ALMA MATER STUDIORUM – UNIVERSITÀ DI BOLOGNA

DOTTORATO DI RICERCA IN

INGEGNERIA BIOMEDICA ELETTRICA E DEI SISTEMI

CICLO XXXIII

Settore Concorsuale: 09/E1

Settore Scientifico Disciplinare: ING-IND/31

PLASMA SYNTHETIC JET ACTUATORS FOR BIOLOGICAL INDIRECT TREATMENT: THE ROLE OF THE CHARGED PARTICLES

Presentata da: Anna Chiara Ricchiuto

Coordinatore Dottorato

Prof. Michele Monaci

Supervisore

Prof. Gabriele Neretti

Esame finale anno 2021

Alla mia famiglia
per esserci sempre stata

Contents

Abstract

Plasma Synthetic Jet Actuators (PSJA) have demonstrated their ability to produce a flow from the surface where the Dielectric Barrier Discharge (DBD) is ignited. This ionic wind is due to the Electro Hydro Dynamic (EHD) interaction. These fluid-dynamic actuators enhance the delivery of reactive species towards the target to be treated. The long-life charged particles are generated within the plasma region and then carried on by the induced flow. The disinfection efficacy of PSJA used to indirectly treat different pathogens was demonstrated. In particular, the inactivation effect of free charges advected by the ionic wind has been investigated. An assessment of the various factors that may affect the production and the effect of the free charges are analysed. It was observed that humidity rate weakly influences the charge deposition. Besides, the most notable effect is an increase of the deposition time for higher humidity rate. In addition, a higher applied electric field produces higher charge deposition rates. Moreover, different geometries and dielectric materials have been considered. Linear actuators have proven to be more effective in charge delivery with respect to annular actuators. The EHD interaction was measured also for a streamer corona discharge utilised for cancer cells treatment.

.

Introduction

In recent years, cold atmospheric pressure plasmas have been considered a promising technology into the biomedical domain. The main features of these non-thermal discharges are their low operational cost, since they can be used at room temperature and atmosperic pressure and the absence of byproduct and toxic emissions. Several works demonstrated the disinfection ability of cold plasma against bacteria, viruses, yeasts and parasites.

A plasma treatment exposes the surface of pathogens or cells to reactive oxygen and nitrogen species, radicals and a significant flux of charged particles, including electrons, positive and negative ions. Two different approaches have been suggested for atmospheric-pressure non-thermal plasma disinfection. These approaches can be classified as direct and indirect treatments. The indirect case presents more advantages, especially in biological field. In fact, the sample is in contact only with the reactive species. In direct case, the tissue itself is an electrode that takes part in discharge creating.

Plasma actuators based on the Electro Hydro Dynamic (EHD) interaction are potentially able to create a preferential channel in which the plasma products are accelerated by the applied electro hydro dynamic forces. In this way, the reactive species delivery towards target increase the treatment efficacy. Plasma local properties and EHD forces have been experimentally studied by means of electrical, optical, and fluid-dynamics diagnostics. This type of actuator names Plasma Synthetic Jet Actuators (PSJA).

Two different plasma sources that use air at atmospheric pressure have been studied and analysed. The former is the Dielectric Barrier Discharge (DBD) and the latter is the Streamer Corona discharge (SC). The EHD interaction effect was investigated for both. Once demonstrated the biocidal efficacy of the PSJA in food and sterilization field, the work focused on the charged particles.

The clinical potential of free charges has been largely ignored in plasma treatments, especially in indirect case. Only recently, their sterilization effect has been investigated, particularly with the PSJA actuator. The charged particles disinfection role was tested against *Candida Albicans* and *Candida Guillermondi*, the agents most frequently implicated in invasive nosocomial fungal infections. Different electrode geometries and dielectric materials have been used to understand which combination is better in the charged particles production. In addition, the influence of external parameters as the air humidity level and the electric field have been analysed. The aim is to understand if the boundary conditions influence the plasma discharge and the charged particles delivery.

The results show the advantage of combining fluid dynamics and inactivation properties of DBD. The charged particles' role in disinfection process was demonstrated. The efficacy of this indirect treatment opens new perspectives in biological field. Further studies must be carried out to understand the role of the free charges on other type of bacteria. It will be interesting to investigate if it is possible to increase the amount of charged particles to enhance the treatment efficiency.

Chapter 1

Non-thermal plasma in biology

1.1 Direct and indirect treatments

The study of non-thermal atmospheric pressure air plasma treatments in medicine and biology have been growing considerably in last decades. The high efficacy in disinfection, healing of wounds, blood coagulation, and in skin diseases has made plasma technologies and in particular cold plasma, very attractive to the scientific community [1]. In addition, the possibility to create a selective tool can kill cancer cells, maintaining alive healthy ones has been shown [2-3]. Besides, it is environmentally friendly and cheap. In fact, there is a limited and controlled pollutants production [4].

Air plasma is able to inactivate a wide range of microorganisms due to the production of reactive oxygen and nitrogen species (RNOS), including ozone, hydroxyl radical and hydrogen peroxide, a significant flux of charge particles, as electrons, positive and negative ions and intense UV radiation [5-6]. All these active agents, show in Figure 1.1, are responsible for the beneficial effects against pathogens and cancer cells [7].

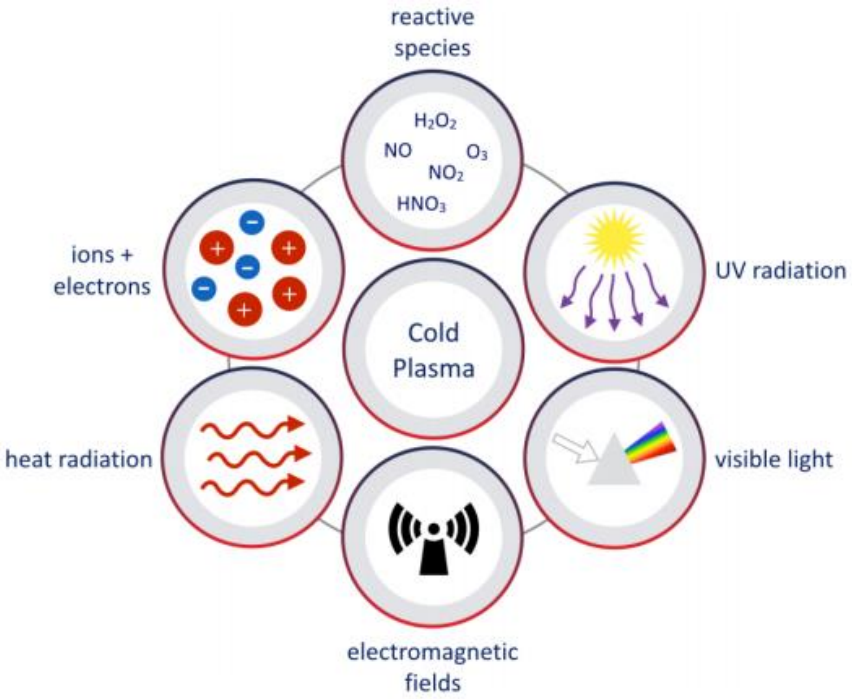

Figure 1.1 Biocidal agents produced in cold atmospheric-pressure plasmas.

The interaction between plasma and living matter is a complex phenomenon still under investigation. Plasma treatments can be direct or indirect. In direct treatment, plasma is directly applied to the biological substrate, the sample is exposed to all plasma elements. In indirect case, the sample is in contact only with plasma afterglow, and thus to reactive species and charged particles solely. In specific situation, the indirect treatments have more advantages than direct one. For example, the plasma reactor can be developed and optimized without considering the target to be treated. It is possible to treat irregular and large surfaces, in homogeneous way, without the contact with harmful voltage potentials. Basically, only the long-life reactive species hit the sample, reaching the surface due to thermal and concentration diffusion. On the other hand, the process is usually slow and isotropic, and so a portion of these is lost.

The indirect treatment also takes in plasma-activated medium (PAM) treatments. The medium is first treated by plasma source, and then, the cells or samples are added to the activated medium. In fact, when non thermal plasma meets water and biological media, antimicrobial or antitumor effects are induced [8]. The plasma discharge produces a relatively long-lasting solution that can be subsequently applied to tissue, cavities, or tumours. This solution has great potential for biomedical application, especially in cancer therapy [9].

This work is focused on indirect treatments. The first part shows the electrical characterization of portable corona plasma source, used for a PAM treatment in cancer therapy [10]. In the second part, non-thermal plasma discharge inactivation effect and the role of the charge particles have been analysed.

1.2 Dielectric Barrier Discharge

Different plasma source configurations have been developed for biomedical applications. They differ for the way in which plasma is created and applied on the target [11]. The most common configuration for indirect treatment is Dielectric Barrier Discharge, or DBD. This concept was first developed in 1857, from Siemens, for ozone generation [12].

The typical DBD configuration, and its equivalent electrical diagram, is shown in the following figure.

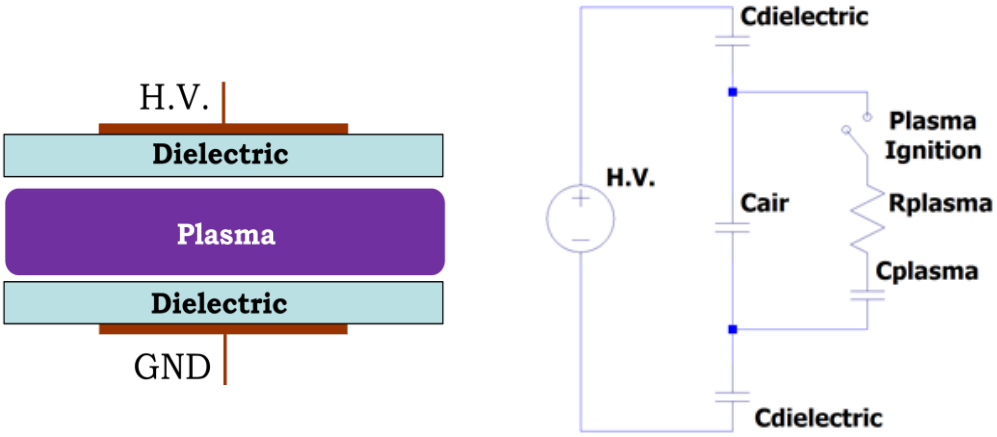

Figure 1.2 Scheme and equivalent electrical diagram of DBD.

The basic configuration of volumetric DBD actuator is composed by two parallel electrodes separated by a gap, filled with gas. One or both electrodes are covered by a dielectric material. In the absence of discharge, the electrical diagram includes three capacitances: two represented the dielectric layers and one, the air gap between the dielectric. C_{plasma} and R_{plasma} are respectively the capacity and the resistence when the plasma switchs-on. If a sinusoidal AC voltage is applied, a displacement current is estabilished and the breakdown of the gas occurs, leading to plasma formation. The dielectric layer is need to self-limit the current and to forbid the transition into an arc regime.

The formation of plasma is based on the avalanche phenomenon. In a plane gap there are the electrons near a cathode. When an electric field is applied, they are accelerated along the electric field lines drifting toward the anode. During this motion, they collide with neutral particles. If the energy owned by the electrons is high enough, they are able to ionize the neutral particles, and so they can extract from the molecules or atoms of the gas one or more “new” electron(s). These electrons are themselves accelerated and are so potentially able to ionize more and more neutral particles. In this way, an avalanche ionization is generated. In plasma discharge the brakdown mechanism is alike to a spark and is based on the streamer concept. The streamers are a series of plasma-filaments. Basically, it is a ionized channel, in which the electrons propagate faster along the electric field lines. In the following figure, it is shown the spark breakdown mechanism and a streamers example, maked by a DBD in air, at atmospheric pressure [4].

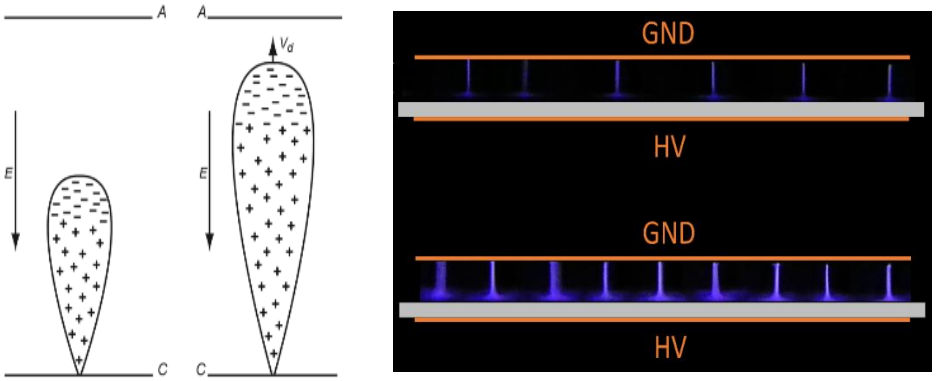

Figure 1.3 Spark breakdown mechanism and DBD streamer picture.

The electron avalanche is self-terminating and only repeats when the applied voltage changes sign. When the streamer channel connects the electrodes, the current may be significantly increased to form the spark. The number of streamers is dependent on many variables including the applied voltage magnitude and frequency, the gas pressure and composition, the electrode material and geometry, the geometry and material of the dielectric layer. During the discharge, the energy from the electric field is accumulated by electrons and than, it is transferred to heavy particles. The majority of the electron energy goes into the

formation of other energetic electrons, instead heating the sorrounding gas. This stored energy, allows to the excitation of the internal energy of the species and limiting the temperature of the plasma itself. For this reason, plasma, formed by a DBD, is known as non-thermal plasma or cold plasma.

The plasma temperature is determined by the average energies of the plasma particles, neutral and charged ones, and their relevant degrees of freedom. In non-thermal case, the relantionship between different temperatures can be conventionally presented in this way: $T_e > T_v > T_r \approx T_i \approx T_0$. The electron temperature (T_e) is the highest in the system, it is followed by the temperature of vibrational excitation of molecules (T_v). The lowest temperature is usually shared by heavy particles (T_0, temperature of translational degrees of freedom), ions (T_i), and molecules rotational degrees of freedom (T_r). In many non-thermal plasma system, electron temperature is about 1 eV (10.000 K), while heavy temperature is usually in the range of 300 ÷ 400 K. For this reason, cold plasma is biocompatible. Basically, it is possible to use it in contact with heat sensitive surfaces. Tipically, a DBD is characterized by electron density in the order of $10^{13} \div 10^{16}$ [part/m^3] and current density in the range of 100 ÷ 1000 [A/cm^2] [13]. An example of voltage and supply current for a DBD is in the figure below.

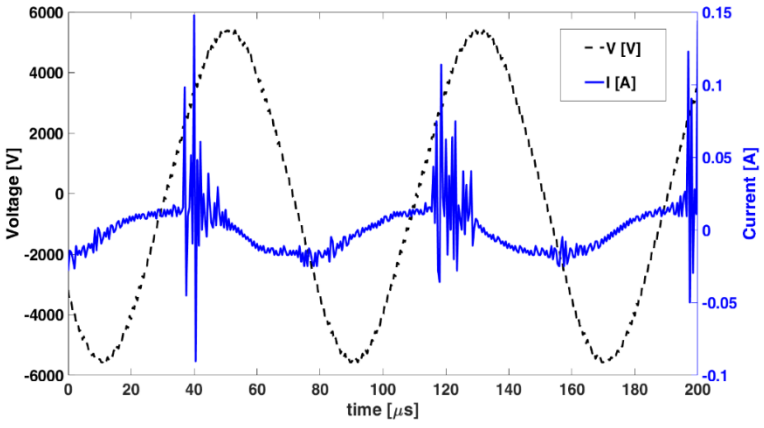

Figure 1.4 Voltage and current for a DBD plasma discharge.

In Figure 1.4 current, rappresented by blue line, is the total of two different contributes. One is the displacement current, due to the capacitive behaviour of the

DBD, (see Figure 1.2) and the other one is the discharge current, represented by the dense repetition of blue peaks and due to streamers formation. The plasma generation occurs only in correspondence of the current peaks, when the high voltage value increase.

1.2.1 DBD sterilization effect

Cold atmospheric-pressure plasma disinfection is a complicated process that involves a wide variety of mechanisms. All biocidal agents produced by plasma, and illustrated in Figure 1.1, are able to completely disintegrate bacteria, viruses, and other micro-organisms without any significant temperature effects. On the other hand, many parts of this process remain largely unclear.

In disinfection process, the first phase is characterized by UV irradiation action. It causes the destruction of the genetic material and a sufficient number of DNA strands lesions. This inhibits the ability of the bacteria to properly replicate. Atmospheric pressure plasma is not so efficient in UV ray production. Usually, a synergy between UV radiation and other sterilizing agents takes place [5]. For example, charge particles play an important role. They deposited onto the cell membrane and can create very intense electrostatic forces is able to break cell membrane itself. Reactive neutral species make a significant contribution into disinfection too. The oxygen-based and nitrogen-based reactive neutral species have strong oxidative effects on the outer structures of cells. The following figure, shown an example of plasma treatment. The bacteria is completeley destroyed after treatment [14].

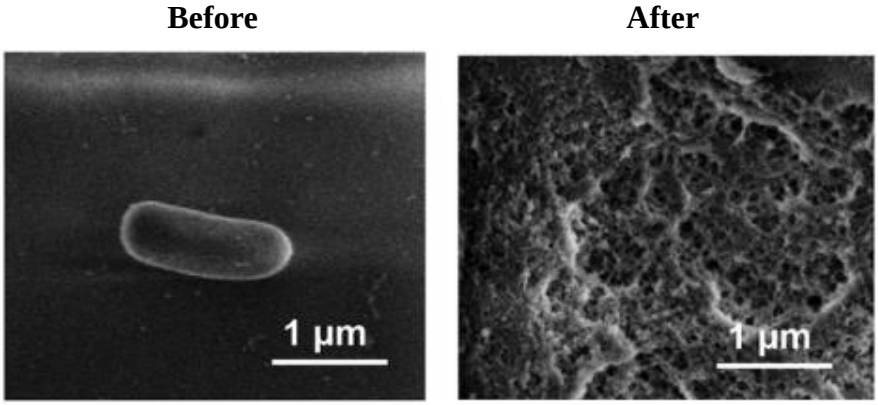

Figure 1.5 Bacteria response before and after DBD plasma treatment.

The most important species responsible in cell membrane destruction is the hydroxyl radical $OH\cdot$. The formation of it starts by water reaction: the ozone dissolves in it, dissociates and reacts with R – H organic molecules:

$$(O_3)_{aq} \rightarrow (O_2)_{aq} + (O)_{aq}$$

$$O + RH \rightarrow \mathrm{R} + OH\cdot$$

The radical $OH\cdot$ triggers a series of reaction making available new organic substrates R and reacts with them to produce a radical ROH · :

$$OH\cdot + RH \rightarrow \mathrm{R} + \mathrm{H_2}O$$

$$OH\cdot + R \rightarrow \mathrm{ROH}\cdot$$

The radical ROH · can be oxidized the cell by means of metal ions and reaction between ROH · radicals. When the cells are not able to repair this chemical attack, they die. The electrons have an important role in $OH\cdot$ formation. They react in water and become hydrated electrons. The hydrated electron can convert oxygen, dissolved in water, into superoxide, the highly reactive O_2^- ion radical. The superoxide is converted into hydrogen peroxide and oxygen by reaction called superoxide dismutation:

$$H_2O + e^- \rightarrow OH\cdot + H + e^-$$

$$2O_2^- + 2H^+ \leftrightarrow O_2 + H_2O_2$$

The H_2O_2 conversion into OH is known as Fenton reaction, a redox process provided by oxidation of metal ions, for example the Fe^{2+}:

$$Fe^{2+} + H_2O_2 \rightarrow Fe^{3+} + OH\cdot + OH^-$$

$$Fe^{3+} + O_2^- \rightarrow Fe^{2+} + O_2$$

In addition, the positive ions M^+, for example N_2^+, are particularly interesting with respect the interaction with water. They rapidly react with water molecules and produce H_3O^+ and OH radicals that play an important role in disinfection:

$$M^+ + H_2O \rightarrow M + H_2O^+$$

$$H_2O^+ + H_2O \rightarrow H_3O^+ + OH \cdot$$

In conclusion the contribution of charged particles into disinfection can be divided into three effects: direct chemical effect of electrons and ions, direct effect of ion bombardment and effect of electric field induced by charged particles.

In previous paragraph, the difference between direct and indirect treatment is described. In direct treatment the discharge and all plasma products reach the sample. In indirect case, the sample is in contact only with the long-life species. These species hit the target by means of thermal and concentration diffusion. It is possible to improve the RNOS carriage with the Electro Hydro Dynamic, interaction.

1.3 Electro Hydro Dinamic interaction

The momentum transfer from charged to neutral particles results in Electro Hydro Dynamic (EHD) body force, also called ionic wind. The first explanation was given by Faraday in 1838 [15]. In plasma discharges, the high electric field locally ionizes the air, producing several charged particles. These particles are accelerated by the applied electric field inducing a macroscopic air flow by means of collisions with the surrounding neutral molecules. In the first studies, direct current corona discharges were used, but different disadvantages have been observed. The biggest limitation was the glow to arc transition [16]. In 1998, Roth demonstrated that an actuator based on plasma, generated by a Surface DBD, was able to induce a tangential flow, at a velocity of some centimetres per second. The velocity was proportional to the magnitude of the AC applied voltage. In this way, a new kind of atmospheric fluid-dynamic actuator was defined [17].

The interest for this phenomenon is growing in aeronautics, astronautics [18-20] and for turbine blade applications [21-22]. For example, the EHD interaction can prevent or induce flow separation, modify the laminar to turbulent transition inside the boundary layer, and stabilize or mix air flow. The EHD effect can also generate convective flows. In recent years, this ability has been investigated in plasma medicine and biology field too. In fact, the ionic wind can be exploited to enhance indirect plasma treatment, increasing the delivery of the plasma reactive species onto surfaces or liquids, thereby intensifying their disinfection and antibacterial efficacy [23].

1.3.1 EHD actuator based on DBD

The asymmetry of the electrodes is the most important characteristic in the DBD aerodynamic plasma actuator. The two electrodes are separated by a dielectric layer. Exposed electrode (the upper, in the figure below) is in direct contact with the fluid, the other is embedded, in order to prevent the plasma formation on it. A sketch and a picture of DBD aerodynamic plasma actuator is shown in the following figure.

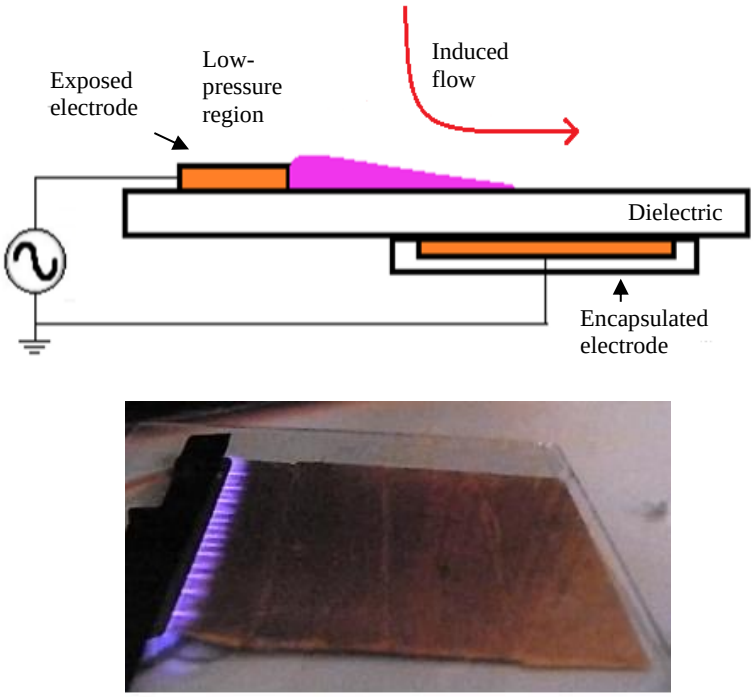

Figure 1.6 Sketch and picture of tipical DBD aerodynamic plasma actuator.

When high voltage is applied to the electrodes, a surface discharge is produced, only in the upper surface correspondingly over the embedded electrode. Due to the asymmetric electrodes a low-pressure region is generated above the exposed electrode. Air enters this depression region and experiences a unidirectional thrust tangentially to the actuator surface. In this way, the ionic wind occurs. The wind speed is limited by the highest intensity of the electric field generated in the actuator. Higher fields can damage the dielectric layer and progressively change the plasma morphology. EHD interaction can be influenced

by streamers morphology, dielectric layer properties, waveform of the voltage feedings, and electrodes geometry [24-26].

1.3.2 Linear and annular DBD actuators

It is already highlighted, that different plasma discharge configurations are used in biology and medicine field. In the past, our research group have studied the linear and annular DBD actuators in order to maximize the velocity, mechanical power and efficiency of the induced jet [27]. In this work, both configurations, linear and annular, have been compared to investigate their ability in the disinfection field.

In linear case, an asymmetric electrode pair is separated by a dielectric slab. In this way, a tangential jet over the actuator surface occurs, as described above (see Figure 1.6). The annular actuator is characterized by a normal tubular flow perpendicularly to the actuator surface itself. The different tangential jets collide and merge when approaching the centre of the circular exposed electrode [28]. The ionic wind direction, due to the EHD interaction, is indicated by arrows in the Figure 1.7, for both geometries.

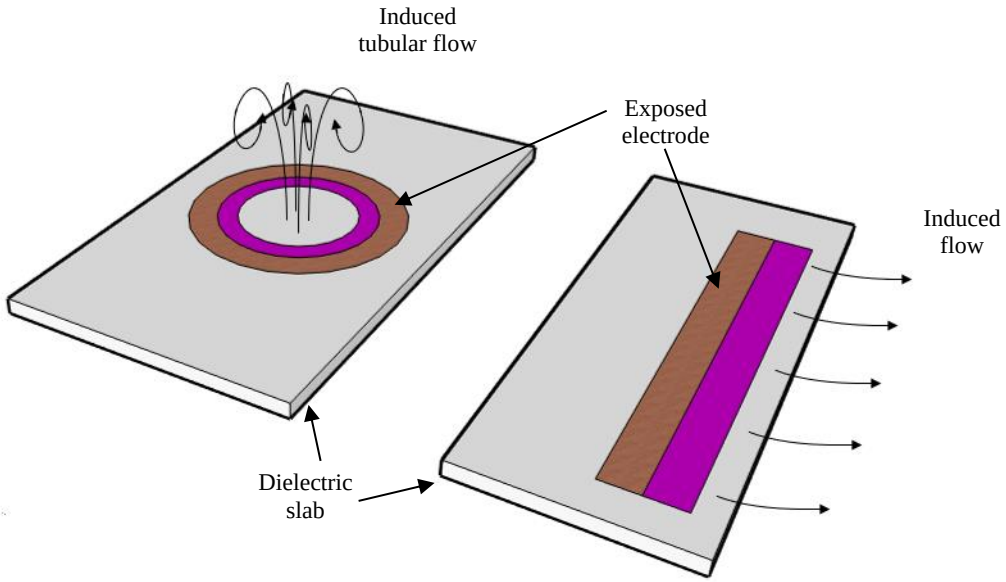

Figure 1.7 Ionic wind direction for annular and linear actuator.

The electrodes are made of copper tape, with a thickness of 35 μm. The dielectric slab analysed is both PVC and Teflon. The annular geometry is changed by an octagonal geometry due to the difficult to build the electrode. It has been demonstrated that this octagonal configuration produces an induced jet similar to generated by an annular actuator [29]. A sinusoidal supply system constituting of a push-pull voltage transformer controlled by Arduino is utilized to feed the discharge. The voltage and frequency are in the ranges 0 – 20 kVp and 15 – 50 kHz, respectively. In order to investigate the electric field role, a supplying frequency value of 4.2 kHz was obtained with another power supply, constituted by a signal generator, a power amplifier, and a step-up transformer.

The atmospheric pressure ambient air is used to ignite the discharge. In fact, the fluid dynamics Plasma Synthetic Jet Actuators (PSJA) are very attractive in different application fields due to their flexibility and low-cost operation [1]. This work is focused on the two configurations and their role in indirect bacteria inactivation [28].

The ability of the ionic wind to transport neutral particles, active species and free charged particles is very interesting in indirect treatments. In fact, the actuators produce a preferential direction in which the plasma products are delivered toward a target to be treated. In particular, the role of the charged particles in the inactivation process is analysed. Their clinical potential has been largely ignored in plasma treatments considered up to know, and only recently, their disinfection effect has been investigated in direct and indirect treatment [30]. The potential distributions induced by charges deposited on an insulating target surface, perpendicularly to the flow have been measured. Several parameters, such as actuator dielectric material and its thickness, electrode geometry, target distance from the actuator surface, time interval of plasma-on and potential of the exposed electrode have been changed and studied.

1.4 Streamer Corona Discharge

In this chapter, PAM treatment for the cancer therapy has been introduced. One of the aims of this work is the electrical characterization of different non-thermal plasma discharge. The portable air plasma corona pen source, analyses in the following, was made in the Faculty of Mathematics, Physics and Informatics, at Comenius University in Bratislava [10].

This discharge is a positive streamer corona (SC). It is a direct-current electrical discharge generating non-thermal plasma in atmospheric air. The device consists of a hollow needle as power electrode and a metallic mesh or a metallic plate as grounded electrode. The geometry is point-to-plane. The needle electrode is surrounded by a quartz capillary. A simplified electrical scheme and a picture of the discharge are shown in the figure below [31-32].

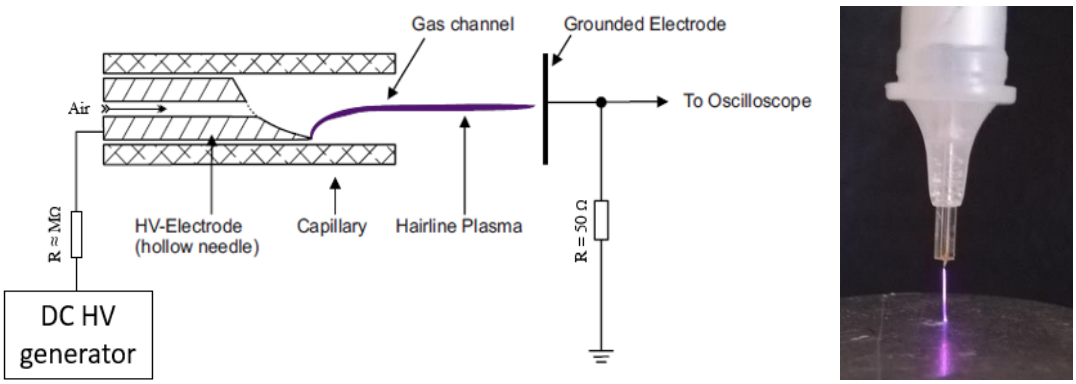

Figure 1.8 Sketch and picture of a SC discharge.

A DC high voltage (HV) was applied through the ballast resistor R (~MΩ) and through the HV cable on the needle electrode. When a few kilovolts are applied to the point electrode SC appears. SC has small current pulses (~10 mA) with a repetitive frequency of 10–30 kHz, during which the discharge voltage remains fairly constant. A typically voltage and supply current for a SC discharge is shown in the following figure.

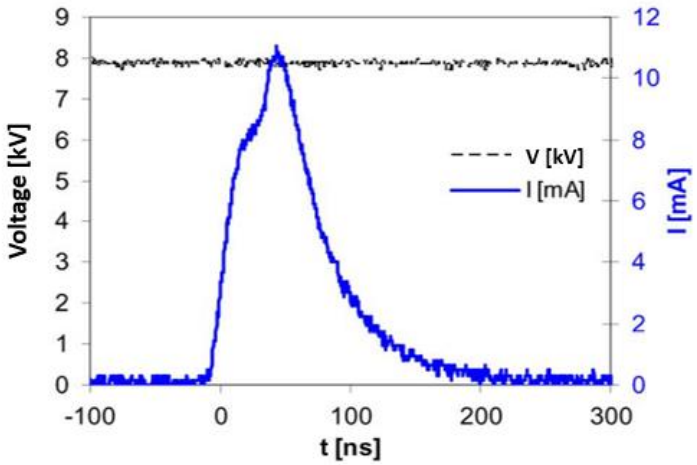

Figure 1.9 Voltage and current for a SC plasma discharge [10].

The corona discharge starts when the electric field is strong enough to create chain reaction. In the same way of a DBD reaction, electrons collide with heavy particles, ionize them and create free electrons. The glow of the corona is caused by electrons recombining with positive ions to form neutral atoms. When the electron falls back to its original energy level, it releases a photon of light. The photons serve to ionize other atoms, maintaining the creation of electron avalanches.

The portable plasma source also enable operation in the transient spark regime, it is described in details in Ref. [10, 33-34]. The source is characteraized with three different needle positions: 1 mm inside glass tube, 2 mm outside and 0 position, the same position between the needle and the glass. When the needle is in the last position a transient spark transition occours. These three configuration are electrically analysed in the following chapter.

1.4.1 SC sterilizazion effect

The most important application of the SC discharge concerns the cancer therapy. This source generates RONS at very low deposition power in the medium, that in a second time, is used to treat the cells [35]. In fact, PAM treatment is able to create a selective tool. Cell death is an important variable in cancer development.

There are two distinct processes: apoptosis, also known as programmed cell death and necrosis, a form of traumatic cell death. The apoptosis is an active process that, can be regulated and controlled. In cancer tharapy, SC plasma treatment induces a massive response against tumor cells, whereas it has no impact on the survival of non-malignat cells. In this way, the tumor cells die for apoptosis. The first step involves the formation of primary singlet oxygen. It inactivates some membrane-associated catalase molecules on at least a few tumor cells. With some molecules of their protective catalase inactivated, these tumor cells allow locally surviving cell-derived, extracellular H_2O_2 and $ONOO^-$ to form secondary oxygen. These species continue to inactivate catalase on the originally triggered cells and on adjacent cells. Optimal inactivation of catalase then allows efficient apoptosis induction. In this way, the RONS are directly responsible for the induction of cell death in the target cells. The PAM treatments are a promising antitumor effects *in vitro* and *in vivo*, in very broad variety of tumor system [9, 35-37].

The EHD effect is also visible in this portable corona pen. It was meausered for the three different needle positions with the aim to understand if the ionic wind influences the RONS carriege and consequently the cancer application.

1.5 Diagnostic techniques

Different diagnostic techniques have been used to analyse and study the plasma sources. They are briefly illustrated in the following.

1.5.1 Schlieren Imaging

The Schlieren imaging is an optical diagnostic sensitive to the refraction of the rays of light. This diagnostic has been largely utilized in the past because it enables to see the presence of pressure and temperature gradients. In this way, it is possible to study the hot jet produced by means of the plasma actuators and to evaluate its shape and velocity. A Schlieren set-up example is shown in the following [38-39].

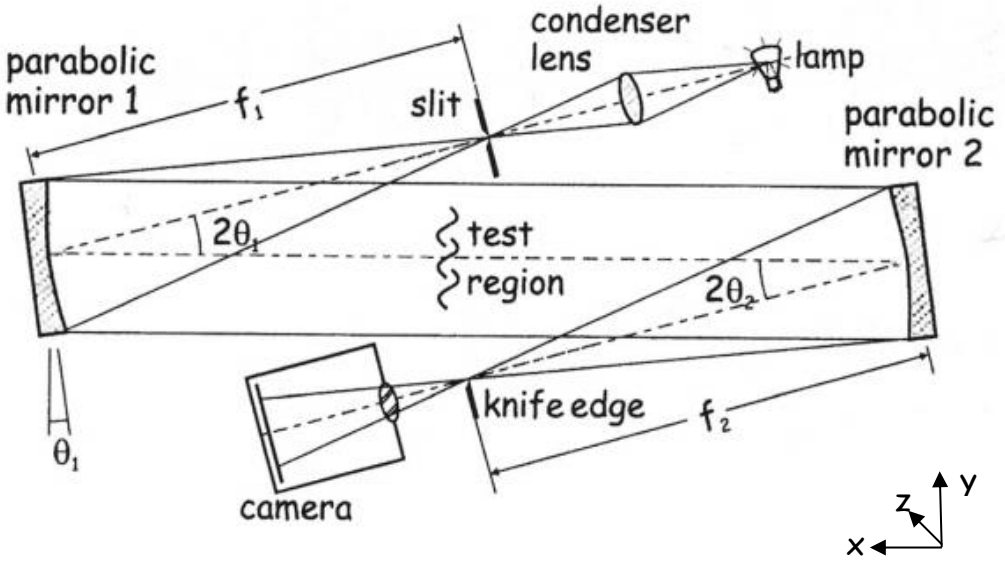

Figure 1.10 Schlieren set-up example [39].

In this diagnostic technique a collimated light beam is focused on target object, this is the role of the first parabolic mirror. The second, refocuses the beam on the knife edge. Finally, the beam proceeds to a viewing system, for example the camera or human eye, where a real inverted image of the test region is formed. In uniform density fluid, it is possible to see a simple bright picture, because all the light emitted from the source arrives undisturbed to the screen. In fact, there are no

change in refractive index in the test section and the knife edge is open. If the knife is slightly closed, less light arrives to the screen, until all the rays are intercepted, and the screen becomes dark. For example, in fluid with density gradients, light beam is distorted and therefore light that is focused in area covered by knife-edge is blocked. In this way, on the screen it is now possible to observe regions that are brighter and others that are darker. This Schlieren description is a Z-type configuration, light rays travel in a z-shaped path [39].

1.5.2 Pitot tube diagnostic

Pitot tube is a flow measurement device used to measurement the punctual fluid flow velocity. It is composed of a thin L-shaped tube, placed against the flow direction, as reported in Figure 1.11. In plasma field, the pitot tube is used to determine the synthetic jets velocity.

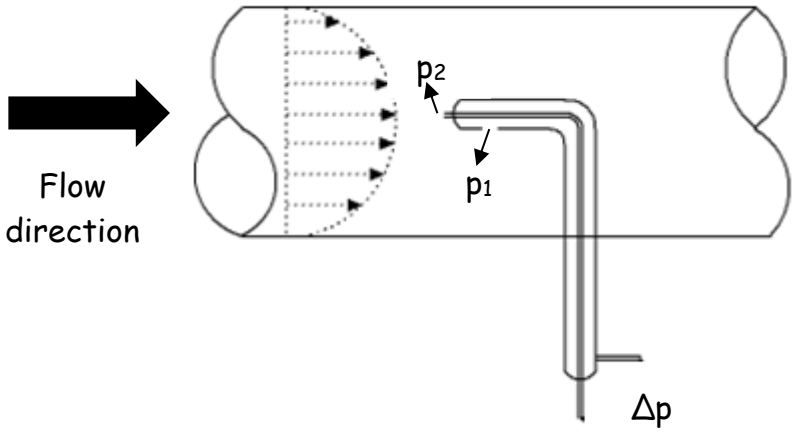

Figure 1.11 Pitot tube device.

The principle of Pitot tube is based on the Bernoulli equation:

$$\frac{u_1^2}{2} + gz_1 + \frac{p_1}{\rho_1} = \frac{u_2^2}{2} + gz_2 + \frac{p_2}{\rho_2} \qquad (1.1)$$

where u, z and ρ are respectively the velocity, the high and the density of the fluid, and g is the standard gravity constant. For the section shows in Figure 1.11, different assumptions can be done:

- The flow is incompressible, $\rho_1 = \rho_2 = \rho$
- The conduct is horizontal, so the highs of the fluid are the same, $z_1 = z_2$
- In the stagnation point the condition of still fluid holds, $u_1 = 0$

Under these conditions the equation 1.1 becomes:

$$\frac{p_1}{\rho_1} = \frac{u_2^2}{2} + \frac{p_2}{\rho_2} \qquad (1.2)$$

In this way, it is possible to calculate u_2 , the velocity of the fluid:

$$u_2 = \sqrt{\frac{2\,(P_1 - P_2)}{\rho}} \qquad (1.3)$$

The plasma actuators studied in this thesis operated in atmospheric pressure air and therefore ideal gas behaviour and consequently the simplify equation (1.3) can be assumed.

1.5.3 Charged particles measurement

To understand the role of the charge particles in indirect treatment is needed to quantify the production of them in the plasma discharge and how many reaches the sample. The potential distribution induced by charges deposited over an insulating target has been measured by using the set-up shown in Figure 1.12.

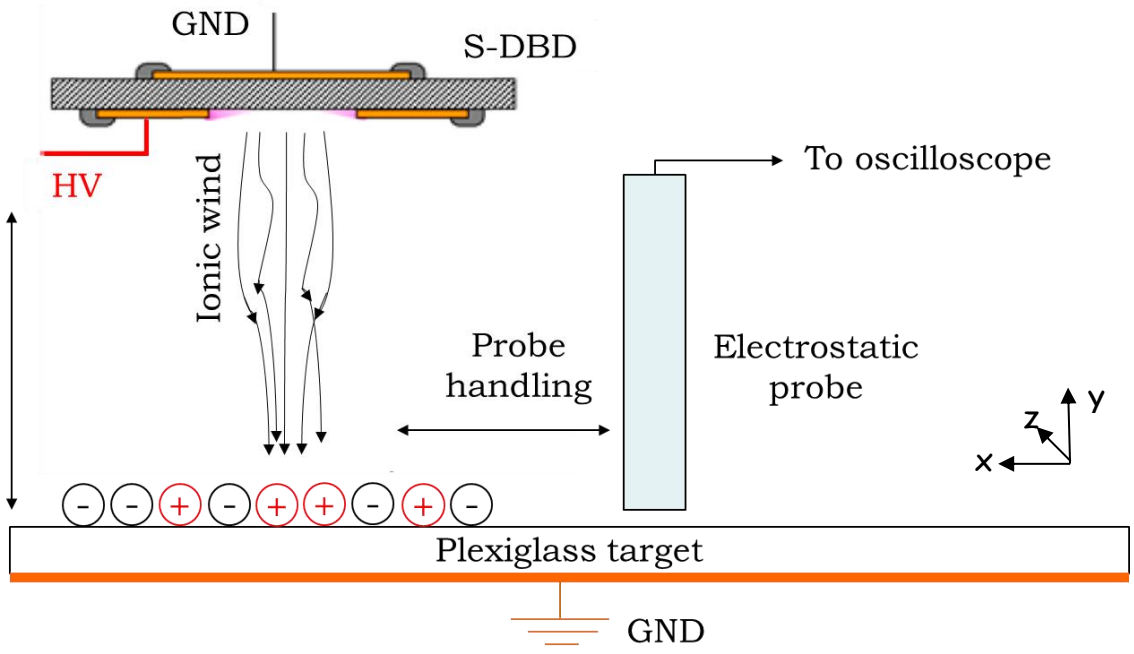

Figure 1.12 Charged particles measurement set-up.

The plasma actuator is placed under the target, in a range 1 ÷ 5 cm, to investigate the maximum distance for which the charges reach the sample. When the discharge is ignited, a jet is formed and the charged particles are transported on the target, in the negative y-direction (Figure 1.12). After the switching-off of the discharge, the electrostatic 341B 20 kV TREK voltage probe scans the target surface, by means of an automated handler, in the x-direction. In this way, the potential induced by charges is acquired on the scope.

The measurements were performed inside an insulating cubic box, to maintain constant the temperature and relative humidity level, and to study the influence of these parameters on the charged particles production and delivering. The box is provided with a glass wall allowing to see inside of it, and a Plexiglas movable tray used to measure advected charged particles. Below this tray, a copper tape was attached and grounded allowing stable and reliable measurements of the induced potential (Figure 1.13).

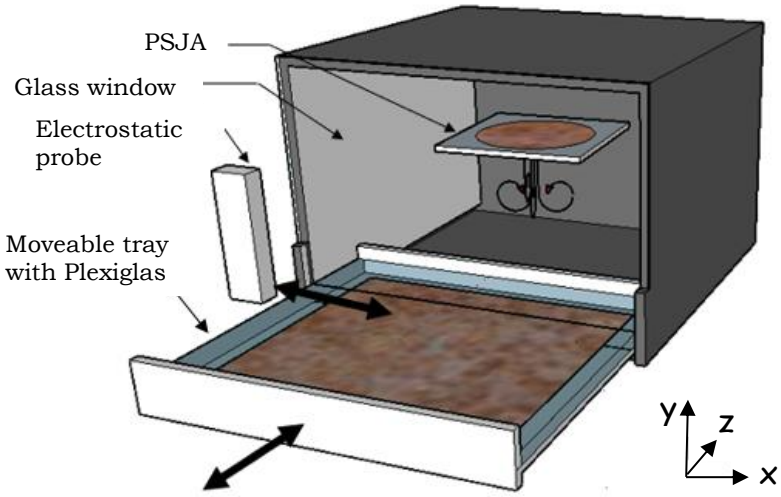

Figure 1.13 Cubic artight box schematic. Electrostatic probe and PSJA position in experimental set-up [40].

1.6 Biological application

The disinfection effect of DBD annular actuators was tested against a Gram-negative food-borne pathogen, as *Escherichia Coli* and other not specified bacteria. Non-thermal plasma technology is a promising tool for different application field, one of this is the plasma food [41].

Meat and agricultural products are contaminated by microbes at distinct stages of the production chain, including the preparation, storage, and distribution stages. Thus, the quality of the products deteriorates, and potential public-health problems develop unless the products are properly handled and preserved. For example, in USA, 76 million cases of foodborne diseases are reported to occur annually leading to 325,000 hospitalizations and this results in high medical costs and in productivity losses. Conventional thermal treatments can inactivate foodborne pathogens, but they can have a negative impact on the nutrient value and the sensory qualities of food. Considerable attention is currently being focused on developing new non-thermal and highly energy-efficient techniques that can be used to effectively reduce microbial contamination in foods.

In this context, *E. Coli* is a typical bacterium presents in food packaging or in food it-self. Different research group have tried to inactive it by a DBD non-thermal plasma source [42-44], but nobody has used the EHD interaction on the chemical species carriage to increase the disinfection effect. Moreover, the DBD annular actuator was used for the inactivation of native microorganisms isolated from fresh fruit juices. This treatment is one of the new technologies to answer to the continuous increase of long-lasting fresh product requirement.

1.6.1 Charged particles role in inactivation *Candida* test

The charge particles' role was investigated against *Candida* species. This species is commonly used as a model organism for fungal pathogens. *Candida* is a common member of the human gut flora but causes systemic infection in an immunocompromised host. This pathogen is implicated in invasive nosocomial

infections. In the last years, nosocomial infection problem is largely increased [45]. It is typical in hospital: during hospital stay, fungal pathogens may cause prolonged stay, disability, and economic burden. The aim to study the inactivation of *Candida* is to have an alternative method to decrease the infections proliferation. The most common fungal species isolated is *C. Albicans*. *Candida Guilliermondii* is widely distributed in nature and frequently isolated from soil, plants, insects, seawater, atmosphere, exudates of several trees, and processed foods, in addition to being a part of saprophyte microflora on the skin and mucosal surface of humans and also of animals [46].

Cold atmospheric pressure plasma treatment is a promising technology in the biological field, as already described. In the past, different research groups demonstrated the sterilization ability of this treatment against bacteria, viruses, parasites and *Candida Albicans* too, but in the literature no information exists about *Candida Guilliermondii* treatments [47-49].

In this work the inactivation power against this *Candida* species is illustrated and it is focus on the charged particles effect. The inactivation effect of free charges, advected by the induced flow, was studied interposing a metallic mesh between the actuator surface and the treated sample.

The tests were repeated with two configurations: in one the mesh is connected to the ground terminal (0-2 configuration in Figure 1.14). In this way, the charges are blocked and have not a role in disinfection process. In the other one (0-1 configuration in Figure 1.14), the metallic mesh is floating, and the charged particles are free to reach the sample. In Figure 1.14 an actuator sketch with the mesh and the related experimental set-up are displayed.

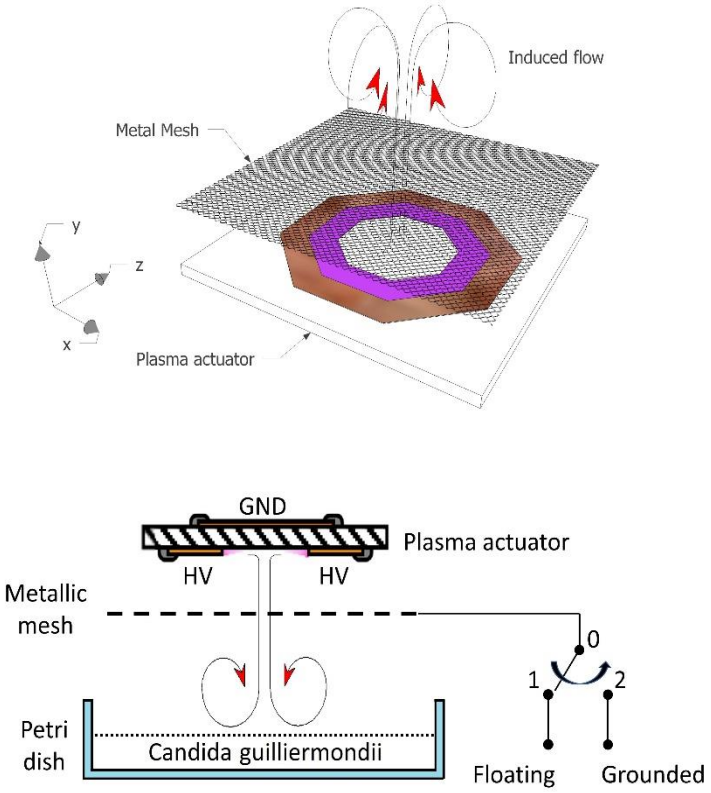

Figure 1.14 Sketch and set up actuator with metallic mesh [29].

In the following chapters, the electrical characterization and the fluid dynamic interaction is studied for SC portable pen and for DBD actuators. The potential distributions induced by charged particles is illustrated for the two DBD configurations actuators, displayed above. Finally, their inactivation ability has been tested against *Candida Guillermondi, E. Coli* and other bacteria. The tests are performed in order to increase the production and the effect of the charged particles.

Chapter 2

Streamer corona discharge

2.1 SC characterization

In previous chapter, portable air corona pen source was introduced. In the following, electrical characterization and ionic wind analysis are presented.

The discharge is a positive streamer corona, generated on the needle electrode in ambient air. The geometry is like the discharge presented in Ref. [31-34]. The particularity of this discharge is the needle position. As already mentioned in Chapter 1, the source is characteraized with three different needle positions: 1 mm inside the glass tube, 2 mm outside and 0 position (the same potision between the needle and the glass). An example is shown in Figure 2.1, 2.2 and 2.3. The aim is to understand if the needle position influences the electrical parameters of the discharge ignition and the ionic wind production. In the following, to simplify the lecture, 1 mm inside position will be called Configuration 1, 0 position will be designated as Configuration 2, and 2 mm outside is Configuration 3.

2.1.1 Electrical charcterization

The discharge was ignited between two metal electrodes: one is the needle, the high voltage electrode and the other one is a metallic plate, the grounded electrode. The discharge voltage, V, was measured by HV probe (Tektronix P6015A). The current, I, was measured on a 50-Ω resistor by a Rogowski current monitor (Pearson Electronics 2877). V and I signals were processed by a 200-MHz oscilloscope Tektronix TDS 2024, see Figure 1.8, Chapter 1.

Three different gaps, distance between the needle and the metallic plate, were performed: 5, 10 and 15 mm, and the three different needle configurations were analysed for each gap. In all tests the voltage was fixed to 14 kV, the same voltage used for the biological application. The current maximum and its average value and the frequency were acquired for all needle positions.

A discharge picture is shown in the figure below. It is possible to note a transition from SC discharge to a spark regime in Configuration 2, when the needle is in 0 position (Figure 2.1.b, 2.2.b and 2.3.b). This behavior is highlighted for the

same configuration, for all gaps analyzed. The transition mechanism is described in Ref [10].

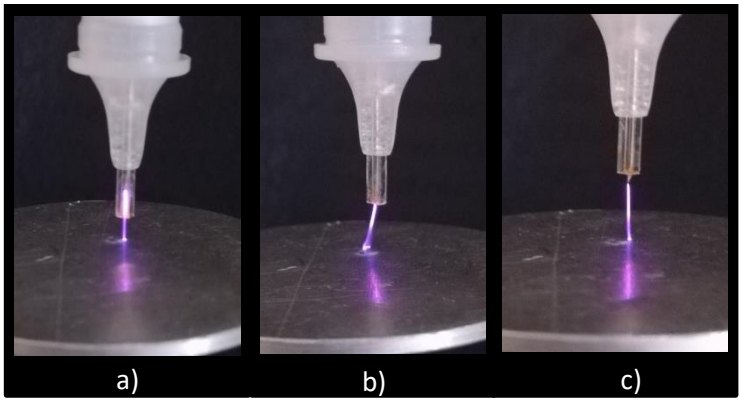

Gap 5 mm

Figura 2.1 SC discharge for the three needle configuration, 1 (a), 2 (b) and 3 (c). Gap 5 mm.

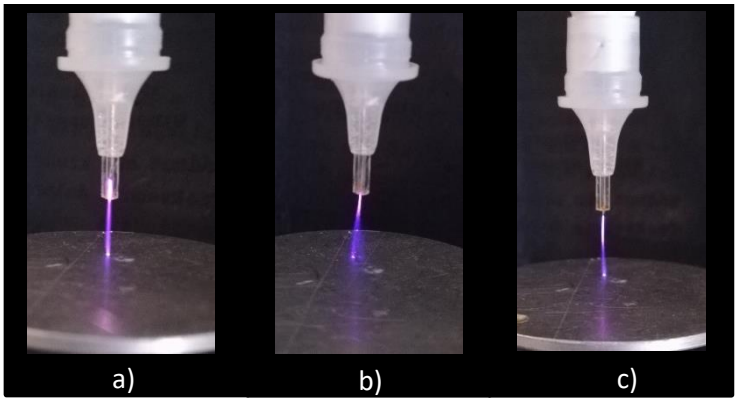

Gap 10 mm

Figura 2.2 SC discharge for the three needle configuration, 1 (a), 2 (b) and 3 (c). Gap 10 mm.

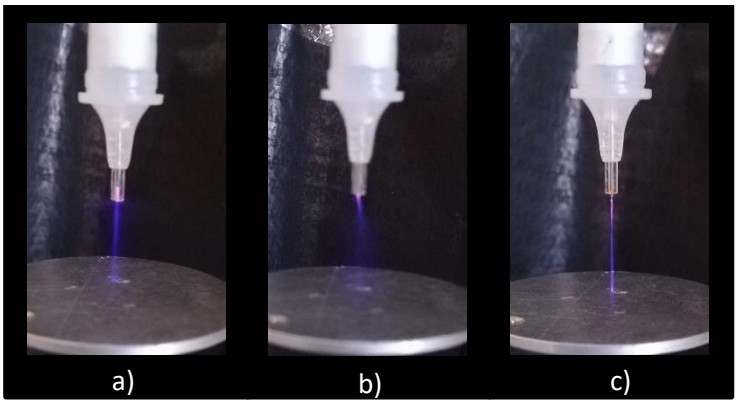

Gap 15 mm

Figura 2.3 SC discharge for the three needle configuration, 1 (a), 2 (b) and 3 (c). Gap 15 mm.

A typically voltage and supply current for SC discharge is displayed in Figure 1.9, in Chapter 1. In the following, the measurement of current and frequency are done in triplicate with a standard deviation error of 6%.

The values are acquired for the three needle configurations and for the intermediate positions: 0.5 mm inside, 0.5 mm, 1 mm and 1.5 mm outside. The results are shown in Figure 2.4. In blue is highlighted the values acquired for a gap equal to 5 mm, in black for 10 mm and in red for 15 mm. All values increase when the distance between the two electrode is small, while for a bigger distance it decreases. This behaviour is shown also in the discharge picture, (Figure 2.3). The discharge glow is very low, for a gap of 15 mm, while it is very intensive for a gap of 5 mm, with the same voltage applied.

The frequency and average current values in the graphs shown a negative peak for a needle position of 0.5 mm outside respect the trend curve. This could be related to spark transition. In addition, the frequency (Figure 2.4.a) decreases for the needle outside position, despite in Configuration 3, and only for the gap of 15 mm, a fast increase is displayed. The values decrease considerably, in configuration whit a gap of 15 mm, in fact a drop of about 70 % is illustrated. On the contrary, the maximum current (Figure 2.4.b) increases for the needle outside position. In fact, the value is 0.05 mA, in Configuration 1, and 0.15 mA, in Configuration 3, with an increase of about 70 % for the gap of 5 mm. The average current (Figure 2.4.c), presented a similar trend curve with the gap of 10 and 15 mm, despite the same fast peak, highlights for the frequency, is displayed, always for the needle Configuration 3 and for the gap of 15 mm. The gap of 5 mm shows a different trend, it has a positive peak, for the needle position 1 mm outside, and then the curve decreases.

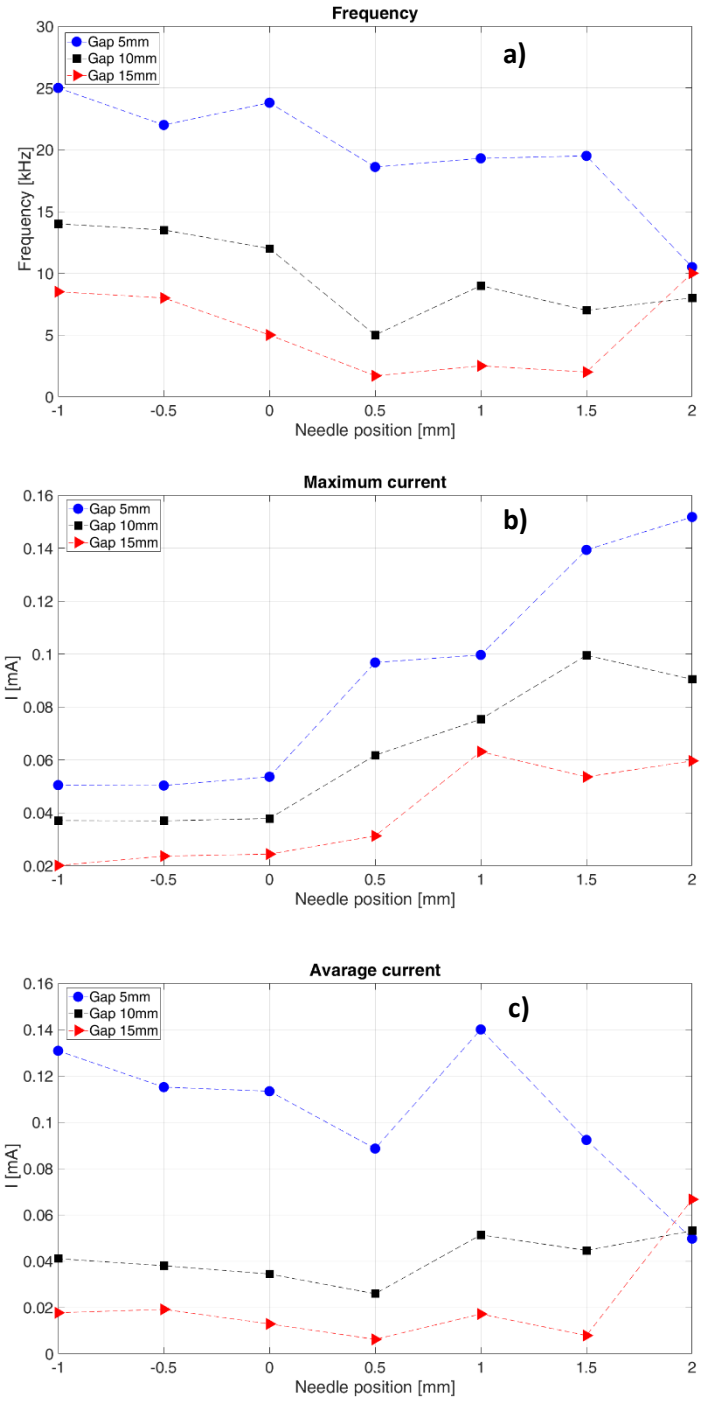

Figura 2.4 Frequency (a), maximum current (b) and avarage current (c) for the three gaps and for the different needle positions.

To understand the different behaviours above mentioned a magnetic hysteresis tests have been done. The charge particles deposited on the quartz tube and consequently the possibility of them to influence the current and frequency measurements have been analysed. The tests were performed changing the position of the needle in two different ways: from inside to outside (IN==OUT), and from outside to inside (OUT==IN), for a gap of 10 mm. The results are shown in the following. The black line is referred to the needle position from outside to inside, while the red line from inside to outside. Frequency trend (Figure 2.5.a), maximum current (Figure 2.5.b) and average current (Figure 2.5.c) have about the same value for the two different needle positions (IN==OUT and OUT==IN). In conclusion, the free particles do not influence the electrical data.

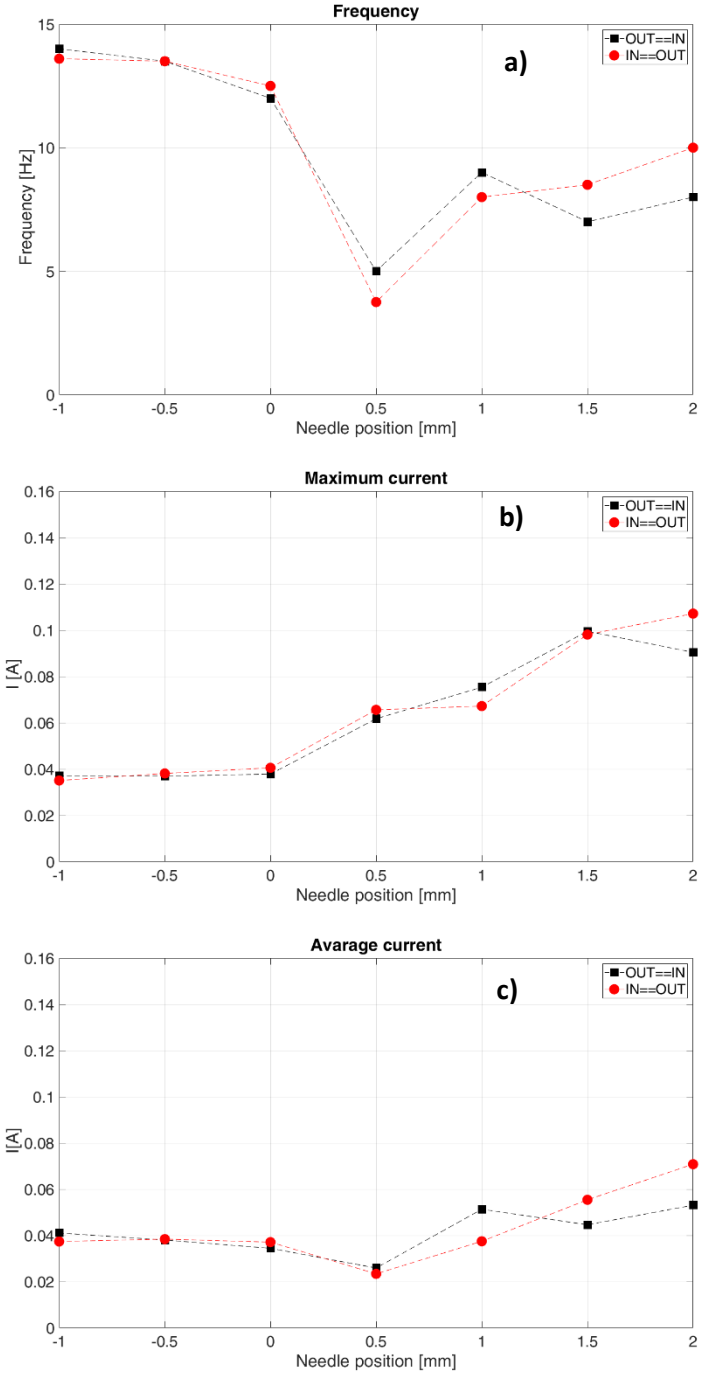

Figura 2.5 Magnetic hysteresis tests for a gap of 10 mm. Frequency (a), maximum current (b) and avarage current (c).

2.2 Fluid-dynamic charcterization

In Chapter 1, EHD interaction and ionic wind concept were presented. In this Chapter, ionic wind was measurements for the different needle positions. Test set-up is shown in Figure 2.6. Needle position changes in x-direction while velocity profiles along y-direction. The grounded electrode is a metallic mesh, with 2 x 1 mm x mm rectangle holes and with a wire thickness of 0.3 mm. In this way, it is possible to measurement the ionic wind velocity without compromised the fluid-dynamic of the jet.

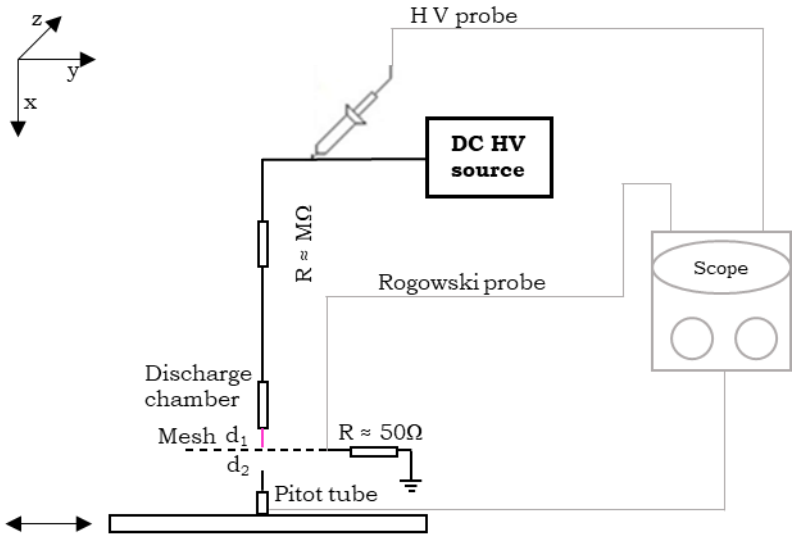

Figure 2.6 Pitot tube measurements set-up.

Needle positions, gaps and voltage are the same analyzed for the electrical characterization. In Figure 2.6, d_1 is the distance from the end of the quartz tube to the mesh. This value was changed for the velocity measurements as a function of needle positions and was fixed to 10 mm for the velocity tests as a function of Pitot tube moving. In addition, d_2, is the distance between the mesh and the Pitot tube device. d_2 was equal to two different values: 0 mm and 5 mm. In this way, the end point of spread ionic wind could be estimated. Pitot tube is placed on the optical table and it was moved on the y-direction (Figure 2.6). It was connected to a DCAL401 Sursense ultra-low pressure sensor with 32 mV Pa^{-1} resolution. The

measurements were averaged over five different tests. The results are presented in the following.

In this first test the two distances, 0 and 5 mm, between mesh and Pitot tube, (d_2 in Figure 2.6), are compared to choose the better configuration. The distance between the mesh and the needle is equal to 10 mm (d_1 in Figure 2.6).

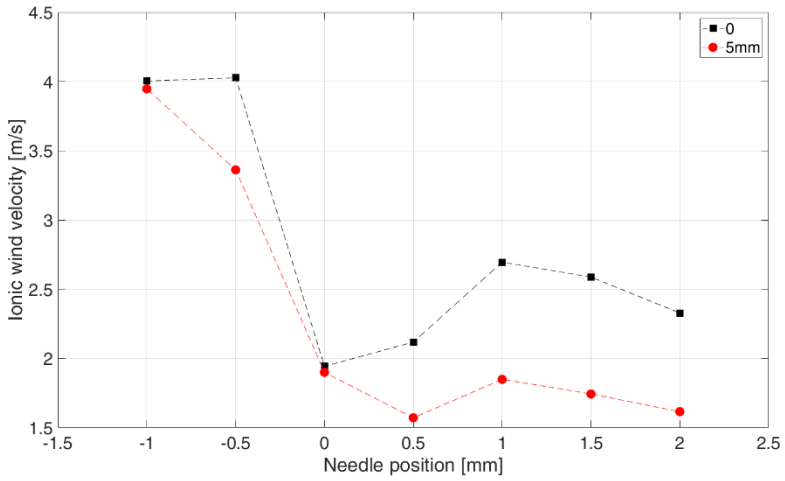

Figure 2.7 Ionic wind velocity as a function of needle position. d_2 is equal to 0 and 5 mm, d_1 is 10 mm.

In Figure 2.7, black line is referred to 0 mm, and red line to 5 mm. Both cases have a fast decrease for the zero needle position, as already highlighted in the previous measurements. In the first case, curve trend is highest than the second. For this reason, in the following, d_2 has been fixed to 0 mm for all tests. Moreover, this suggests that ionic wind have not a long spread in the x-direction (Figure 2.6).

In Figure 2.8, ionic wind velocity as a function of needle position, for the three gaps are displayed. In the graph, in blue is highlights the values acquired for a gap equal to 5 mm, in black for 10 mm and in red for 15 mm. The highest values were obtained for the gap of 10 mm and for the needle position in Configuration 1. In fact, in this case the maximum ionic wind velocity value is equal to 4 m/s. Trend curve is similar for 15 mm and 10 mm gaps, but the velocity for 15 mm is less of about 18 %. This difference is about 33 % with gap of 5 mm. The velocity has a

fast decrease for the needle Configuration 2, for the gap at 10 mm and 15 mm. This behaviour is highlighted for the needle position at 0.5 mm outside, for the gap of 5 mm. The decrease could be related to the spark transition. In needle outside configurations, ionic wind velocity is less than inside needle position. The different is about 18 %. In conclusion, the gap of 10 mm is the best distance in term of ionic wind velocity. For this reason, the distance of 10 mm between the mesh and the needle was chosen for the velocity measurement with Pitot moving.

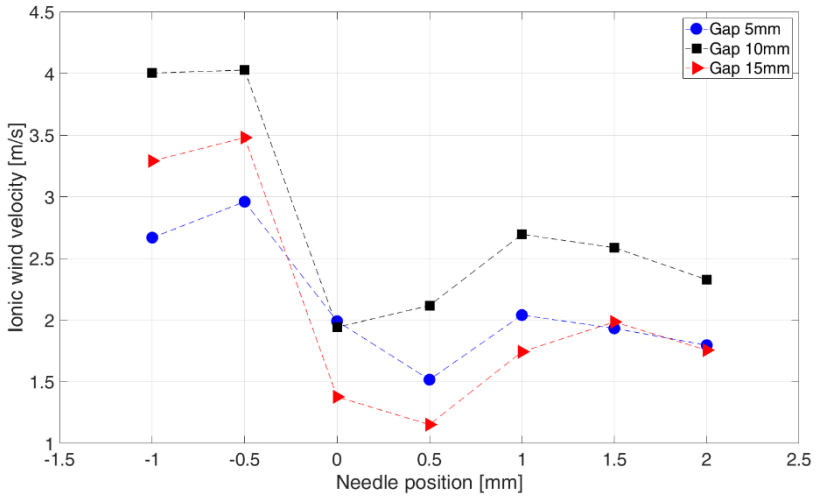

Figure 2.8 Ionic wind velocity in fuction of needle positions, for the three gaps analyzed.

In the second test, Pitot tube was moved of 2 cm, in the y-direction (see Figure 2.6). Zero Pitot position, in the graph below, is the perfect alignment between Pitot tube and the needle. Pitot tube moves 1 cm on the right and 1 cm on the left, of the corona discharge. The measurements were acquired for the three needle configuration and are displayed in the following plot. Configuration 1, needle 1 mm inside) is the continuous blue line, Configuration 2 (0 position) is the dotted black line, and Configuration 3 (needle 2 mm outside) is the red line.

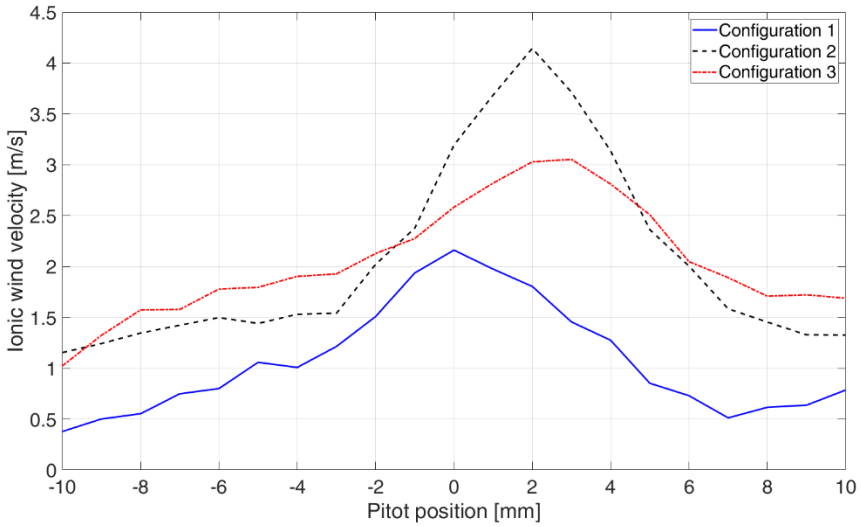

Figure 2.9 Ionic wind velocity in fuction of Pitot tube moving.

In this case a different behavior was highlighted. Highest value was obtained for Configuration 2, while in previous tests Configuration 1 was the best needle position related to ionic wind velocity. In fact, the maximum value of 4 m/s was reached, for the needle in 0 position. On the contrary, the velocity increases and reaches the maximum value of 3 m/s with Configuration 3. Moreover, the velocity peak is not in 0 position but 2 mm on the right, for Configuration 2 and 3. For Configuration 1 the maximum value is obtained with needle in 0 position, but this value is half than the first measurement (see Figure 2.8). A possible explanation consists in the needle geometry. It has not a square end but a triangle shaped. This could be influencing the direction of the corona discharge formation.

These measurements have been very difficult to perform. Minimal differences in the set-up, have highlighted a strong change in ionic wind velocity. Despite this, it is possible to conclude that the streamer corona discharge produces an ionic wind velocity in the order of 4 m/s, at 10 mm of the end of the quartz tube. This result can be utilized in cancer therapy, to facilitate the reactive species carriage into the sample.

In the following Chapters electrical and fluid-dynamic characterization for different DBD reactors, and their biological applications are presented.

Chapter 3

Annular PSJA

3.1 Annular PSJA characterization

In this chapter the annular PSJA configuration is analysed. The actuator scheme shown in Figure 3.1, is the same describe in Chapter 1. The inner diameter chosen is equal to 30 mm. In a previous study [27], this value has been already optimized to maximize velocity, mechanical power, and efficiency of the jet. The dielectric slab is made of PVC. It has better performance on the charged particles production and deposition than other, for example glass or FR4 (vitrinite for PCB). In fact, in Ref. [29], these three dielectric materials are analysed and compared.

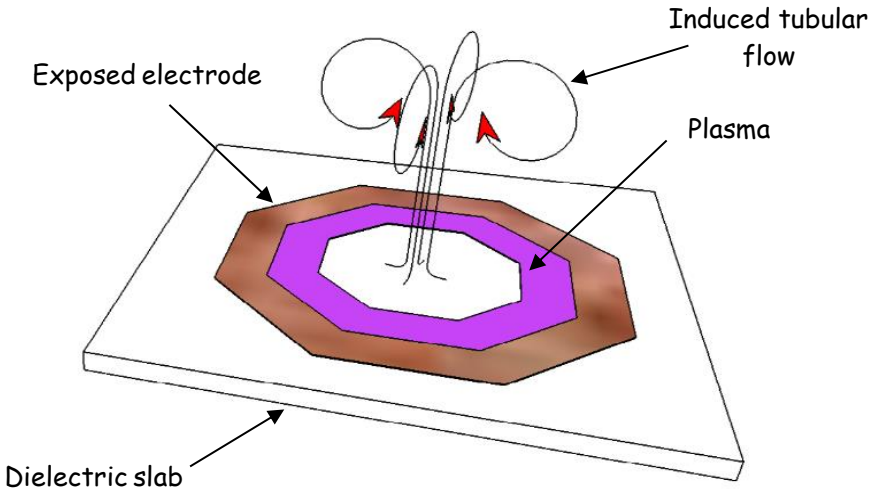

Figure 3.1 PSJA rendering [30].

3.1.1 Electrical characterization

The applied voltage frequency is fixed to 31 kHz and the peak voltage is set to 6 kV, in order to produce a homogeneous and stable discharge. These parameters lead to an average power supplying the plasma equal to 10 W. The average power is evaluated by using Lissajous figure method [50]. Power was calculated by the equation (3.1):

$$P = {}^{1}/_{T} \oint v_{out}(t)\, dq_m \qquad (3.1)$$

The integral result is the energy delivered to the discharge in a voltage period and corresponding to the area inside the voltage-charge cycle of the Lissajous graph, Figure 3.2.

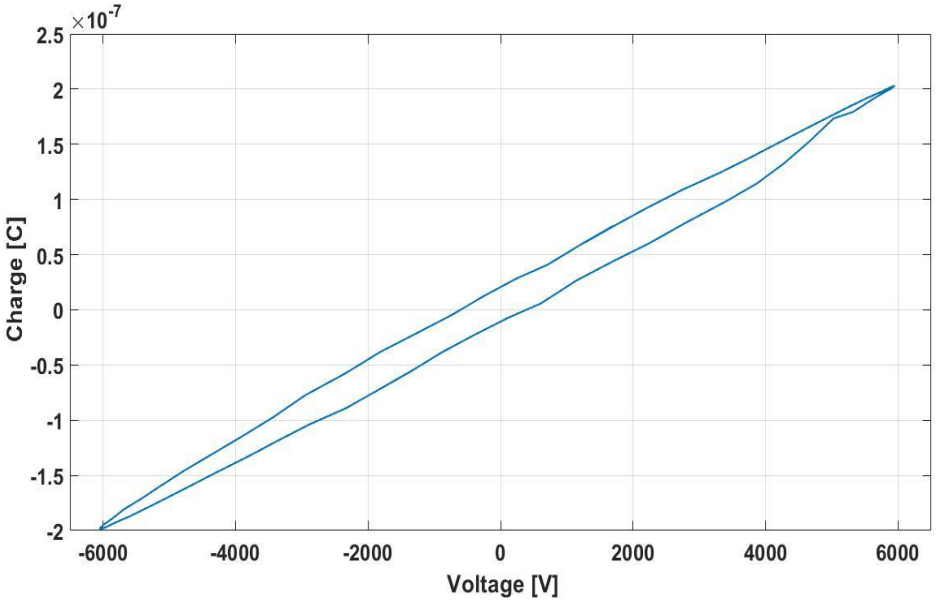

Figure 3.2 Lissajous figure.

3.1.2 Fluid-dynamics characterization

EHD effect is analysed by Schlieren Images, it is shown in the following figure. The images highlight the fluid-dynamics jets behaviour in three different plasma-on time: at the begging, after 30 ms and after 60 ms, in this way a complete picture of the development of the jets is obtained. Every side of the octagon produce a tangential jet, as illustrated in Figure 3.1. In the actuator centre, they collide and merge together, and so the normal flow is generated. At the begging of the discharge, the flow is tubular and axisymmetric for a time equal to 10 ms. The turbulences appear when the discharge time increase. After 30 ms from discharge ignition, the height of the jet is about 60 mm.

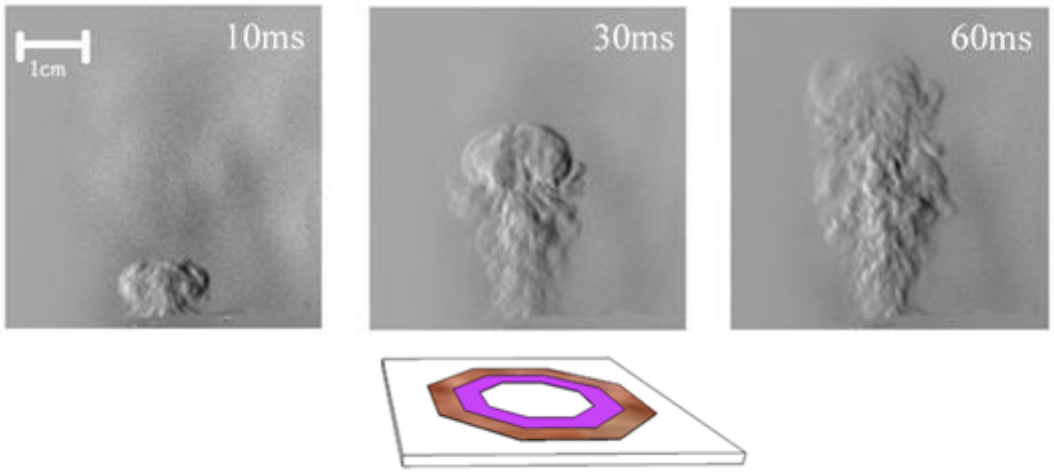

Figure 3.3 Schlieren Images of the induced jet generated by PSJA.

The normal velocity component of the induced flow (y-direction in Figure 3.4) was measured by using a Pitot tube device, placed at 5 mm from the actuator surface and moved parallel to it (x-direction in Figure 3.4). In the following figure the complete picture of the velocity profile found in the jet is shown. The maximum velocity is observed at the centre of the actuator, where the zero position is imposed.

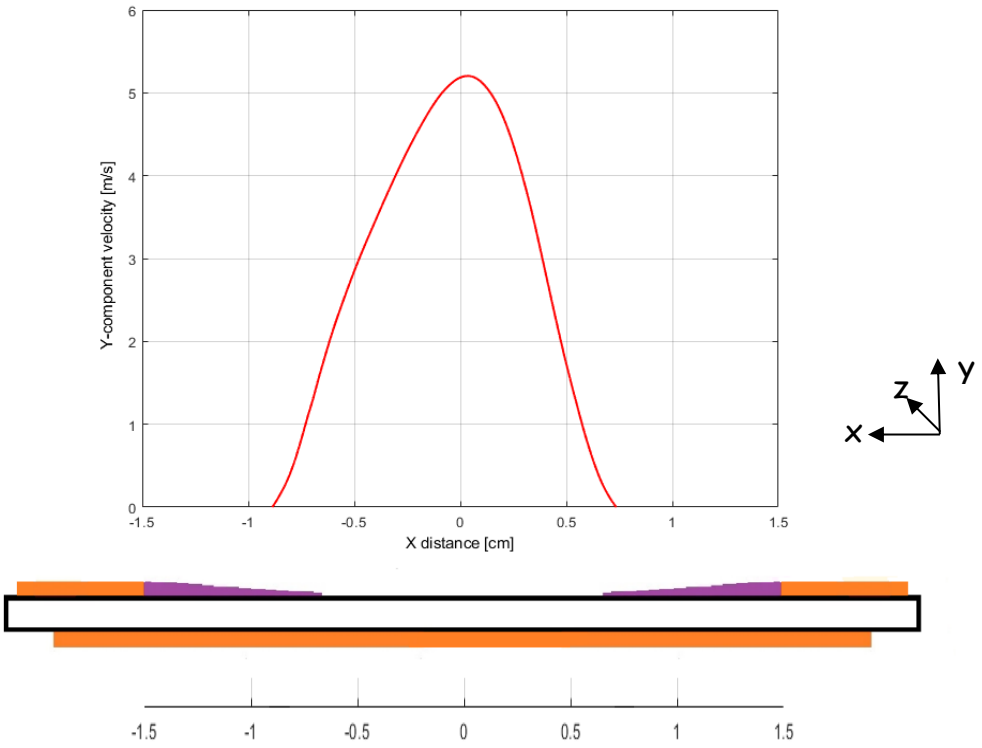

Figure 3.4 Ionic wind velocity at a distance of 5 mm from the actuator surface.

3.2 Charged particles measurement

As already mentioned in Chapter 1, this work is focused on the free particles' carriage from the actuator surface to the sample. In this paragraph, the charge flux hitting the target surface is estimated. Moreover, the potential distribution induced by charges, deposited on an insulating surface perpendicularly to the flow, is measured. In the tests, distance between the target and the actuator and plasma-on time are the two parameters varying to understand the best conditions for biological treatments.

3.2.1 Measurement set-up

The measurements were performed inside an insulating box, to maintain a constant air temperature at 25 °C with the values of humidity rate at 40% ± 5%. Controlled atmosphere was chosen due to difficult to have repeatable measurements. In fact, in the next chapter the humidity rate role is investigated. The set-up used for the surface potential distribution measurements induced by charged particles is represented below.

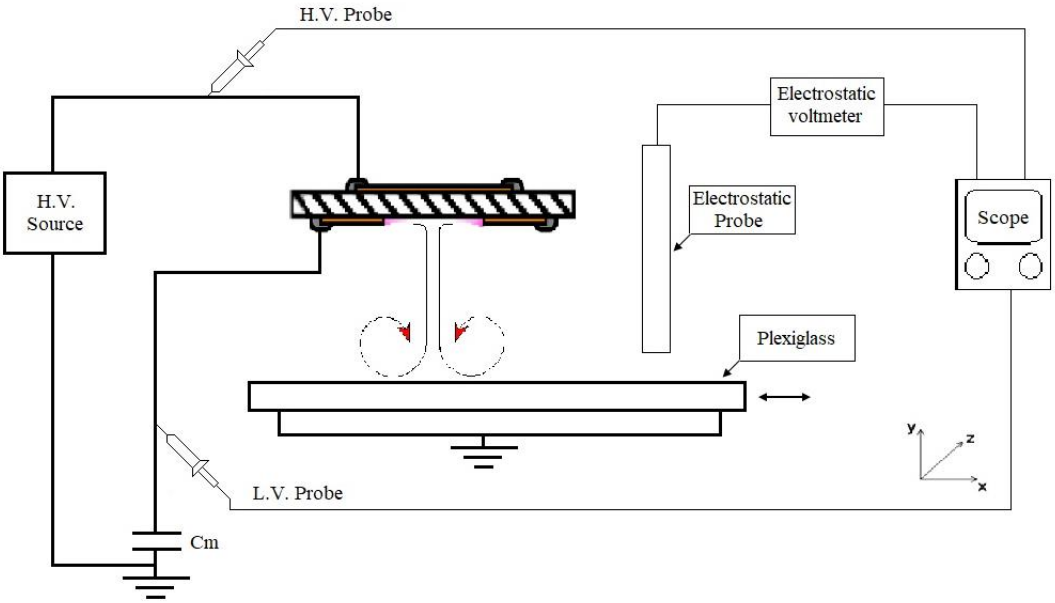

Figure 3.5 Charged particles measurement set-up [30].

The high voltage applied to the electrodes has been measured by means of a Tektronix P6015 capacitively compensated high voltage probe with a bandwidth up to 75 MHz. The voltage across the measuring capacitor C_m of 1 nF, used to evaluate the charge flowing within the discharge and the power, has been detected by a Yokogawa low voltage probe with 75 MHz bandwidth. Both signals have been acquired by a Yokogawa DL1740 4-channel, 500 MHz bandwidth, 1 GS s^{-1} oscilloscope.

The acquisition process on the scope is the same describe in Chapter 1. The discharge was ignited for time interval from 5 ms to 20 s, and, after it is switched off, the electrostatic voltage probe scanned the surface. It has been moved by means of an automated handler with a resolution of 0.1 mm. The target is in Plexiglass and under it, a copper tape was attached and grounded, to have a zero-potential reference for the probe. The actuator is placed perpendicular to the target at 1, 2 and 5 cm, and the exposed electrode is connected to the high voltage. The measurements have been repeated five times, leading to standard deviations within 5%. The experimental procedure is the same describe in [30] and it is reported below:

1. The sealed box was opened.

2. The Plexiglass surface was wiped by using a wet rag and then heated for 10 s with a hot gun to eliminate possible traces of humidity.

3. The sealed box was closed, and the electrostatic probe was moved over the Plexiglass surface, checking the presence of a zero-voltage signal. If the zero condition was not achieved, steps 1 and 2 were repeated.

4. Discharge was ignited for a defined time interval. Suddenly, after the switching off the discharge, the electrostatic probe was moved over the Plexiglass plate, in the region where the induced jet hits the surface. The induced potential signal was acquired.

The measurements have been repeated with exposed electrode connected to the ground terminal. In this case the fluid-dynamic analysis, done by the Schlieren

technique, shows that induced jet propagates faster when the exposed electrode is connected to the high voltage terminal [30]. For this reason, high voltage connection was chosen for biological treatments.

3.2.2 Results

Surface potential and charge density distributions obtained over the Plexiglass surface placed at 1, 2 and 5 cm from the actuator and for increasing switching-on time of the discharge are shown in Figure 3.6, respectively in a, b, and c. The zero 'probe position' refers to the centre of the jet over the Plexiglass surface. The switching-on time investigated are different for the three actuator positions, because by increasing the distance between actuator surface and target, charged particles needed a longer time to reach it. In all considered cases, the behaviours of surface potentials are comparable.

An M-shaped potential profile symmetric with respect to zero position is observed, up to several tens of milliseconds of discharge ignition. By leaving the discharge ignited for longer time intervals (hundreds of milliseconds), the amount of charges deposited over the surface increases, filling the inner space within the 'M' too, and creating a bell-shaped distribution.

In Figure 3.6.a, a further increase in the discharge on-time leads to a decrement in the potential distribution peak, and an increment in the potential values in the wings of the distribution, for 1 cm of distance. This behaviour can be related to additional charges, advected by the incoming flow, and it is able to push to the side of the slab the charges already deposited over the Plexiglass surface. These charges are then accumulated far away from the region, where the jet core hits the surface by the flow spreading.

A second set of measurements are performed at 2 cm from the actuator surface. The results shown in Figure 3.6.b, are comparable with the graph at 1 cm (Figure 3.6.a). Also, in this case, by increasing the plasma-on time, a transition from M-shaped to a bell-shaped distribution is obtained. Potential values are about one and half of those measured with the target at 1 cm when the distance is 5 cm (Figure

3.6.c). In this case, the longer distance and time to reach the surface allows for a portion of the charges to recombine. Potential distribution evolutions follow the same behaviour already obtained for shorter target distances.

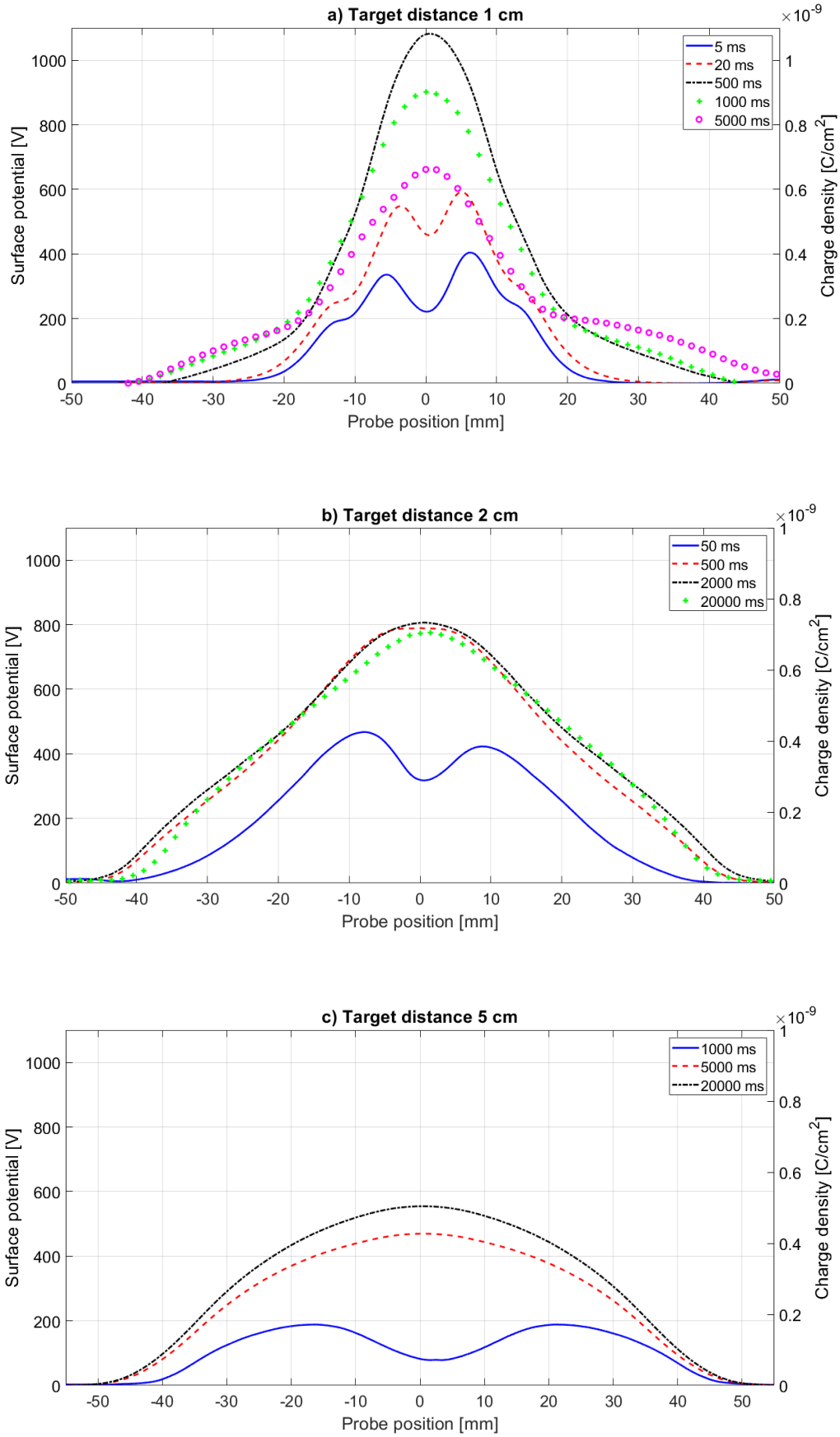

Figure 3.6 Surface potential distribution and charge density over the targate suface placed at 1, 2 and 5 cm from actuator surface, by increasing plasma on-time, [29].

The transition from M-shaped to bell-shaped distribution is related to the Schlieren Images of the induced jet impinging the target surface, by increasing plasma-on time, placed at 1 cm from the actuator surface, displayed in Figure 3.7.

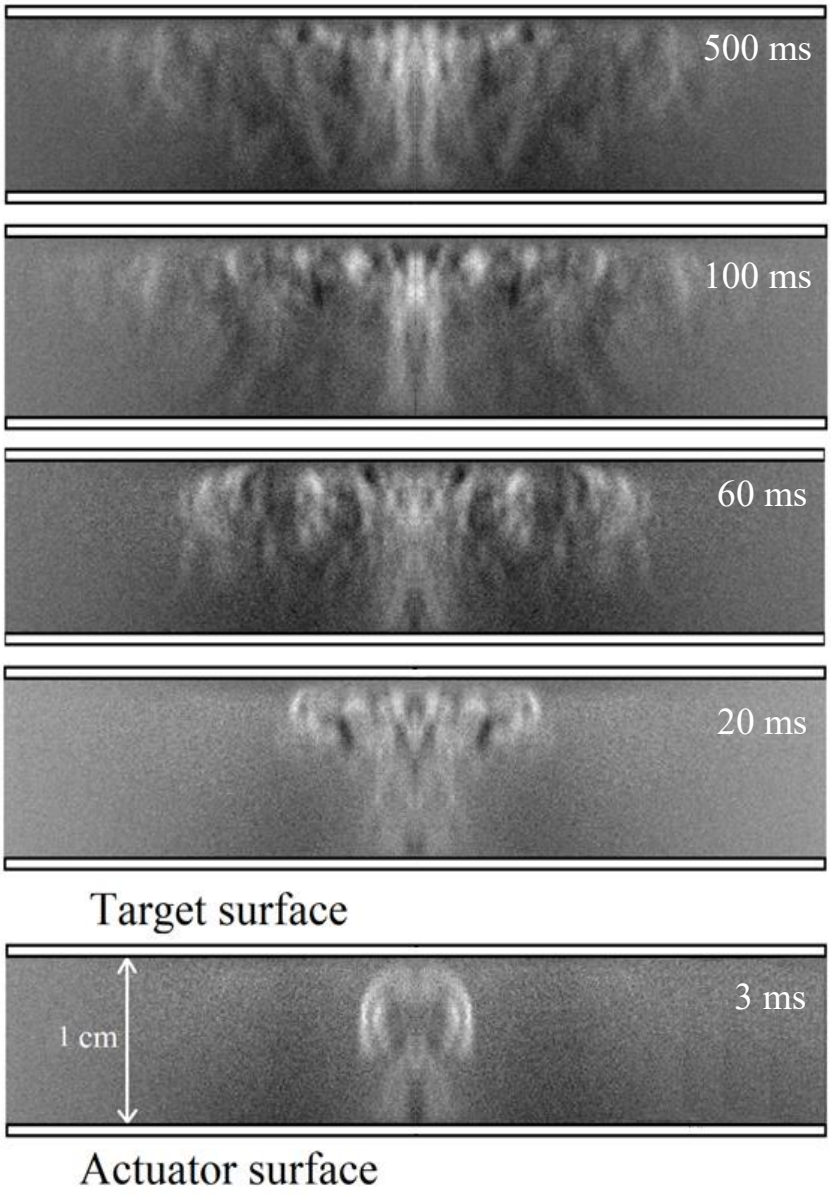

Figure 3.7 Schlieren Images of the induced jet hitting the target surface.

In the first image, at 3 ms, the jet hits the surface and after 20 ms starts to spread over it. The recirculating regions could be related to the mushroom-shaped tubular flow that is produced at the ignition of the discharge (see Figure 3.3) and subsequently hits the target surface. Despite the induced tubular jet core has a

diameter of about 1 cm, as displayed in Figure 3.3, for longer times, jets spread depositing charges on the surface for a width of about 8 cm. In fact, in Figure 3.6, the surface potential distribution covered a length of about 10 cm. The charges are carried by the flow hitting the surface and then, they are deposited on the target spreading on it.

In all graphs in Figure 3.6, the charges deposited over the Plexiglas surface always induce positive potentials. A possible candidate is H_3O^+ ion because it is quite stable at atmospheric pressure [4]. Moreover, the flux of positive particles hitting the surface is estimated:

$$\Phi^+ = \frac{Q}{\Delta t\ e}\ \left[\frac{particle}{cm^2 s}\right] \qquad (3.2)$$

where Q is the charge density obtained by surface potential measurements, Δt is the amount of time charge build-up effect takes place, and e is the charge of the electron equal to $1.6 \cdot 10^{-19}$ C. An average flux of charges Φ^+ of about 10^{11} particle/cm^{2}s was calculated, by considering the distance of 1 cm and the ignition plasma of 5 ms. Increasing plasma-on time, as mentioned above, the charged particle partially attaches to the surface and partially repel away incoming new charges, due to the electrostatic interaction. In this case, an underestimation of the charge flux would be realized.

3.3 Biological application

In the first chapter, it is mentioned the different PSJA applications. Annular geometry analysed above, was tested both in food field and in biological context.

3.3.1 PSJA against *Escherichia Coli*

Annular PSJA was used to treat *E. Coli* in saline solution, with the aim to evaluate the inactivation efficacy of indirect treatment, in collaboration with the Department of Agriculture and Food Science at the University of Bologna. The Gram-negative bacteria was chosen because it is characterised by good resistance to several chemical-physical stresses and physical treatments [51-52].

Test set-up is the same illustrated in Chapter 1, Figure 1.14, without mesh. The distance between actuator and Petri Dish is 2.8 cm. The electrical parameters are the same used in this chapter, a sinusoidal voltage of 6 kV and a frequency of 31 kHz. Different treatment time intervals are investigated: 5, 10, 15 20 and 25 minutes. The duty cycle of the discharge is 1 second on and 1 second off. In this way, the translation temperature of both discharge and dielectric surface are maintained low and the energy dose utilizes to treat the sample is lower. All tests are performed in a sealed box container.

E. Coli NCFB 555 was cultivated in Brain Heart Infusion (BHI, Oxoid, Basingstoke, Hampshire, UK) at 37 °C for 24 h. An aliquot (1.0ml) of overnight cultures (~9 log CFU/ml) was transferred into 400ml of BHI and incubated at 37 °C for 12 h. Subsequently, cells were harvested by centrifugation (5,910g for 10 min), washed twice with sterile saline solution (0.9% NaCl, w/v, Merck KGaA, Germany) and re-suspended into 400 ml of sterile saline solution. The final cell load of 8.4 ± 0.6 Log CFU/ml was obtained. At the end of each treatment microbiological analysis and the measurement of pH (pH meter BasiC 20, Crison) were carried out in triplicate [53]. Enumeration of the surviving cells was done by serially diluting 1 ml of treated samples and surface-plating the appropriate dilutions onto BHI agar plates. Plates were then incubated at 37 °C for 24 h, and colony-forming units were counted. Results are shown in the figure below. The pH

time course is highlighted by the dotted red line, while the CFU reduction is the continuous black line.

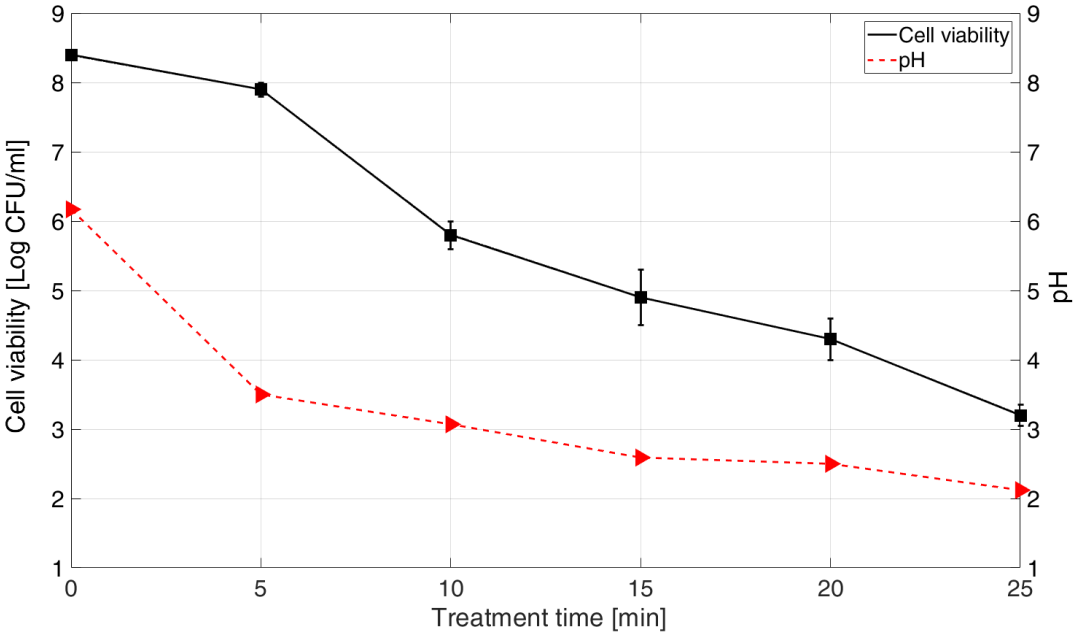

Figure 3.8 *E. Coli* CFU reduction and time course of pH.

A pH values strongly decrease from 6.3 down to 3.7 already after a treatment time of only 5 min was displayed. Weak changes were recorded prolonging the treatments up to 25 min being 2.4 the final pH value. These measurements were repeatable, in fact the error bars do not compare into the graph.

E. Coli indirect treatment highlights that a long time of treatment is more effective. In fact, a 4 log CFU/ml reduction was achieved following the 20 and 25 min of plasma discharge turned-on. The inactivation curve is not linear having an initial plateau and a tail, which indicate the presence of a portion of resistant population.

Cell viability and pH trends suggest that microbial inactivation is related not only to pH reduction, but also to additional factors, for example the accumulation of reactive species generated by the plasma treatment.

3.3.2 PSJA against microorganisms in fruit juices

Annular source was tested for inactivation of native microorganisms isolated from fresh apple juice, in plasma food field. These measurements have been done in collaboration with the Department of Chemical Science and the Department of Molecular Medicine, at University of Padova.

In this occasion, a glass material was chosen to build the dielectric of the plasma source. In a previous study glass and PVC dielectric materials were compared in term of fluid-dynamic performance and amount of charge particles advected by the flow [29]. It was demonstrated that dielectric material slightly influences these parameters. For these reasons, glass was used. Basically, it is more inert than PVC. The glass dielectric pollutes less the chemical species produced by the plasma discharge. In addition, the chemical changes of the juice composition were also investigated.

The home-made fresh apple juice was contaminated by two different native microorganisms isolated from the juice itself, named *J10* and *J11* (their characterization is in progress) with an initial concentration of 10^7 CFU. 10 mL of microbial suspensions were exposed to the plasma treatment and the same quantity was not treated. It was used as a reference to compare the effect of plasma between treated and untreated samples. Immediately after the treatment, the juice samples were collected, opportunely diluted, and plated on agar culture media. The plates were turned upside down and incubated at 37°C for 16 hours. Microbial growth was quantified by colony forming unit (CFU) enumeration. To assess the long-term antimicrobial effect of plasma treatment, aliquots of juice were stored at room temperature and at 4°C up to 4 weeks. In this way, it was possible to evaluate the fruit juice shelf life. Every 7 days, samples were aseptically taken and were appropriately diluted and sown to evaluate the effect of the plasma treatment over time. As a comparison for bacterial growth, the corresponding untreated plasma samples were sown in parallel, with the same dilution. All the analyses were performed in triplicate.

The homemade juice was extracted using a domestic juice extractor. Then the juice was centrifuged and filtered through a membrane filter Stericup Quick Release Filter Millipore Express of 0.22 μm, to remove impurities and coarse particles.

Test set-up is the same used for the previous *E. Coli* treatments. A sinusoidal voltage of 5.2 kV and a frequency of 28.4 kHz was used, with average power of 11 W. Different distance between Petri dishes and plasma actuator are analysed in term of reactive species to choose the optimum value for the treatment.

The juice chemical composition was analysed to understand if the non-thermal plasma treatment modifies the taste of the drink. The most typical juice components including polyphenols, organic acids, and sugars. Their plasma degradation was investigated by means of High-Performance Liquid Chromatography technique, HPLC/ultraviolet−visible (UV−vis). HPLC analyses were carried out with an Agilent Technologies 1260 Infinity II instrument (G7112B Binary Pump, G7129A Autosampler, G7114A VWD detector) for the organic acid. Phenomenex Kinetex column (5 μm EVO C-18 100Å, 150 mm length and 4.6 mm internal diameter) was used for the polyphenols analysed. The chemical procedure is the same used in Ref. [54].

Species produced by the plasma into water exposed to the treatment for different exposure times and different distances between the actuator and the sample, are quantified to complete the characterization of the plasma source. Hydrogen peroxide, H_2O_2, and ozone, O_3 concentrations are determined. The procedure is the same describes in [28]. The results are shown in the graphs below.

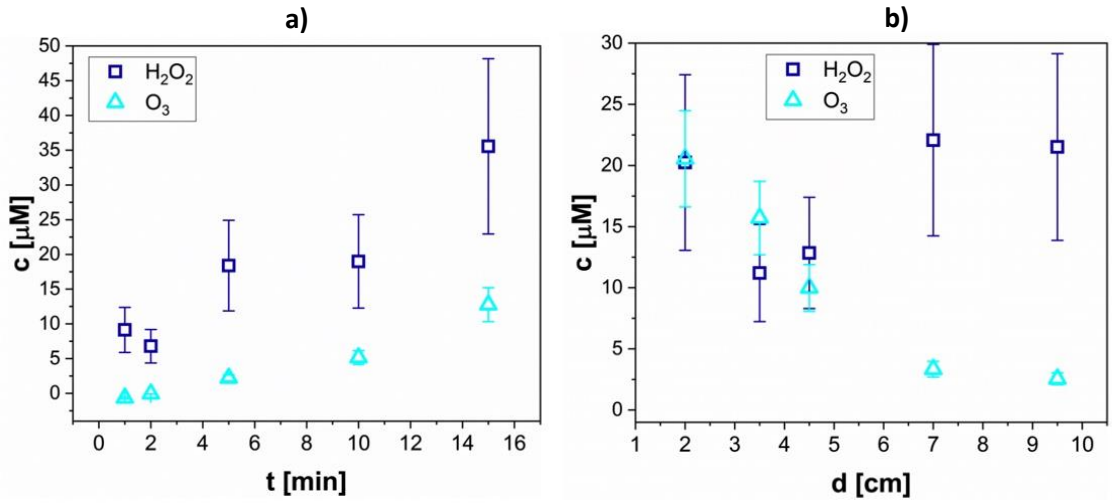

Figure 3.9 Species produced in water by plasma treatment as a function of treatment time (a) and as a function of distance sample-source (b).

In left graph (a), the distance sample-source is 4.5 cm, on the right (b) the plasma treatment time is 10 min. The ozone concentration increases with the treatment time and decreases when the distance sample-source grows. The hydrogen peroxide and ozone concentration have the same trend in both cases. After these measurements, 3.5 cm distance and a plasma on-time of 10 min was chosen for the apple juice treatments.

The juice was analysed 4 weeks and compared to the control to evaluate the answer of the treatment. The results are shown in the graphs below.

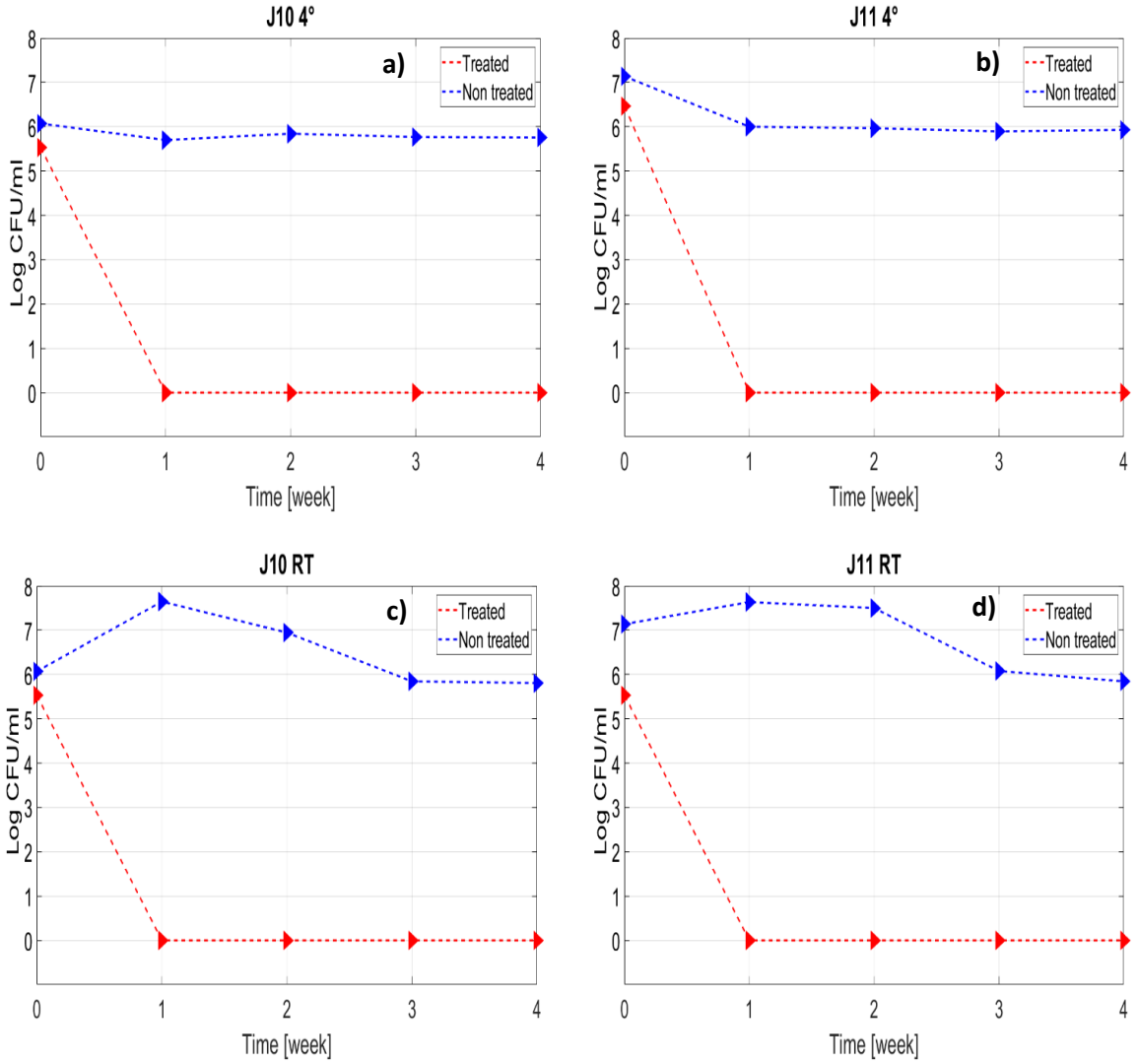

Figure 3.10 *J10* and *J11* reduction and comparison with the control sample.

In the graphs, red line refers to CFU microorganism reduction, while blue line represents the CFU in the control sample (without non-thermal plasma treatment). The juice was stored at 4°C (Figure 3.10.a and 3.10.b) and at room temperature (RT), (Figure 3.10.c and 3.10.d). Both microorganisms presented an instantaneous reduction, about 80 %, and a complete inactivation after one week from treatment. This inactivation was stable for all 4 weeks, no changes were detected. In fact, the apple juice pasteurization was obtained. The chemical analysis has been done before and after the plasma treatments. An important decrease for polyphenols was observed. About the organic acid an important change of nitric acid was identified. A probable reason of these different is the ozone produced by non-thermal plasma discharge.

The results obtained are very interesting. The indirect treatment with the annular actuator has demonstrated his efficacy in inactivation process against microorganisms. It is important to modulate in a correct way the distance between the sample and the source to sterilize the juice without compromise its chemical composition.

3.3.3 Charged particles role against *Candida Guillermondii*

After demonstrating the efficacy of actuator in disinfection field, the study was focus on charge particles inactivation role. *Candida Guillermondii* was treated as already describe in Chapter 1. In this indirect treatments, electrical parameters are the same analysed above. The distance chosen, between actuator surface and Petri dish, is 2 cm. In this way, there is enough space to interpose the metallic mesh through the induced jets by plasma discharge. The mesh is placed at 1 cm from the actuator surface, to block the charged particle, determining the influence of these in inactivation process. The set-up is the same describe in Chapter 1, section 1.4.4.

The surface potential distribution, on the Plexiglass target, with the metallic mesh, was measured by using the same procedure and set-up described in Figure 3.5. The measurements were acquired after a plasma discharge of 30 s and are shown in Figure 3.11. Red continuous line indicates the case without mesh, black dashed line is test with mesh floating and when mesh is grounded, magenta line with plus signs. Charged particles distributions are similar for both first two conditions (with and floating mesh). As a matter of fact, mesh does not drastically modify the behaviour of transported and deposited charges. It has the tendency to create an isopotential surface and it is possible to observe a more uniform charge distribution. Charge's role is negligible when the mesh is grounded. In fact, above 90% of it are drained to the ground terminal.

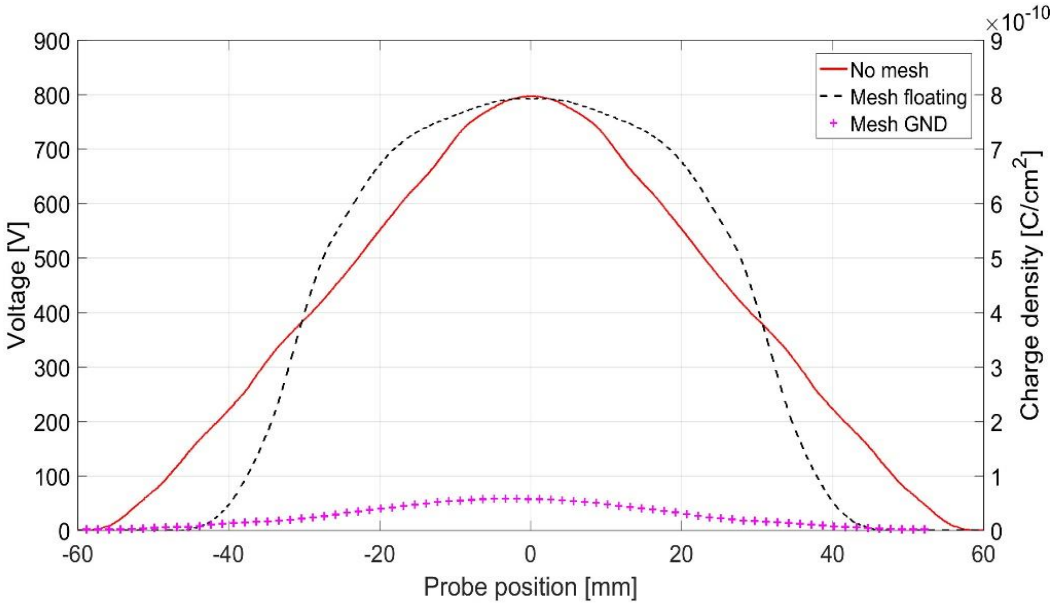

Figure 3.11 Metallic mesh role in the surface potential distribution and charged density [29].

Schlieren technique was used in order to understand in which way, the metallic mesh influences the fluid dynamics of the induced flow. In Figure 3.12, comparison of Schlieren images of the induced jets generated by plasma actuator without (Figure 3.12.a) and with (Figure 3.12.b) metallic mesh is illustrated, for an increase plasma-on time. The presence of the mesh does not influence the fluid dynamics of the flow. In fact, images are similar and only for the case of 10 ms a "comb" spreading of the jet is visible suddenly downstream the metallic grid.

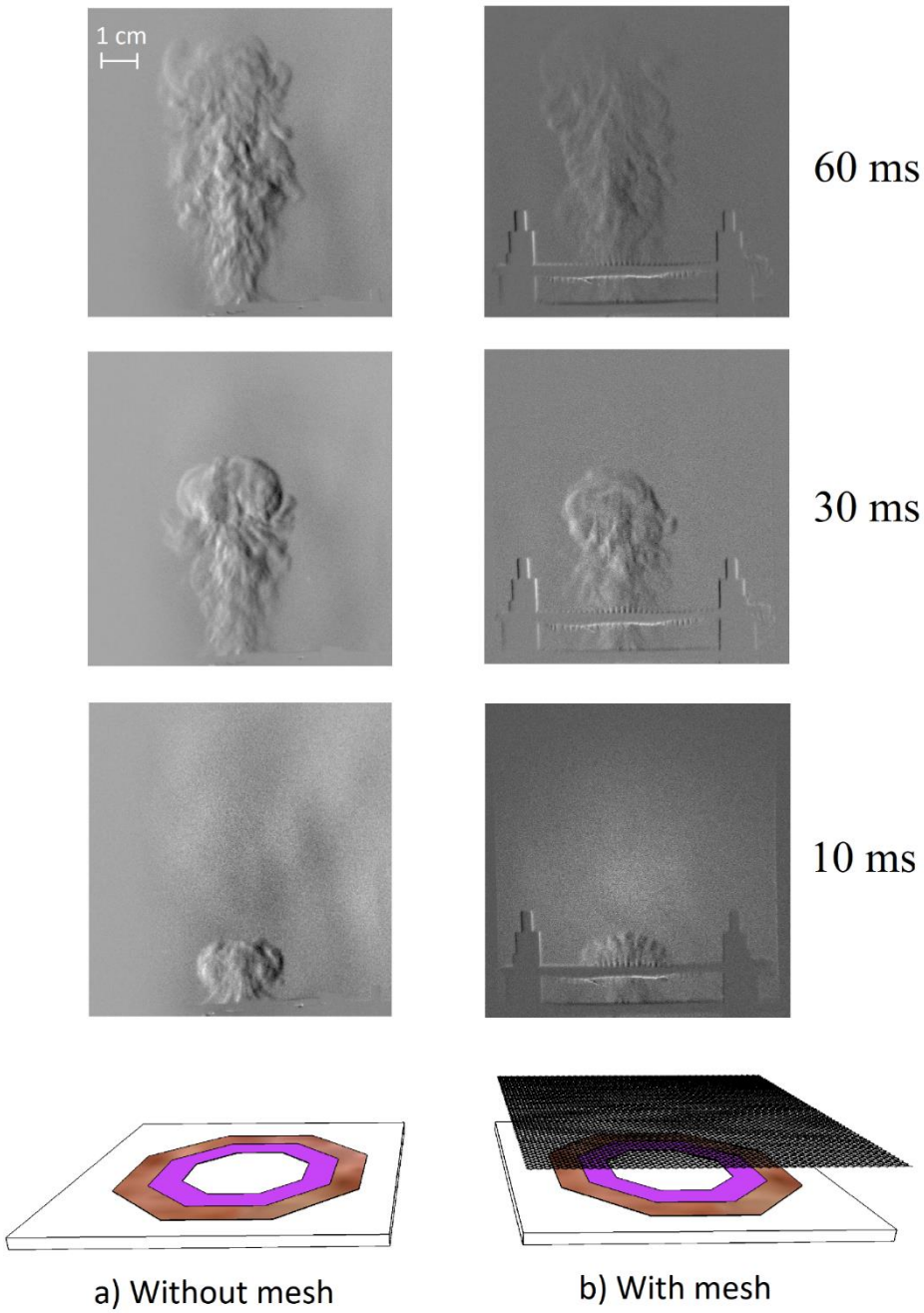

Figure 3.12 Schlieren images of the induced jets without (a) and with (b) metallic mesh for increase plasma-on time [28].

Species produced by the plasma into water exposed to the treatment have been quantified, with and without metallic mesh, to complete the characterization of the plasma source. OH radicals, ozone, hydrogen peroxide, pH and concentration of nitrate ions have been measured. No appreciable differences are highlighted with both configurations used (mesh grounded and floating).

The tests are performed with the Department of Chemical Sciences, at University of Padova, [28]. The results are showed in Figure 3.13.

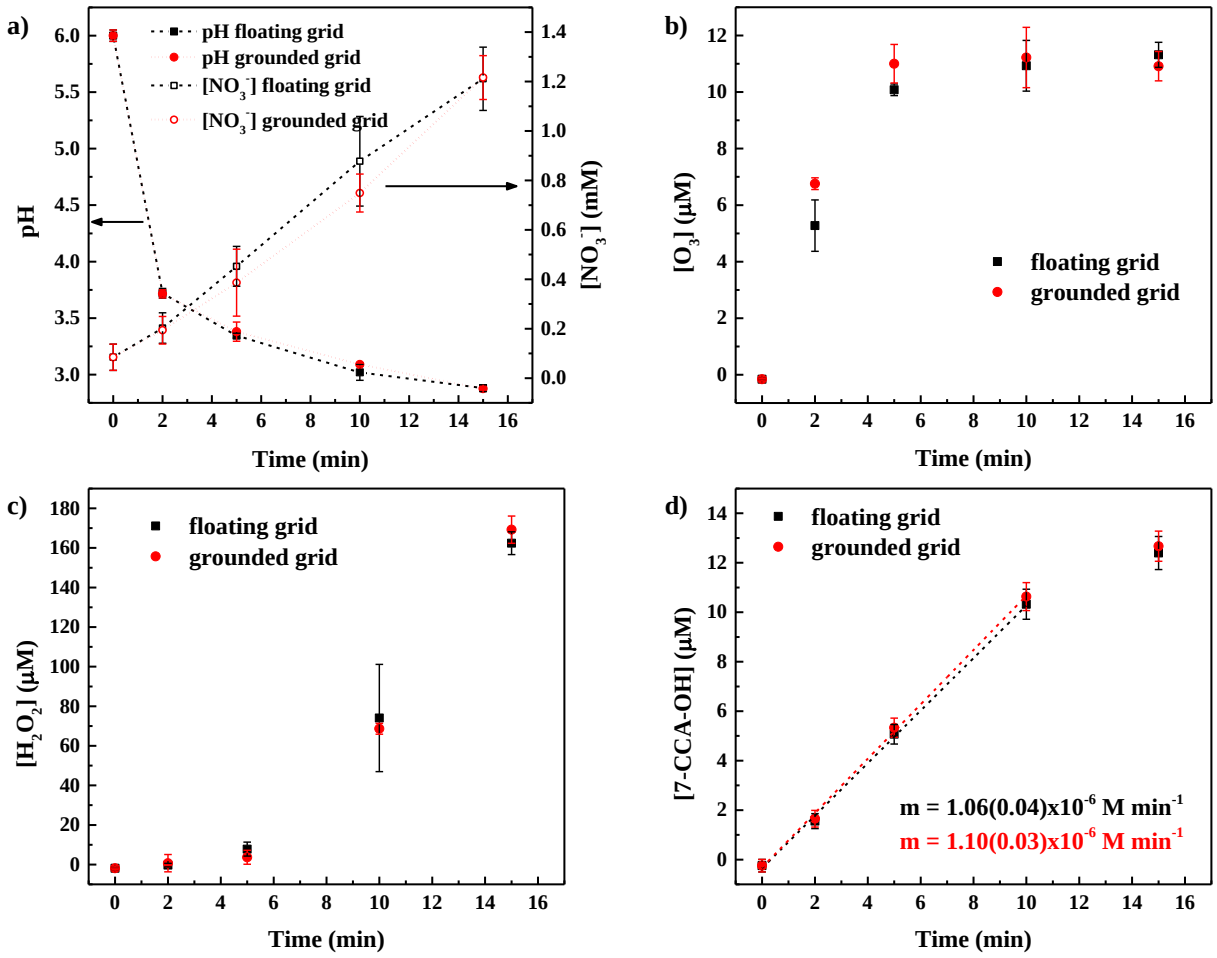

Figure 3.13 Species produced in water by plasma treatment as a function of treatment time with the metal grid floating (black points) or grounded (red points). pH and nitrate ions concentration (a); concentration of ozone in solution (b); concentration of hydrogen peroxide (c); concentration of 7-CCA-OH (in these experiments a CCA aqueous solution was used instead of pure water, see text for details) (d). The dashed lines in Fig 3.13a are just a guide for the eye; those in Fig 3.13d are the interpolation of the first 4 points using straight lines [28].

The pH of the solution drops by increasing the plasma treatment time reaching a value of about 3 after 15 minutes. The same behaviour highlights in the *E. Coli* treatment. At the same time a linear increase of nitrate ions concentration is observed, (Figure 3.13.a). H_3O^+ and of NO_3^- ions increase consistently, reaching a value of about 1.2÷1.3 mM after 15 min treatment, suggesting that both derive by the dissociation of nitric acid in solution. Ozone and hydrogen peroxide

concentration are displayed in Figure 3.13.b and 3.13.c, respectivily. Ozone increases rapidly during the first minutes of treatment, reaching a plateau value of about 11 μM. On the contrary, hydrogen peroxide concentration instead remains very low during the first five minutes of treatment and then increases rapidly following an approximately linear trend. After 15 min treatment, a measurement hydrogen peroxide concentration of about 170 μM is obtained. In Figure 13.3.d, the rate of OH formation in solution is equal to $(2.34 \pm 0.06)\cdot10^{-5}$ M min^{-1} when the metal grid was connected to ground and $(2.26 \pm 0.09)\cdot10^{-5}$ M min^{-1} when it was left at floating potential [28].

In all measurements, as already mention, any significant different, with the two metallic mesh configurations, was observed. These results suggest that, under these conditions, the main ways of formation of the species quantified do not involve the charged species present in the air plasma but only neutrals. It can be deduced that H_3O^+, which is detected in the liquid phase, is formed mainly by the dissociation in water of nitric acid formed from NOx according to reactions presented in these papers [44, 55-56]. This conclusion, which is supported by the matching concentrations of H_3O^+ and NO_3^- determined in solution, suggests that there is not major contribution due to direct transfer of H_3O^+ from the gas into the liquid phase [28]. Two option to explain the results have been hypothesised. The first not exclude, that these positive ions present in the air plasma interact directly with *Candida* cells on the surface of the medium, saline solution or Agar, without dissolving into the medium in the absence of the cells. The second, that other ionic species, or species derived by ionic reaction that have not yet been identified and quantified are involved to produce the biological effects of non-thermal plasma.

Candida Guillermondii was treated both in agar substrate and in saline solution. Petri dishes were prepared by the Department of Veterinary Medical Sciences, University of Bologna [28]. Number of Colony Forming Units of untreated suspension initial is 10^6. All tests are performed in open air at temperature of 25 °C ± 2 % and a relative humidity of 41% ± 5 %. The results are shown in Figure 3.14. All treatments have been repeated with the metal mesh left floating, (the continuous line in the figure) and grounded (the dashed line). The charged particles are free to reach the sample, in the first case, while their effect is blocked, in the second one. The Petri dishes were treated with a plasma-on time of 1, 2 and 5 minutes in agar substrate (the red line) and 5, 10 and 15 minutes in saline solution (the blue line). The plasma discharge work in discontinuous mode, 1 second on and 1 second off, the same in all treatment presented in this Chapter. In this way, the fluid dynamics of the jets can completely develop within the Petri dish, delivering reactive and charged species onto the whole surface.

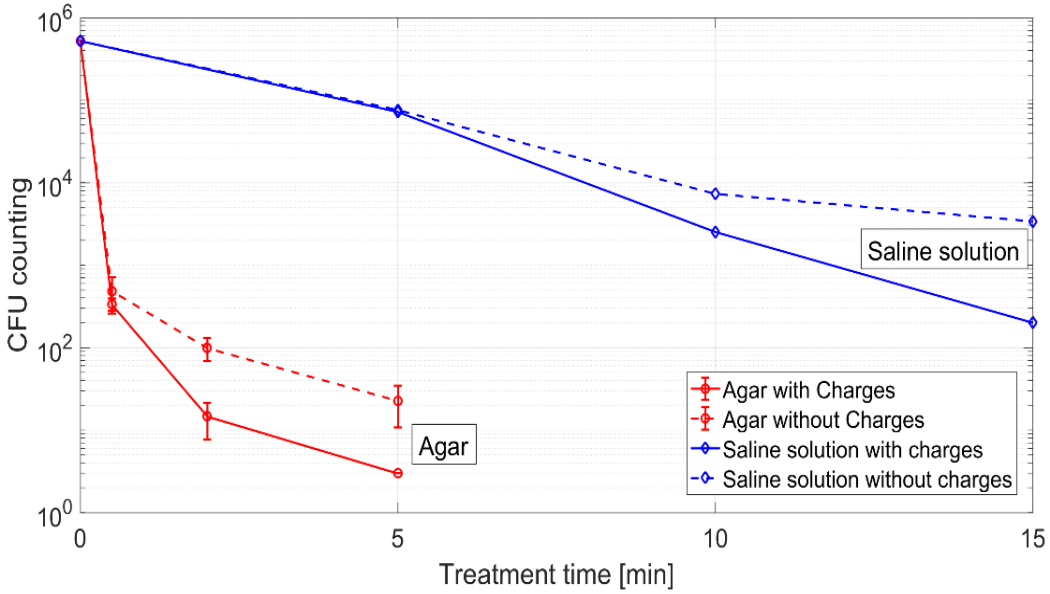

Figure 3.14 *Candida Guillermondii* CFU reduction [29].

Treatments in agar have been repeated in triplicate. Error bars underline the consistency of results. In agar substrate a complete inactivation was obtained after 5 min of treatment, with a 5-log reduction. Moreover, a log 3 decrement it is shown already after 30 s. In water, treatment times is longer, because plasma products need

more time to reach *Candida* cells. In fact, after plasma products hit the surface, they diffuse in the liquid volume and subsequently the inactivation process starts. On the contrary, in the agar substrate, the cells are in directly contact with plasma products. For this reason, a log 3 reduction has been achieved after 15 min of treatment in saline solution. An additional 1 log CFU reduction is obtained, for the longest treatment times, when the charged particles are free to reach the sample. In fact, their presence can eventually trigger chemical reactions responsible for the additional inactivation process. An important result is shown in the following figure.

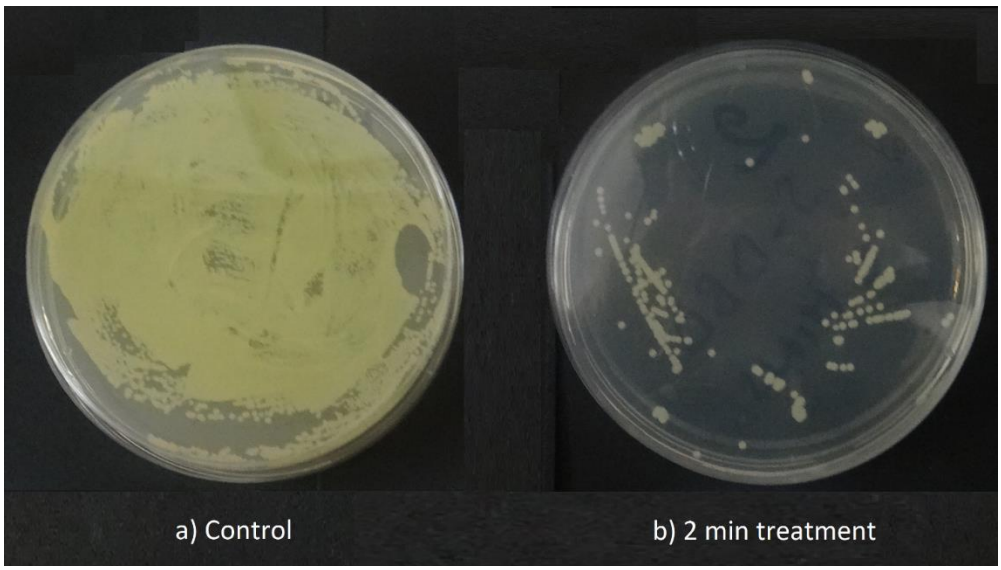

Figure 3.15 *Candida* CFU reduction in agar substrate in a control sample (a) and after 2 min of plasma treatment (b) [28].

The picture of the two Petri dishes, highlights the homogeneity of the disinfection process before (a) and after 2 min of indirect plasma treatment (b), on *Candida* cells in agar substrate. In fact, as mention above, although the induced tubular jet core has a diameter of about only 1 cm, the inactivation process covers all Petri dish surface. The tubular jet core corresponds to an area of 0.8 cm^2, on the target surface, while the Petri dish area is equal to 64 cm^2. This effect is also described by Schlieren image in Figure 3.7. The induced flow reaches the target

and then the jets spread over it for a width of about 8 cm, the Petri dish diameter is 9 cm, about the same length.

The energy dose concept has been already introduced in the previous paragraphs. In this case, it is needing an energy dose of 33 J/cm^2 to obtain a 5 log CFU reduction in Agar substrate, and therefore the complete inactivation effect. Plasma average power of 14 W was used, with 50 % duty cycle and treatment time of 5 min.

In conclusion, the results obtained show the indirect treatment PSJA efficacy combining fluid dynamics and inactivation properties of DBDs. The charged particles enhance the inactivation effect. Farther studies must be carrying out to investigate and to understand the nature and the role of free charged in interaction with biological sample. In order to increase free particles quantity, the external parameters, that could influence the discharge, have been studied. In fact, in the next chapter, the humidity rate and electric field role are presented.

Chapter 4

Humidity rate and electric field role

4.1 Humidity rate role

One of the focus of this thesis is the charged particle's role in disinfection process. In the previous chapters PSJA ability to inactivate *Candida Guillermondii* was demonstrated. An additional log 1 CFU reduction was obtained with the free particles action. Now, the effect on the discharge of humidity rate and of electric field are investigated. The main goal is to understand if these parameters can influence the charged particles production.

Experiments have been performed in a controlled environment. Insulating box was used, to maintain temperature and relative humidity level constant. The box has been described in Chapter 1, Figure 1.13. Five humidity rates (HR) values have been investigated: 5 %, 25 %, 45 %, 60 % and 80 %. As far as the results obtained at 25 %, 45 % and 60 % humidity rates were the same (within the experimental errors). Data acquired for 5 %, 45 % and 80 % tests solely will be reported and discussed. The rates of 5 % and 80 % are at extreme and opposite conditions and the rate of 45 % is intermediate and usual ambient condition (usually between 40 % and 60 %). In the box, the air temperature was maintained at 25 °C. Humidity and temperature have been measured by using two sensors controlled by an Arduino UNO microcontroller.

4.1.1 Electrical characterization

Actuator and its electrical parameters are the same describe in Chapter 3, paragraph 3.1. The discharge was ignited with a sinusoidal voltage of 6 kV peak and a frequency of 31 kHz, by increasing plasma-on time intervals from 50 ms to 20 s. Distance between actuator surface and target is the same used in biological application and equal to 20 mm. The average power supplying the discharge has been evaluated by using Lissajous figure method (see Chapter 3). The measurement has been repeated for three humidity rates investigated (5 %, 25 %, and 80 %). For all cases, the results are equal to 10 W. In fact, the voltage-charge cycle of Lissajous graph is perfectly overlapped, as shown in Figure 4.1.

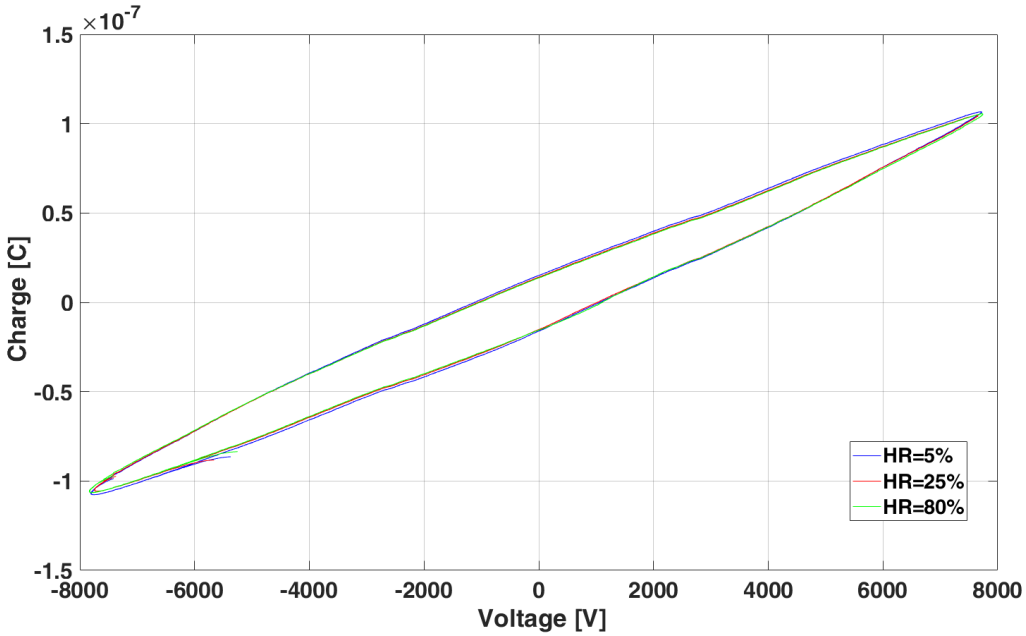

Figure 4.1 Lissajous figures with 5 %, 25 % and 80 % relative humidity [41].

4.1.2 Measurement set-up

Test set-up is shown below. The electrical devices are the same described in Chapter 3 (section 3.2.1) used for the first charged particles measurements. In this case, to vary the humidity level, a bubbling bottle was added. A portion of the synthetic air flows through the bottle filled with room temperature Demi water. The dry/damp air flow rate was controlled by a mass flow rate controller F-201CV with a flow rate of 6 l/min. Similarly, for the previous measurements, after the discharge is switched-off, the movable tray is extracted, in the z-direction (see Figure 4.2), and a scan, in the x-direction of the surface potential induced by the charge build-up, is carried out.

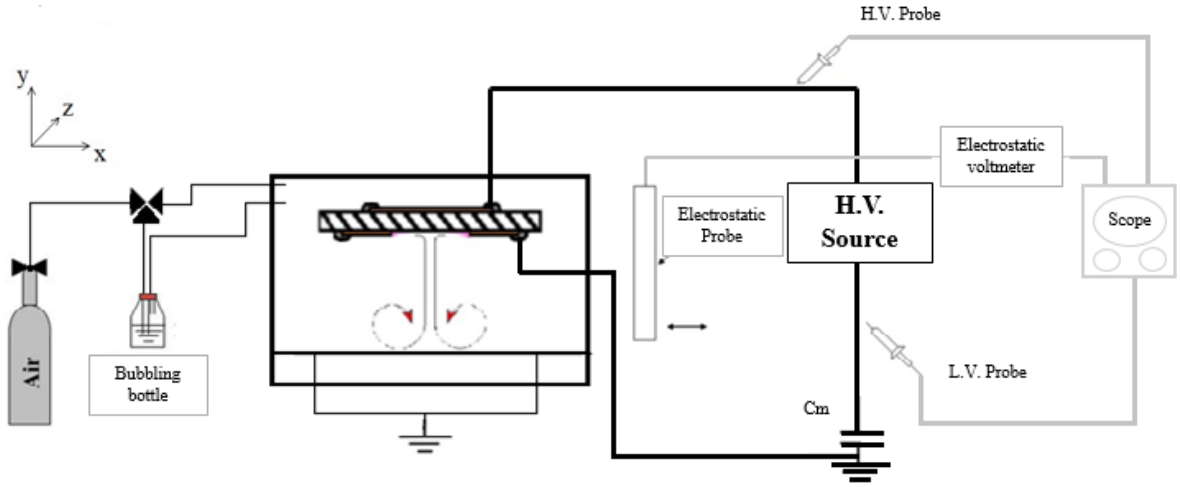

Figure 4.2 Experimental set-up [41].

The experimental procedure has been performed through the following steps (same procedure described in Ref. [40]).

1. The box is closed. The humidity is set to the selected value by using the bubbling bottle and the mass flow controller.

2. The mass flow controller is switched off and the discharge is switched on for the defined time interval.

3. The discharge is switched off, the moveable tray is opened, the electrostatic probe is moved over the Plexiglass surface (along the x-direction) in the region where the induced jet impinges the surface, and the induced potential signal is detected. The time between the two operations is only the time needed to open the movable tray, only few seconds.

4. The Plexiglass surface is wiped by using a wet cloth and then heated up for 10 s with a hot air gun to eliminate possible traces of humidity.

5. The electrostatic probe is moved back on the Plexiglass surface to make sure that a zero-voltage signal is present. When the zero-voltage condition is not achieved, steps 3 and 4 are repeated.

6. The movable tray is closed, and the set-up is ready for another test.

Steps 1 to 6 have been repeated for discharge ignition time intervals between 50 ms up to 20 s, for all humidity rates considered, with the actuator exposed electrode either connected to high voltage terminal and grounded. For each condition, five measurements have been done, reaching a standard deviation within 7 %.

In order to understand if the humidity rate could affect the recombination rate or the migration of the charged species deposited on the Plexiglass target, a preliminary test has been done. In the first case, the measurement of the surface potential distribution has been acquired with the electrostatic probe, on the movable tray open, immediately after the discharge switches-off. In the second case, the measurement has been done after 10 minutes, during which the tray has been closed in a controlled humidity environment. The test has been repeated for all humidity rates. The comparison of two results shows that, for all case, the charged particle recombination and/or migration from Plexiglass surface is slightly dependant on the humidity rate. In addition, it was observed that the charged particles remain attached to the Plexiglass target for very long-time.

4.1.3 Results

The measurements have been performed with the exposed electrode connected to the high voltage terminal and to the grounded. As already mentioned, in the case of grounded connection, the propagation velocity of the jets, and the amount of the charges deposited on the target surface are lesser than the case in which the exposed electrode is connected to high voltage terminal.

The results are shown in Figure 4.3. Zero ‘probe position’ refers to the centre of the jet over the tray, as described in Chapter 3. In the left-hand side of the graph, the exposed electrode is connected to the high voltage terminal, in the right-hand side to the ground. The measurements are acquired for four switching-on time intervals: 50 ms, 250 ms, 1 s, and 20 s, and for the three humidity rates. In all graphs, the charges deposited on the Plexiglass surface induce a positive

potential, in according with the results shown in Chapter 3. Moreover, the trend curves are similar. In fact, the potential distribution and, consequently, the amount of the charges deposited increase when the plasma-on time interval increases. In addition, the same transition from M-shaped distribution to bell-shaped is highlighted.

Apparently, the humidity rate does not significantly influence the discharge regime and therefore, the surface potential distribution. As a matter of fact, in all considered cases, similar behaviours are observed. By increasing the humidity rate, a charge build-up phenomenon takes place in a longer time, leading to about a 15 % decrement of the induced potential for long plasma-on intervals. When humidity level increases, the plasma kinetics within the jet varies and so, the charged particles density and their deposition velocity decrease. The potential measured, in zero-position, has been of 800 V for a humidity rate of 5 % and 700 V, for a humidity rate of 80 %. Similar results have been obtained when the exposed electrode has been connected to the ground terminal. Main differences are related with the lower values of the potential reached at 20 s and the longer times needed to transform the M-shaped potential distribution into the bell-shaped one. This indicates that, when the exposed electrode is connected to the high voltage, the jet propagates in a faster way with respect the one generated when the grounded electrode is exposed.

Potential bell-shaped distribution is large with wings which do not reach the zero-value on the tray surface, for long plasma on time intervals. The reason is in the small dimensions of the box utilized in these measurements. In fact, for long plasma ignition time intervals, the charged particles are transported and accumulated inside the Plexiglass tray. Therefore, the potential induced in the wings of the bell-shaped distribution increases. In this case, the PVC cubic airtight box has a 15 cm long edge. This dimension has been chosen to have a small control volume to guarantee quick humidity conditions before each test.

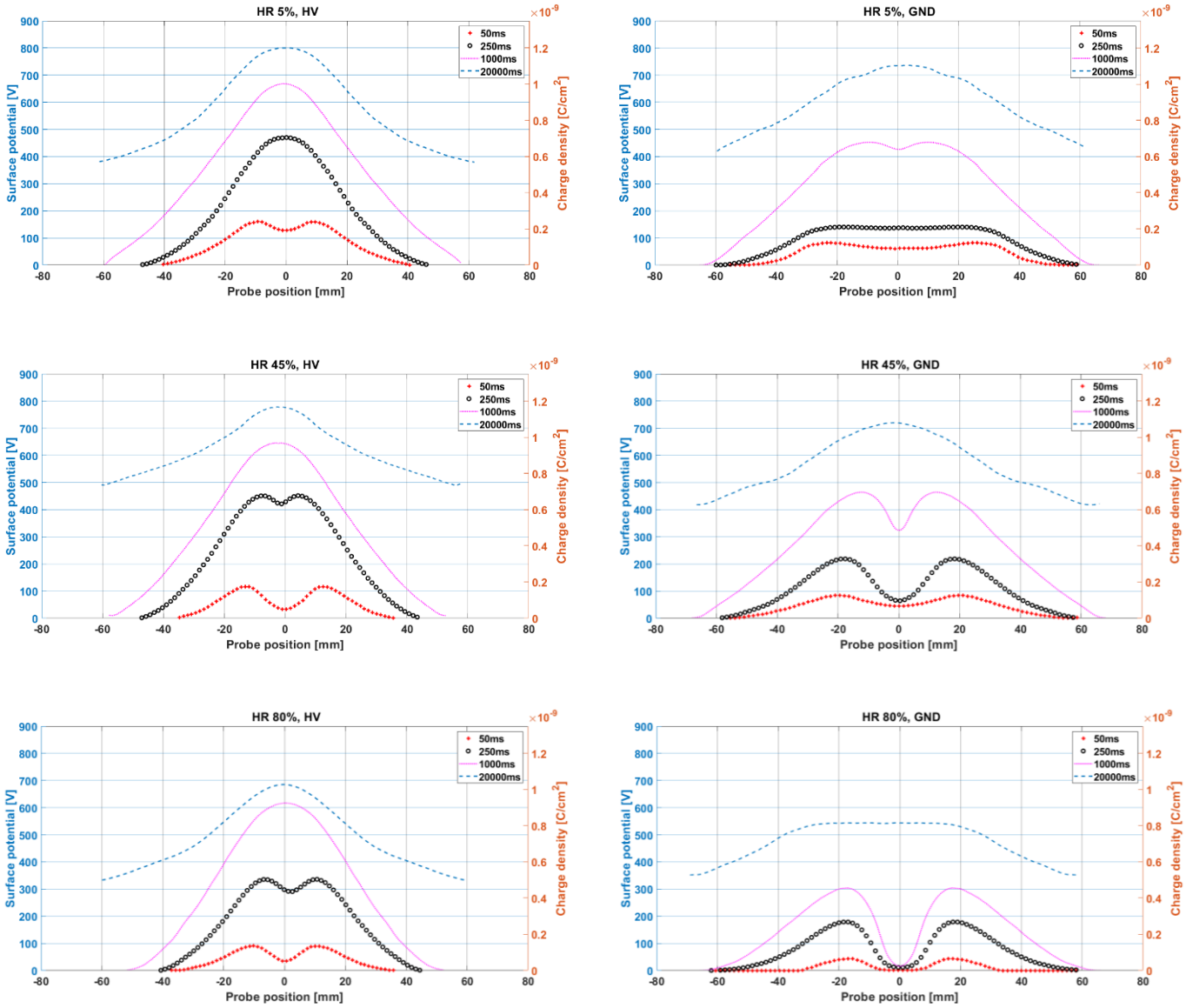

Figure 4.3 Surface potential distribution measured by increasing plasma-on time and under different humidity conditions. On the left-hand side, exposed electrode is connected to high voltage and on the right-hand side to the grounded. [40]

In Figure 4.4, the maximum value of the potential distribution as a function of discharge on-time are shown. In this way, deposition rate of the charges on the plate can be evaluate. In Figure 4.4.a the exposed electrode is connected to the high voltage terminal, in Figure 4.4.b to the grounded. For M-shaped graphs (see Figure 4.3) the maximum value has been evaluated as the average between the maximum and the value measured at the centre of the M-shape.

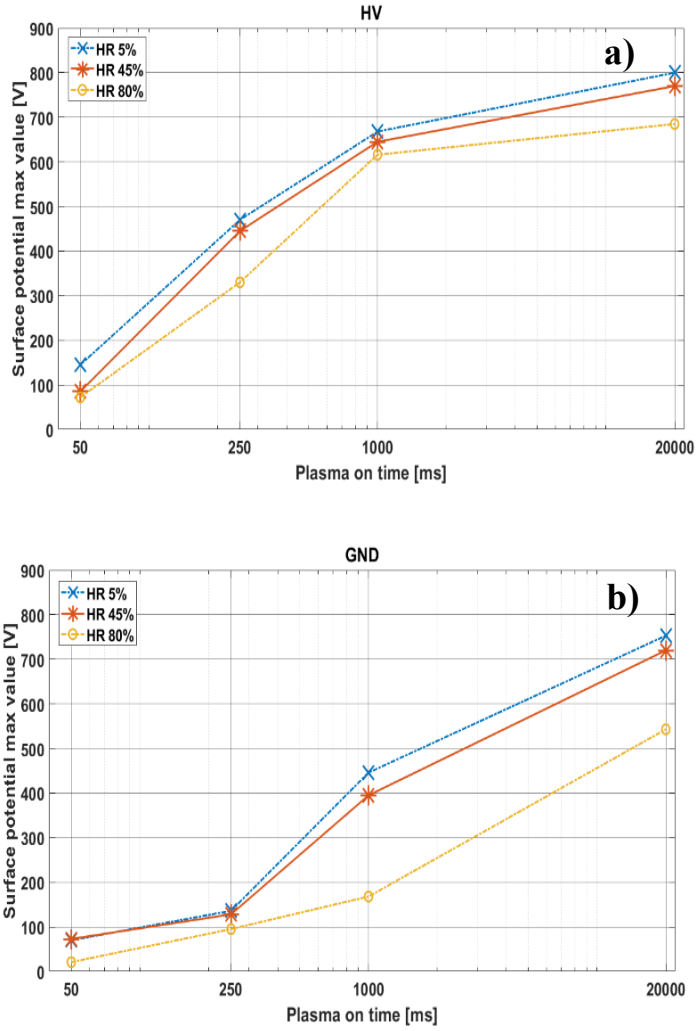

Figure 4.4 Surface potential maximum value by increasing plasma on time, for different humidity level. Exposed electrode is connected to the high voltage (a) and to the grounded (b) [40].

Graph comparison clearly illustrates that the charges deposition is faster in the first case (Figure 4.4.a) when the exposed electrode is connected to the high voltage. In fact, up to 1 s of the discharge-on time intervals, the curve trend is exponential and for a longer time a saturation is observed. On the contrary, when the exposed electrode is grounded, it needs more time to start to deposit charges, and the saturation effect is not detectable.

Induced potential values are about 50 % lower, for 80 % humidity rate, with respect the lowest humidity rate (5 %) for the discharge on-time of 50 ms. By increasing plasma on-time, this difference decreases and reaching the value of 15 % after 20 s. In both configurations, the results obtained in ambient condition (the orange lines in Fig. 4.4) with HR equal to 45 %, are very close to the measurement at lowest humidity (the blue lines) with HR equal to 5 %. In addition, the maximum values of the two curves are greater than the values obtained under 80 % of humidity rate. This result suggests that ambient condition is already an optimized working environment. A high number of free charges are deposited by the PSJA without the need of a controlled atmosphere. For this reason, it is possible to considerate this device cheap and applicable for the disinfection purpose.

4.2 Electric field role

Electric field is another possible parameter that could influence the discharge and charged particles production. A second series of experiments has been performed supplying the actuator with a sinusoidal voltage of 12 kV and a frequency of 4.2 kHz, at the same power feeding the discharge and consequently the same induced flow. The results shown that the number of charges deposited on the target is about four times than the first measurements, when the PSJA is supplied by 6 kV at 31 kHz.

4.2.1 Electrical characterization

In this test, a different supply system has been utilized. It is constituted by a signal generator, a power amplifier and step-up transformer, as described in [57]. The signal generator (HP-Agilent 33120-A) produces a low-voltage AC signal with a frequency of 4.2 kHz that is delivered to the amplifier (Elgar Model 3001 AC). It allows to change the frequency in the range of 4 – 15 kHz. A high voltage ferrite transformer is then used to reach the desired output high voltage. The power supply has been set at 12 kV peak sinusoidal output voltage, with an average power of 10 W, which is the same value used in the previous tests. In this way, the EHD effect is the same. The electric field distribution on the actuator surface for both power supply systems is reported below. It has been carried out by using FEMM Software [58], avoiding the presence of both discharge and free charges. The input of the simulation is the voltage applied to the electrode: 6 kV and 12 kV. The value of the electric field for the voltage of 12 kV is about twice of the value obtained at a voltage of 6 kV.

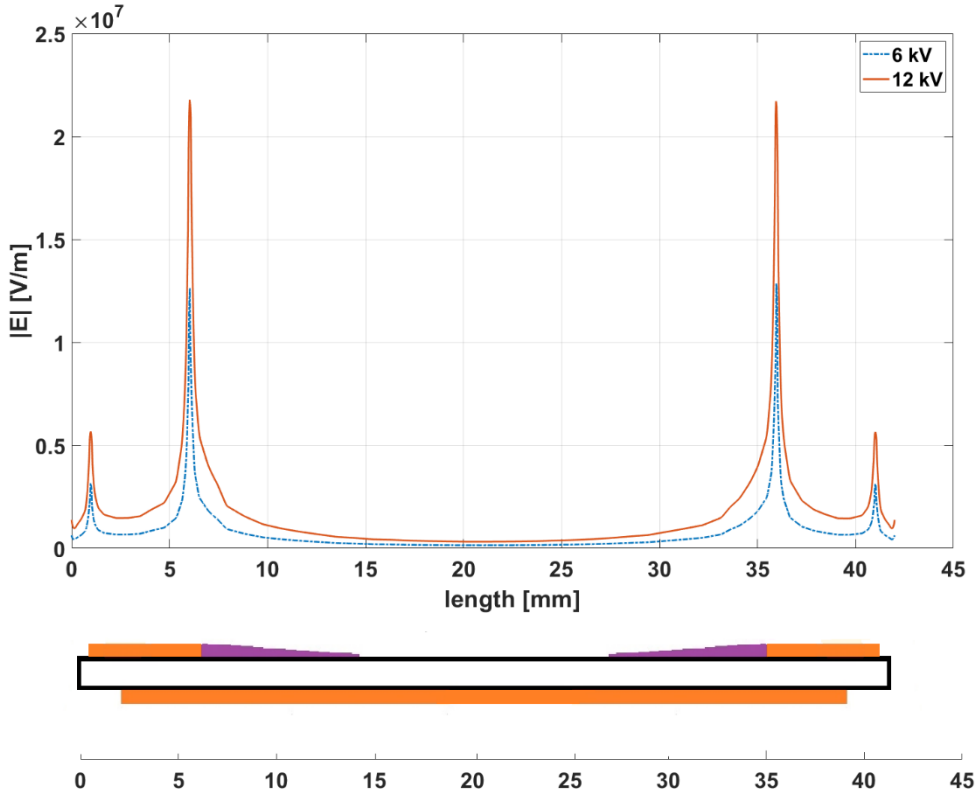

Figure 4.5 Electric field simulation results for the two power supplies system [40].

4.2.2 Results

The tests were performed with the same procedure describe in Paragraph 4.1.2. In this case, tests have been done with the exposed electrode connected only to the high voltage terminal and for the humidity rate of 45 %, due to the difficult measurements repeat. In fact, the previous results shown that the ambient condition is already an optimized working environment. The discharge-on times investigate are: 50 ms, 250 ms, 1000 ms and 20000 ms. In Figure 4.6, the results show that after 50 ms the amount of deposited charges is about four times than the measurement with a voltage of 6 kV. In all case, the surface potential distribution appears to be bell-shaped, and after 20 seconds it reaches a value 18 % higher than the first test (see Figure 4.3).

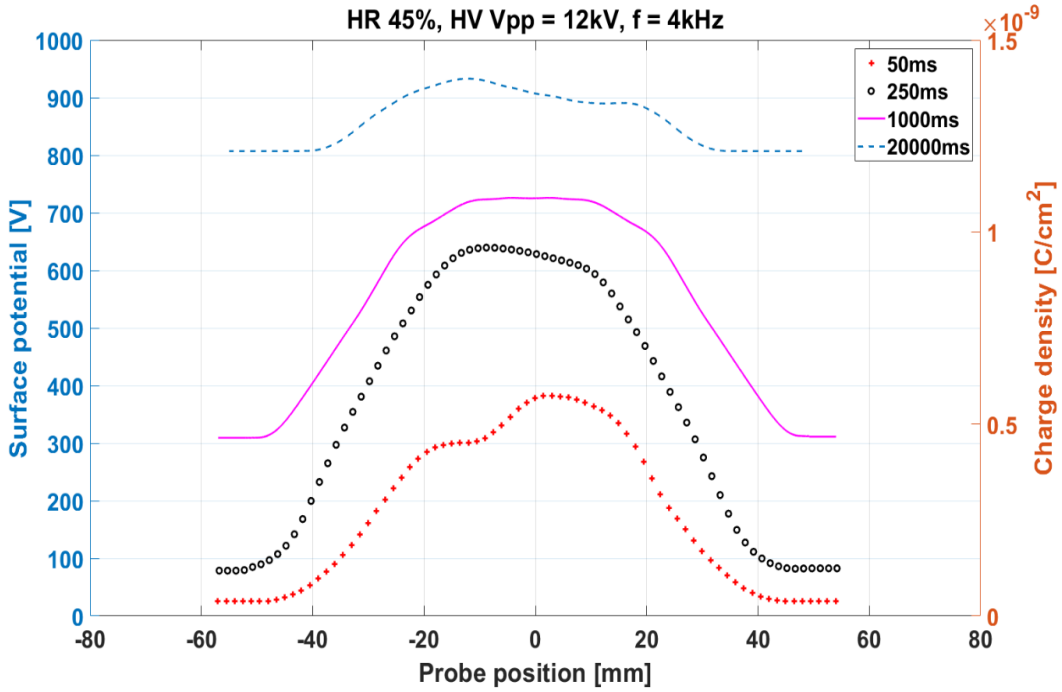

Figure 4.6 Surface potential distribution obtained with a voltage of 12 kV, a frequency of 4 kHz, at a humidity rate of 45% and for four discharge-on time intervals [41].

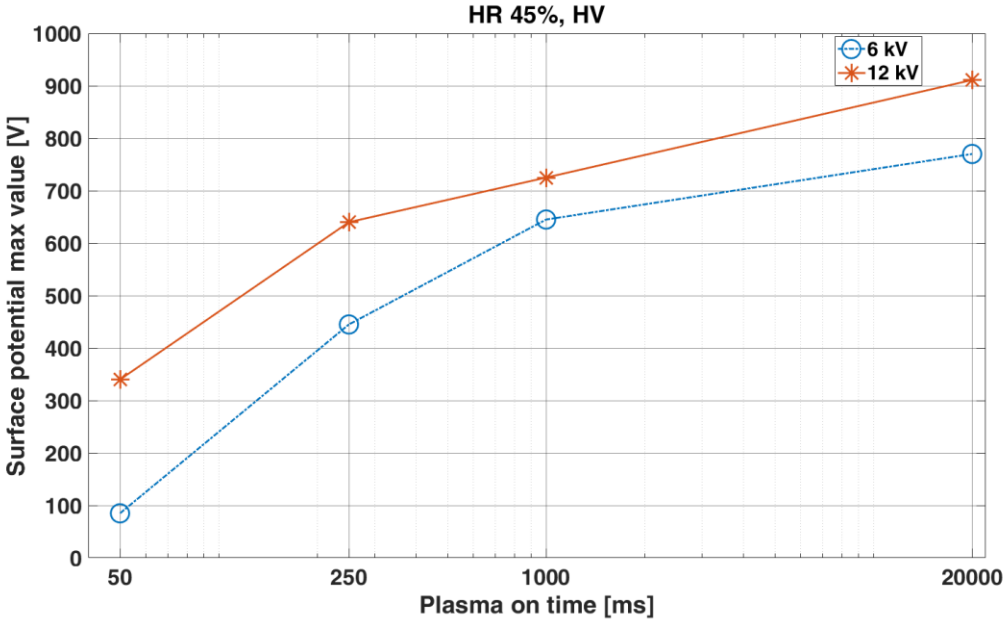

Figure 4.7 Surface potential values induced by the two power supply systems, as a function of plasma-on time [40].

In Figure 4.7, the maximum values of the potential distribution as a function of the discharge are comparison for the two power supply systems. The

humidity rate is 45 % and the exposed electrode is connected to the high voltage terminal.

In the graph it is easy to note that after 50 ms of plasma-on time, the potential maximum value induced by the high voltage of 12 kV (red line) is about four times larger than the one obtained by the high voltage of 6 kV (blue line). When the discharge-on time increases, the charges are driven forward and are accumulated on the lateral area of the surface. In this way, they increase the surface potential of wings of the bell-shaped distribution. This is clear in Figure 4.6, with the magenta and blue lines that represent the surface potential distributions acquired after 1 second and 20 seconds of plasma-on. As a matter of fact, a considerable amount of charge deposition in the first tens of milliseconds, limits a further significant increase of the surface deposition in front of the actuator. Already at 250 ms, charges are attached onto side walls and preventing the potential distribution wings to reach the zero value. This behaviour is shown by the charge distribution of long discharge-on time intervals (20 s). It is almost flat and indicating that many charged particles reach the box walls.

In conclusion, electric field can influence the amount of deposited charges transported by a PSJA. Basically, when the electric field is double the charged particles deposited on the target surface increase of 300 % respect the first electric field condition, after a discharge time of 50 ms, with the same power discharge and EHD effect. On the contrary, the humidity rate not significantly influence the discharge regime. This could lead to an increase of biocidal effects in ambient air of this device without increasing its power consumption, and thus, increasing both efficacy and efficiency.

Actuator dielectric layer, its material and thickness, and electrode geometry are others possible parameters could be influencing the amount of charge deposited on the target surface. For this purpose, in the next Chapter, a new linear actuator is characterized and it is compared with the performance of annular PSJA.

Chapter 5

Linear PSJA

5.1 Linear PSJA characterization

In previous Chapters, several parameters influencing charged particles production in PSJA discharge, are investigated. In the present analyse, a linear actuator geometry with different dielectric slabs has been utilized. After their electrical characterization, both linear actuators performances in charge delivery efficacy were compared respect to the annular PSJA, analysed in Chapter 3. In this way, the better geometry able to maximize delivered free charges, for biological applications can be chosen.

The linear geometry consists of an asymmetric electrode pair, separated by a dielectric slab. The electrodes are made in copper tape with a thickness of 35 μm with a width of 5 mm for High Voltage (HV) and 12 mm for Ground (GND) (see following figure). The length of both in the z-direction is 50 mm. Two different dielectric thickness are used: 2 mm for PVC and 6 mm for Teflon, to produce a homogenous discharge. In this way, the length of plasma discharge, P-quotation in Figure 5.1, is 5 mm for the actuator made in PVC and 8 mm for the other one. The distance from the end of the plasma discharge and the end of the dielectric slab is 10 mm for both actuators. Teflon material was utilized instead of PVC, because the former is less sensitive to heat problems arising when a stronger surface discharge is ignited.

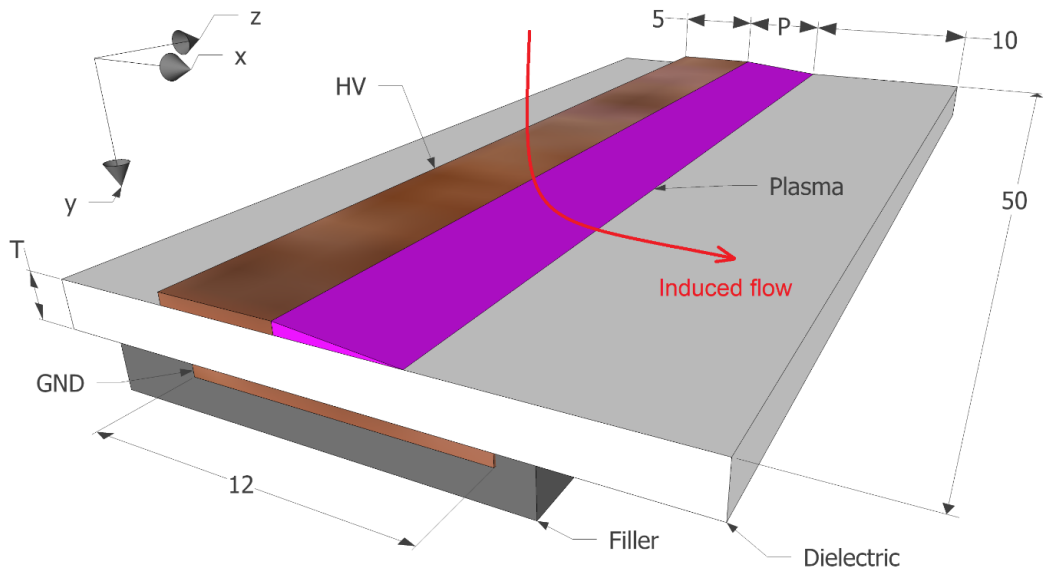

Figure 5.1 Linear actuator sketch [59].

In the following, to simplify the reading, PVC linear actuator will be called Actuator 1, Teflon linear actuator will be designated as Actuator 2 and Actuator 3 is the annular PSJA.

5.1.1 Electrical characterization

Power supply is the same used in Chapter 3. In this case, for Actuator 1 and 3, a sinusoidal voltage of 8 kV peak with a frequency of 27 kHz was chosen, despite in previous Chapter the couple voltage-frequency has a different value. These new parameters were used because it guarantees a stable, strong and homogeneous plasma fulfilling impedance matching requirements between voltage generator and DBD load. It has been verified that for Actuator 3, the PVC annular actuator, plasma appearance, average power, induced jet, and transported charges are the same already analysed in the previous Chapter. This is ascribable to similar plasma behaviour because of the same average power supplying the discharge. In this way, a first comparison is possible, to verify the influence of the actuator geometry respect the charged particles production, without changing the supply quantities. A sinusoidal voltage of 14 kV peak with a frequency of 36 kHz was used to supply Actuator 2, in order to produce a homogeneous and stable discharge. The change of supply voltage and frequency is due to dielectric thickness. In fact, it has been used to increase the plasma extension, induced jet velocity, and charge particles' amount. As reported in Chapter 4, an increment of the applied voltage increases the amount of charge particles deposited onto the target surface. The average power has been evaluated by using Lissajous figures [50]. The value is 6.8 W for Actuator 1 and 18 W for Actuator 2, with a standard deviation error of 6%.

5.1.2 Fluid-dynamics characterization

In linear actuators, induced jet propagates tangentially onto reactor surface. The flow, due to the EHD interaction, is induced in the positive x-direction (see Figure 5.1) and hitting the target, placed perpendicular to the jet. In this way, the merging of the tangential jets occurring in the annular PSJA configuration is avoided, and the recombination of the charged particles produced in the plasma is reduced. The fluid-dynamic behaviour of both Actuators, 1 and 2, was firstly

analysed by means of Schlieren technique, to understand in which way, the dielectric thickness influences the ionic wind production. The speed of the induced wind was, subsequently, measured by using Pitot tube device.

Schlieren images were acquired after increasing time intervals from discharge ignition, after 10 ms, 30 ms, 50 ms and in steady state operation (Figure 5.2).

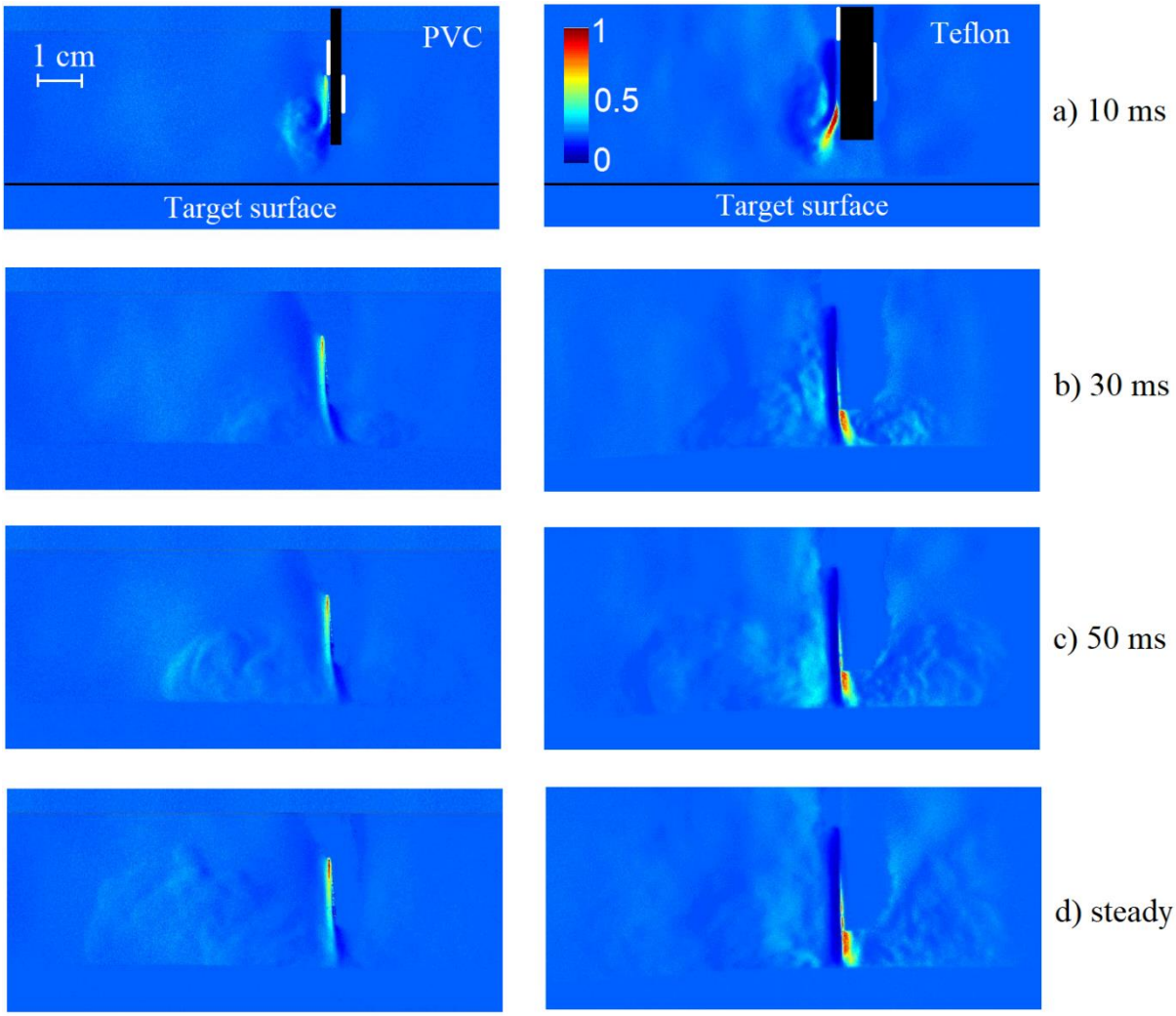

Figure 5.2. Schlieren images of induced jets generated by Actuator 1 (on the left), and Actuator 2 (on the right) after 10, 30, 50 ms from discharge ignition and in steady state operation [59].

In Figure 5.2, Actuator 1 behaviour is reported in the left-hand side, while in the right-hand Actuator 2 is displayed. In first images, linear actuators are

presented in a black rectangle, and the two copper electrodes in white. A colormap representing the light intensity in per unit is highlighted. The distance between the actuator and the target surface is 1 cm, and 2 cm from the end of the plasma discharge, the same distance used by Actuator 3, in Chapter 3, for biological treatments.

The figure highlights that Actuator 2 generates a faster jet. In fact, it shows a wider spreading region of the jet onto target surface. Both actuators produce quite similar induced jets. A curl propagating in the x-direction (see Figure 5.1) occurs after 15 ms. The jets hit the target surface and starts to spread over its, after 30 ms. In addition, the induced jet does not spread in a symmetric way with respect the y-direction (Figure 5.1). The jet propagation is enhanced in front of the HV electrode, on the side of the negative y-direction, then on the one of the positive y-direction.

Pitot tube measurements confirm the higher velocities of the jets induced by Actuator 2. The velocity profiles were measured along the x-direction (Figure 5.1) by means of a glass Pitot tube moved by a step motor with a linear resolution of 0.03 mm. The Pitot tube (outer diameter of 1 mm) was connected to a DCAL401 Sursense ultra-low pressure sensor with a 32 mV/Pa resolution. The measurements were averaged over five different tests, leading to a standard deviation error of 5 %. The velocities are measured in three different points: the zero position (x=0) corresponds to the end of the plasma discharge. The second point (x=1 cm) is immediately beyond the actuator's edge. The last one (x=2 cm) is the same distance used in all tests, equal to 1 cm from the actuator and thus 2 cm from the end of the plasma discharge.

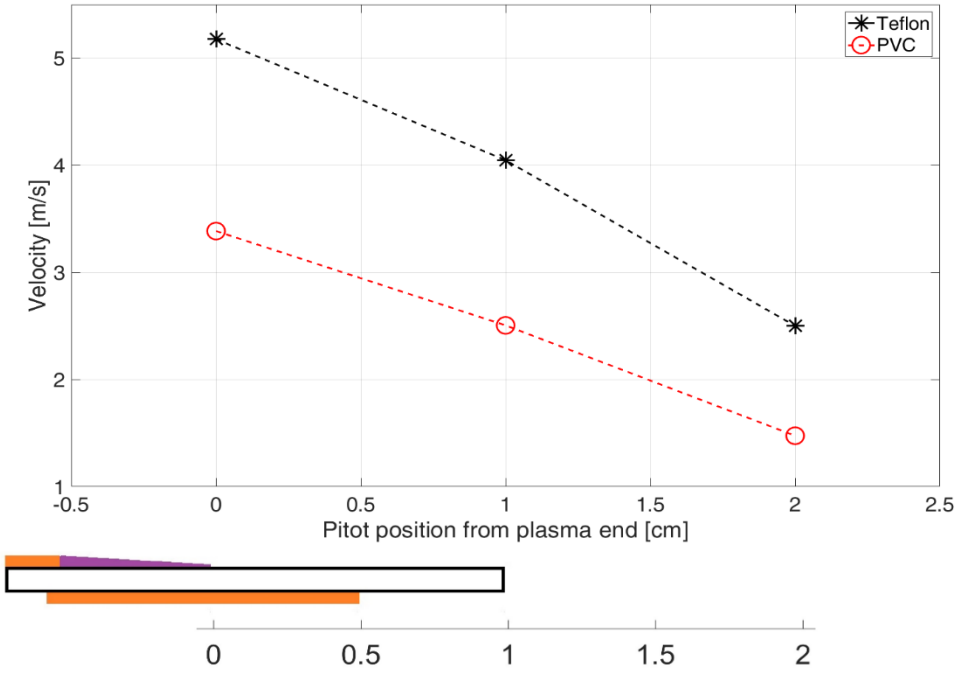

Figure 5.3 Ionic wind velocity at distance of 0, 1, and 2 cm from the end of the plasma discharge for Actuator 1 (black) and Actuator 2 (red).

The graph shows that Actuator 2 (black starts), produces an ionic wind velocity about of 50 % higher than Actuator 1 (red circles). This increment in induced speed is accompanied to a higher average power consumption, generated by this actuator. In addition, this higher velocity is related to the longer plasma extension (x-direction in Figure 5.1), obtained by increasing the applied voltage.

The velocities profile for all actuators, at 2 cm from the end of the plasma discharge, were acquired. The velocity map in the cross-section of the jet is displayed in the figure below. As already mentioned in previous Chapter, Actuator 3 produces a tubular induced jet characterized by an axisymmetric geometry. This agrees with the results shown in Figure 5.4, in which Actuator 3 has a velocity profile broader and faster with respect linear actuators. Moreover, the Actuator 2 has the maximum values double respect the Actuator 1, as highlight in Figure 5.3.

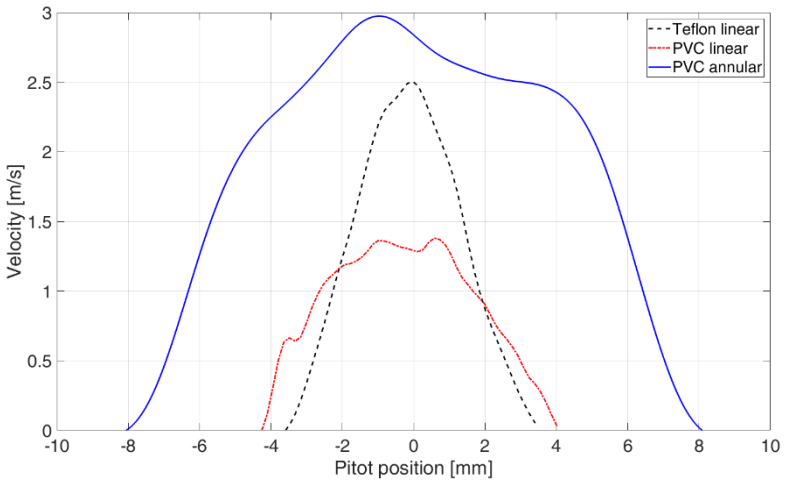

Figure 5.4 Velocity profiles at 2 cm from the end of the plasma discharge for the three actuators [59].

5.2 Charge particles measurement

The goal of this Chapter is to understand which electrode configuration and dielectric material is better to increase the charged particles deposition on a target surface.

5.2.1 Measurement set-up

Induced potential distribution on the surface has been measurement for the two Actuators 1 and 2 and it have been compared with the data acquired in the previous Chapter, using Actuator 3. Set-up scheme and electrical device are the same used in all tests described previously and it is shown in Figure 5.5.

A plexiglass target was placed at a distance of 1 cm from the actuator end (in the x-direction in Figure 5.5) perpendicularly to the actuator dielectric slab. The electrostatic voltage probe scans the target in the y-direction: on the right-side, the reference is positive and on the left-side, it is negative. The zero position in the y-direction corresponds to the plasma discharge plane extension on the target surface. This point represents the position where the jet, hitting the surface, has the highest speed. The experimental procedure, used to measure surface potential distribution, is performed through the following steps:

1. The Plexiglass surface was wiped by using a wet rag and then heated for 10 s with a hot gun to eliminate possible traces of humidity.

2. The electrostatic probe was moved over the Plexiglass surface checking the presence of a zero-voltage signal. If the zero condition was not achieved, step 1 was repeated.

3. Discharge was ignited for a defined time interval. Suddenly, after the switching-off the discharge, the electrostatic probe was moved over the Plexiglass plate, in the region where the induced jet hits the surface. Induced potential signal was acquired.

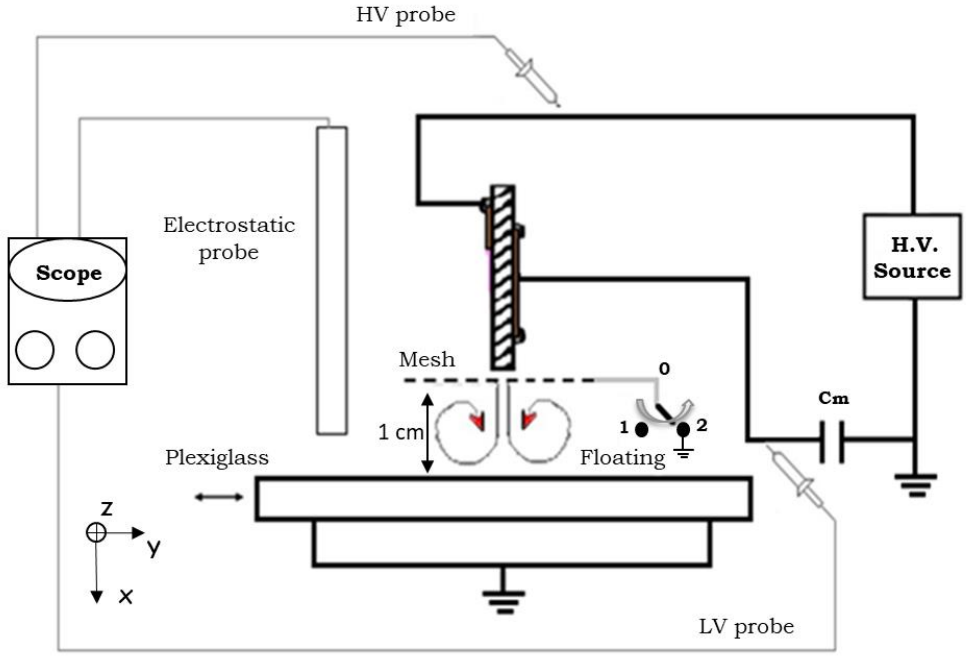

Figure 5.5 Experimental set-up scheme.

5.2.2 Results

All tests have been performed in open air, with a temperature of 20 °C ± 1 °C, and a humidity rate of 45% ± 5%, by increasing plasma-on time, for both Actuator, 1 and 2. In Figure 5.6, the comparison is shown. In Figure 5.6.a, there is the surface potential distribution obtained by using Actuator 1 and in Figure 5.6.b by Actuator 2.

In all graphs, charges deposited over the Plexiglass surface always induce positive potentials. This agrees with all tests shown previously. In according with the Schlieren Images (Figure 5.2), the potential distribution on the target surface increases in value and extension by increasing the plasma switching-on time interval. In addition, the charge build-up takes place in shorter times for Actuator 2, due to faster jet produced by this actuator. In fact, after a plasma on-time of 250 ms, the maximum value of the induced potential is 1 kV, about the 60% of the final regime value. For Actuator 1, after the same plasma on-time only one third of the regime value is achieved.

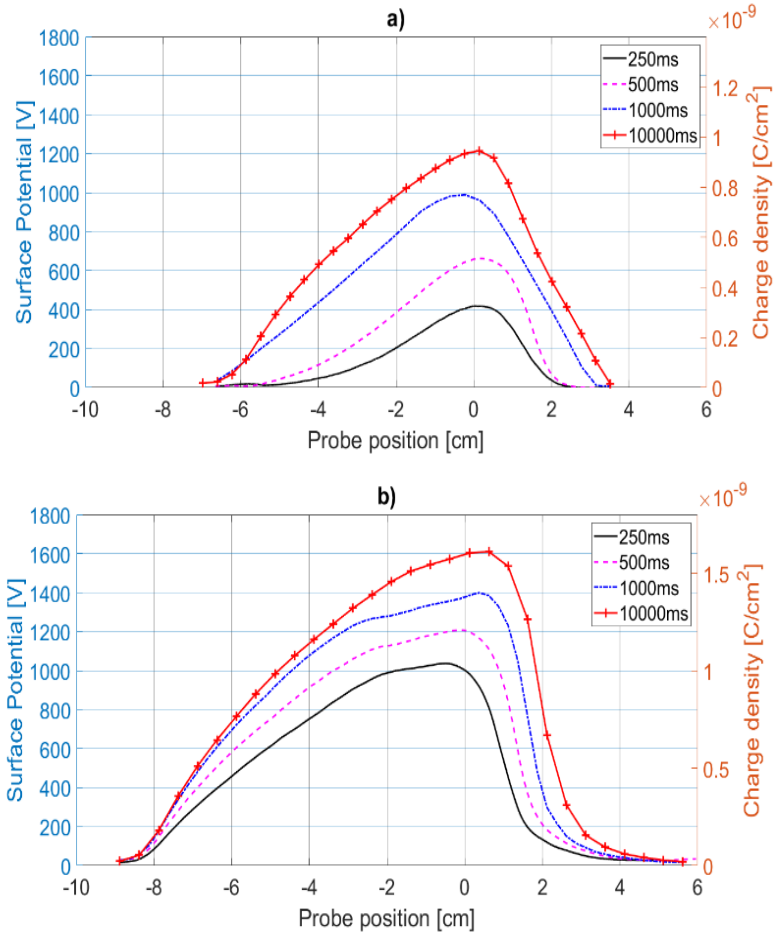

Figure 5.6 Surface potential distribution measured by increasing plasma on time for Actuator 1 (a) and Actuator 2 (b) [59].

To understand which geometry is better for the charged particles deposition, the potentials induce by three actuators, after a plasma-on time of 10 s, at the same distance of 2 cm, are acquired (Figure 5.7). It is possible to compare these measurements with the Pitot profiles shown in Figure 5.4. The induced potential increase of 50 % for Actuator 1 (red line in Figure 5.7) respect Actuator 3, (blue line in Figure 5.7) despite the Pitot profile of Actuator 3 is two time larger than Actuator 1 (Figure 5.4). This is probably due to a different fluid-dynamic interaction between an incoming jet and the dielectric surface. In fact, for Actuator 3 (PVC annular) the jets merging together in perpendicular one. This interaction, between the jets, probably enhance the recombination of free charges, and a lower amount of charged particles is deposited on the target surface. For this reason, the maximum values of the potential obtained by the linear actuators largely exceed the values induced by the annular one.

Moreover, the potential distribution profile for linear actuators is not symmetric with respect the axis normal to the target surface (x-direction in Figure 5.5), as already highlights in Schlieren images reported in Figure 5.2. For Actuator 1, the potential is 50% higher with respect to Actuator 3, going from a maximum of 800 –1200 V. This important increment has been obtained by changing only the reactor geometry. In fact, materials and electrical parameters are the same.

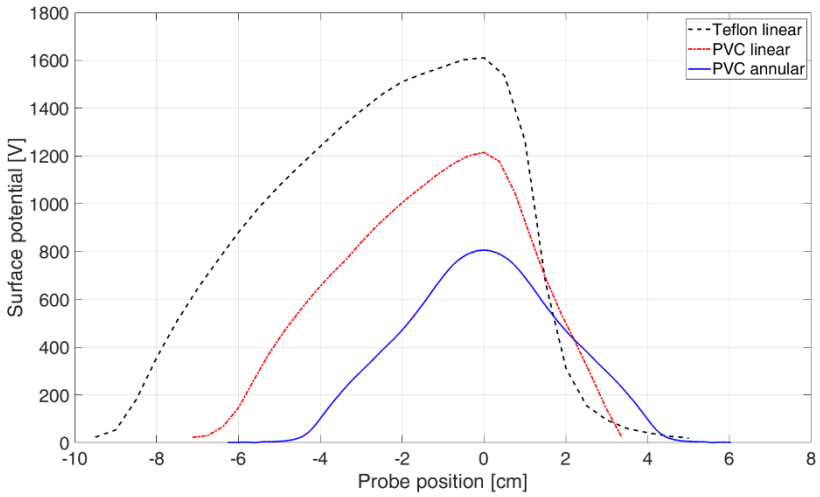

Figure 5.7 Surface potential distribution measured for three actuators, after 10 seconds of plasma switching-on [59].

As a matter of fact, the interaction of the tangential jets induced in Actuator 3, which merges in perpendicular jet, favours the recombination of charged particles. Therefore, a reduced quantity of charges is deposited on the target surface, despite a higher ionic wind velocity. For the Actuator 2, the maximum induced potential value reaches 1600 V, two time of that of Actuator 3. This is agreement with the Pitot profile, in which Actuator 1 has a velocity lower than Actuator 2. In conclusion, it is possible to strongly increase the amount of charged particles transported by a plasma actuator by modifying actuator geometry and supply conditions.

5.3 Biological application

As already illustrated in Chapter 3, the object of this thesis is PSJA biological applications and free particle's role. A metallic mesh has been added between the linear actuator and the target surface to verify the possibility to prevent charged particles to reach the sample. The mesh was placed 1 mm from the actuator surface (in the x-direction, see Figure 5.5) to stop the free charges transported by the induced flow. This mesh is a square with a size of 10 cm with a 2 x 1 mm^2 rectangular hole and a 0.3 mm thick wire.

5.3.1 Mesh analysis

Tests had been performed only with Actuator 2. Teflon linear actuator was chosen because it deposited, on the target surface, the higher amount of free charges (see Figure 5.6). Potential and jet velocity distribution are compared respectively in Figure 5.8.a and 5.8.b. These tests have been repeated with the mesh connected to the ground, switch position 0 – 2 in Figure 5.5, and with the mesh left floating, switch position 0 – 1.

In Figure 5.8.a, the surface potential distribution on the target had been acquired in three different mesh conditions. The continuous blue line refers to the potential when the mesh is not present, the black dashed line when the mesh is floating, and the red line represents the case with the mesh connected to the grounded. The results show an increase in the surface potential by 25 % when the mesh is floating respect with the potential measured without grid. This behaviour is different respect was shown in the previous Chapter 3 (section 3.3.3), in which the maximum values acquired with the mesh is equal to the value without mesh. A possible explanation for this increment, is a different fluid-dynamic regime for the two geometries. When the mesh is connected to the ground, about 95 % of the charged are blocked, limiting the number of charge particles that reach the sample.

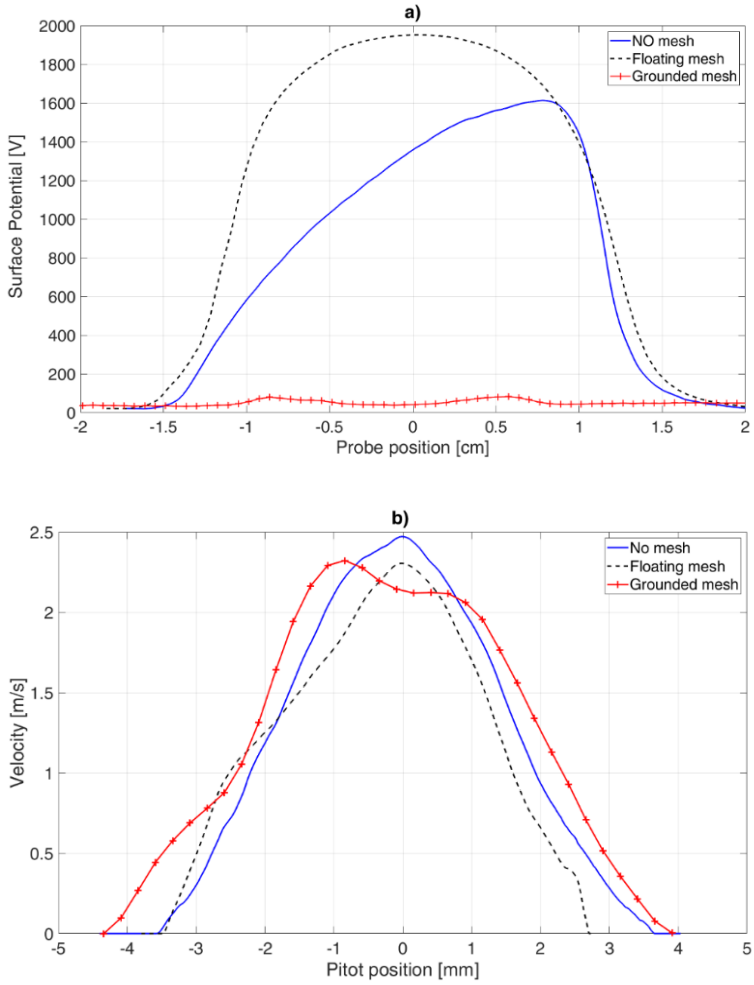

Figure 5.8 Mesh effect on surface potential distribution (a), and velocity profile acquired with the same mesh condition (b) [59].

In Figure 5.8.b, the velocity profile has been measured with the same mesh condition, at 2 cm from the end of the discharge. All profiles are similar. In fact, the differences of the three velocity are within the standard deviation error, about 5 %. This result highlights that the increase in the potential, induced on the target surface when the mesh is floating, is not related to the variation of the induced flow. The floating wire mesh is an equipotential plane orthogonal to the flow direction. Therefore, the electrodynamics on this region is changed and, as a consequence, its interaction with the fluid-dynamics is different.

Measurements had been repeated by increasing plasma-on time and then compared with the surface potential distribution without mesh, due to interesting results obtained with the mesh floating. In Figure 5.9, the surface potential distribution had been acquired with mesh floating (Figure 5.9.a), and without mesh (Figure 5.9.b). The distance from the target surface and the discharge time intervals are the same used in the previous tests.

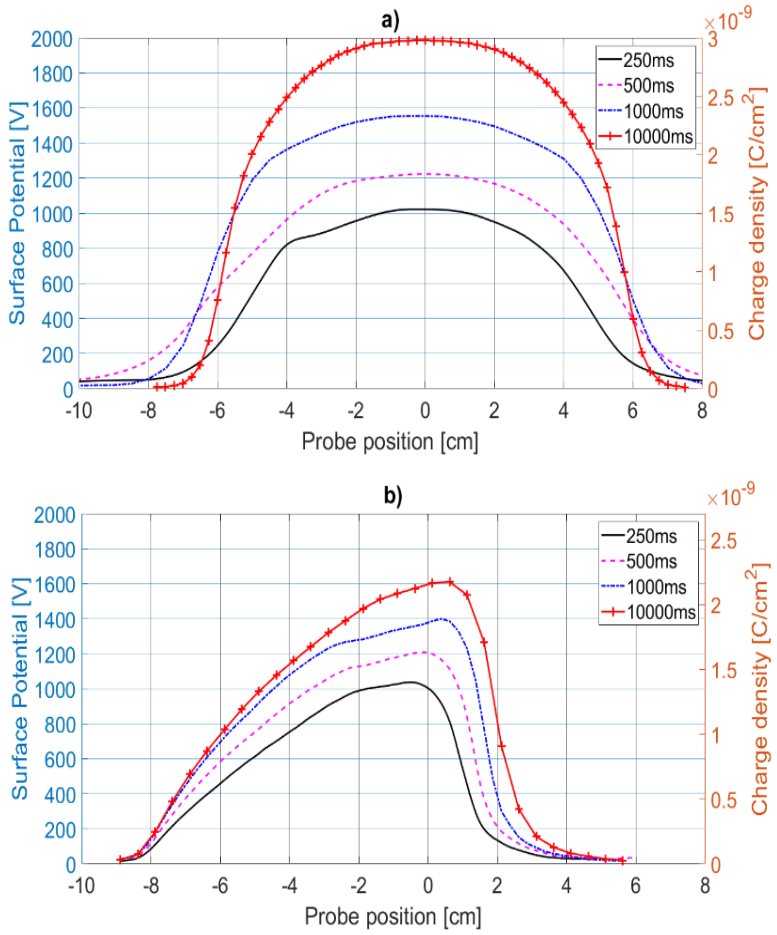

Figure 5.9 Surface potential distribution measured by increasing plasma on time, with floating mesh (a), and without (b) [59].

As already mentioned above, the potential value increases when the mesh is floating, and the maximum values became larger by increasing the plasma-on time. This behaviour is due to the equipotential plane of the mesh that leads to a symmetric potentials' distribution on the target surface on the side of the flow. In fact, after a discharge of 500 ms, the maximum value reached is the same for both

configurations. When the plasma-on time increase, after 10 s, the maximum value with floating mesh is 2000 V and without mesh is 1600 V, it is 25 % higher. This is shown in the figure below. In Figure 5.10.a, the maximum potential values on the target surface, for different plasma-on time, without mesh (black line) and with the floating mesh (red line) are displayed. In Figure 5.10.b the potential of the mesh as a function of time, after the discharge ignition, is presented. The time zero corresponds to the discharge ignition.

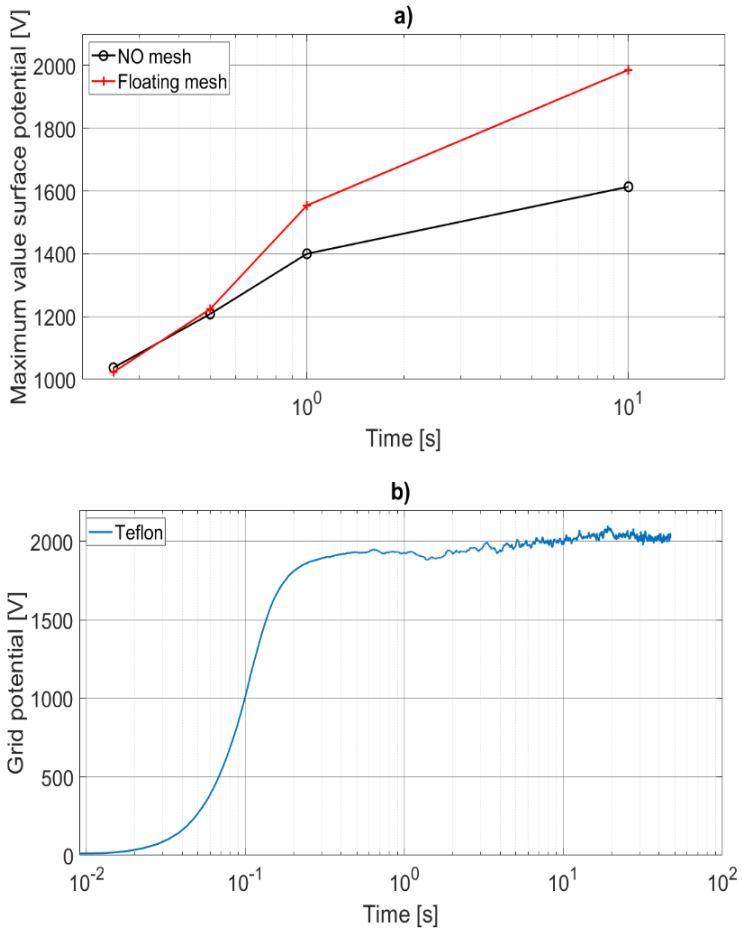

Figure 5.10 Mesh analysis as a function of time [59].

After about 10 ms, the mesh potential starts to increase as the induced jet approaches it surface. The final potential of the floating mesh is the same measured on the target. Despite this, the charge deposition dynamics, on the target surface, is slower than the mesh changing mechanism. This is due to the time needed for free charges to reach the target after overcoming the potential barrier generated by charges that have already reached the surface.

5.3.2 2D finite element analysis

To understand the mechanisms by which electric field affects the transport of electric charges by the jet, a 2D finite element analysis was carried out. A two-dimensional electrostatic problem, governed by the equation for the electric scalar potential φ has been considered:

$$\nabla \cdot \epsilon_r \nabla \varphi = -\frac{\rho}{\epsilon_0} \qquad (5.1)$$

where ϵ_r and ϵ_0 are the relative and vacuum permittivity, respectively, and ρ is the electric volume charge density. Charge separation can produce a charge density capable of modifying the applied electric field in the region where the DBD develops, that is, in the close proximity of the powered electrode. Here, during the streamer formation, regions with a characteristic size of tenths of micrometres and a lifetime of a few nanoseconds are observable, in which the charge separation produces a significant electric charge density [60]. However, due to the limited size of these regions, charge separation affects locally the distribution of the electric field. In the region of the jet produced by the DBD, the conditions of low density of the free charges and relatively low temperature allow to apply a quasi-neutrality assumption. In this analysis, therefore, the charge density will be considered zero, and the electric field distribution is assumed to be dominated by the applied voltage and the charge deposit.

The Ansoft Maxwell 2D electrostatic solver was utilised to solve the equation (5.3) on the considered 180 mm x 120 mm rectangular calculation domain shown in Figure 5.11. On the outer boundary except the electrode portion, a balloon boundary condition has been assigned. This condition is used by the Maxwell software to approximately simulate an infinite region extending beyond the boundary. The grounded electrodes have been assigned a zero electric potential, while the power electrode is assigned a potential equal to the voltage applied by the power source. Additionally, the presence of the charge deposit is simulated by assigning to the target surface exposed to the jet the measured potential due to the deposited charge [59].

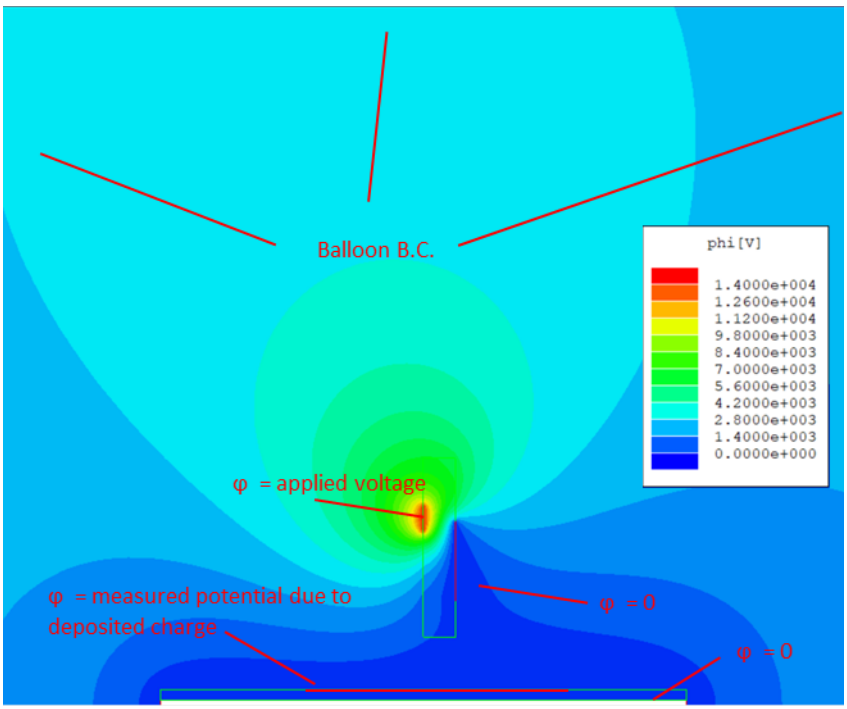

Figure 5.11 Calculation domain and boundary conditions [59].

In Figure 5.12, the contour plots are displayed. In left-hand there is the Actuator 1 and in the right-hand, the Actuator 2. The powered electrode is set to the potential equal to the amplitude of the sinusoidal supply voltage. The distribution of the x-component of the electric field E_x along the line Γ running from the powered electrode to the target is shown in Figure 5.13. Actuator 1 is on the left-hand and Actuator 2 on the right-hand. Considering the reference system in Figure 5.12, a positive electric field E_x represents a force on the positive charge particle per unit charge toward the target. A negative E_x represents a force on the positive charge in the opposite direction.

In all graphs the electric field E_x is plotted for three different values of applied sinusoidally voltage, V_0, equal to -8 kV, 0 and 8 kV. Three different discharge switch-on time have been used in the simulation. The results are shown after 0, 1 and 10 s, for Actuator 1 and 0, 0.25 and 10 s for Actuator 2. The electric field produced solely by the deposited charge is represented by the plot for $V_0 = 0$.

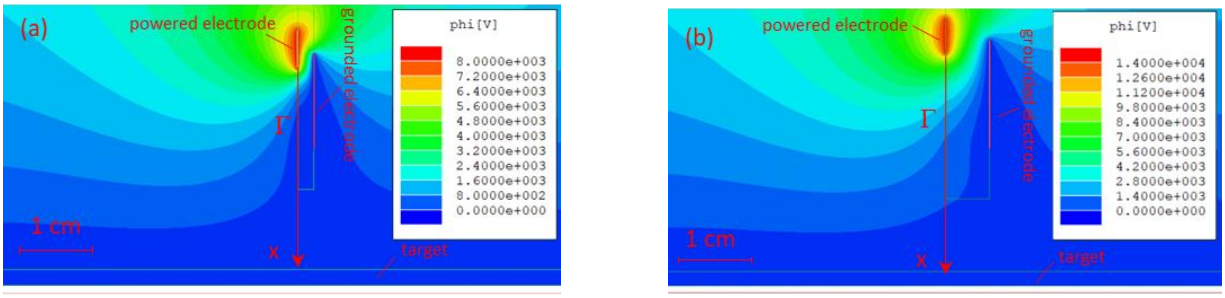

Figure 5.12 Electric potential contour plot for Actuator 1 (a) and Actuator 2 (b) [59].

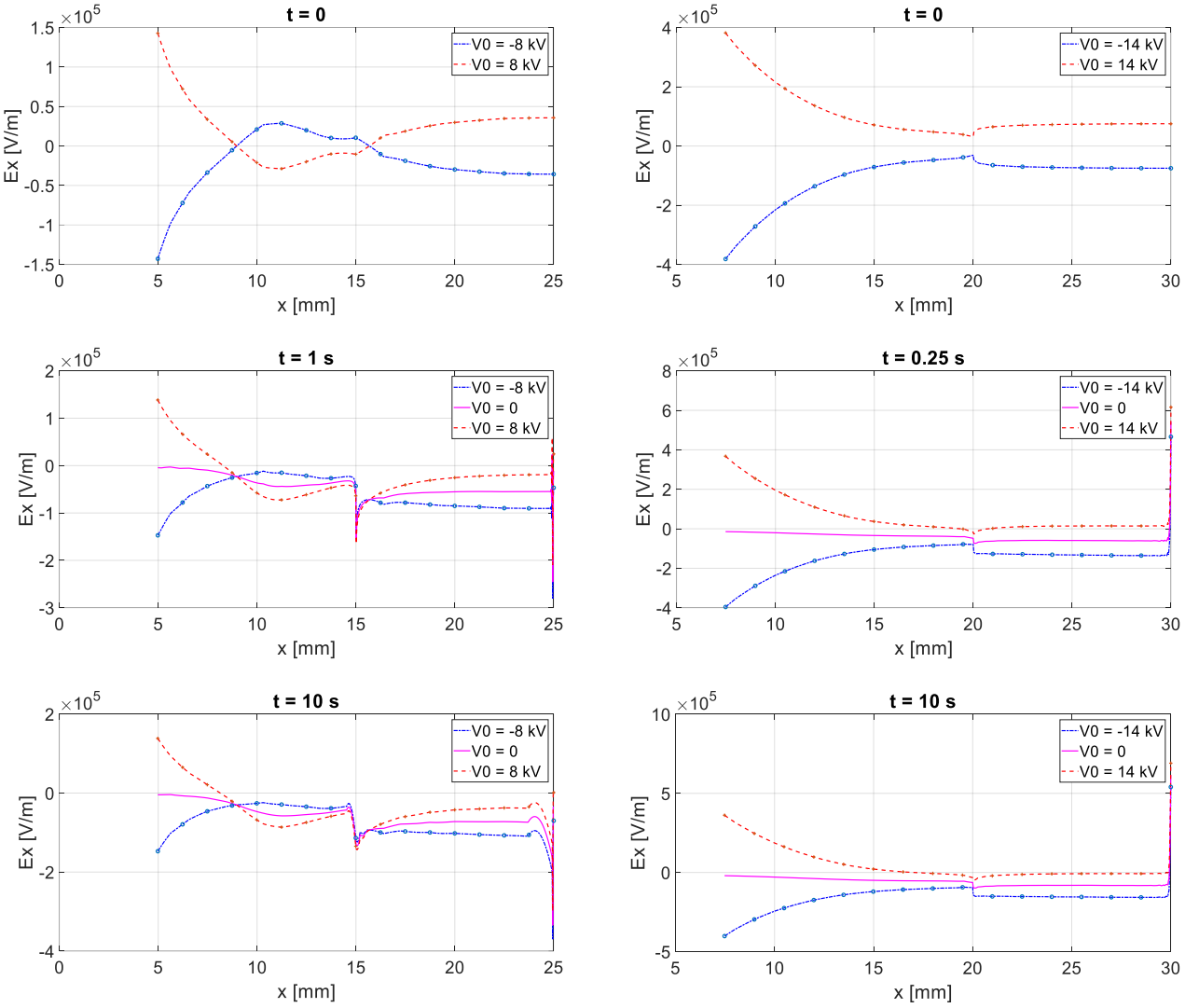

Figura 5.13 Distribution of the x-component of the electric field along Γ for Actuator 1 (on the left-hand) and for Actuator 2 (on the right-hand) [59].

For Actuator 1 (see Figure 5.11.a) the distance between the actuator lower edge and the target is 15 mm. For it, the region between 15 and 25 mm represents the airgap between the actuator and the target. In this region the electric field is low, it varies between 35 and -35 kV m^{-1}. At t=1 s, on the target the electric field is negative for the entire cycle duration, with an average value of about - 45 kV m^{-1}. Despite of this, the charge build-up continues. In this phase, the jet produced by the actuator is responsible for a convective ion flux which prevails on diffusion flux due to the adverse electric field. In fact, while the electric charge settles on the target surface over time, an adverse field is formed, which exerts a repulsive force on ions. After an approximately 10 s switch on time, an equilibrium condition is eventually reached, as the charge build-up produces an electric field that is sufficient to compensate the incoming convection ion flux on the target wall.

For Actuator 2 (see Figure 5.13 on the right), the actuator lower edge is located at x = 20 mm, and the airgap region between the actuator and the target is in the range of 20 ÷ 30 mm. The electric field behaviour is like Actuator 1. An adverse field is formed in the airgap region between the actuator and the target due to the deposited charges. E_x is observed to assume negative values for almost the whole supply system period at t=250 ms. Nevertheless, the positive charge continues to cumulate up to t=10 s, when an equilibrium condition is reached.

5.3.3 2D finite element mesh analysis

The numerical analysis was repeated with interposing the floating mesh between the actuator and the target. As already mentioned in this Chapter, the floating mesh created an equipotential plane, and therefore a symmetric potentials' distribution on the target surface. Figure 5.14, in fact, shows a vast region downstream of the mesh itself in which the distribution of the electric field is fairly uniform and substantially independent of the applied voltage. The mesh is indicated by the horizontal dot line below of the dielectric edge. In this figure, is reported also, the distribution of the x-component of the electric field E_x along the line Γ running from the powered electrode to the target with the floating mesh.

It is possible to note that the rate at which the charge deposited on the target is lower than the rate at which the charges and the potential of the mesh increases. As a result, a positive E_x develops in the region between the mesh and the target. E_x field is negative during the entire electric supply period in the region between x=15 mm and the mesh, for at t = 0.25 s. Also, in this case, ion convection dominates over the repulsive electric force. Despite the adverse electric field reaches a value of -125 kV m^{-1}, an ion flux is delivered past the mesh. In this region the E_x electric field becomes positive and is distributed in the whole width between the mesh and the target. Therefore, it promotes a uniform charge deposition.

The electric field is roughly constant during the supply system period. Its time behaviour is governed by the loading dynamics of the mesh and the target. The equilibrium condition is reached when the potential acquired by the target due to the deposited charges equals that of the wire mesh. In this condition, the ion diffusive flux produced by the adverse field balances the convective one. At the same time, the electric field in the region past the wire mesh takes on an almost zero value (see Figure 5.14, t=10 s).

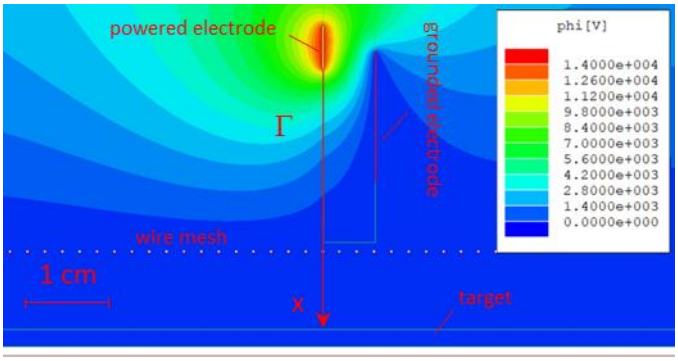

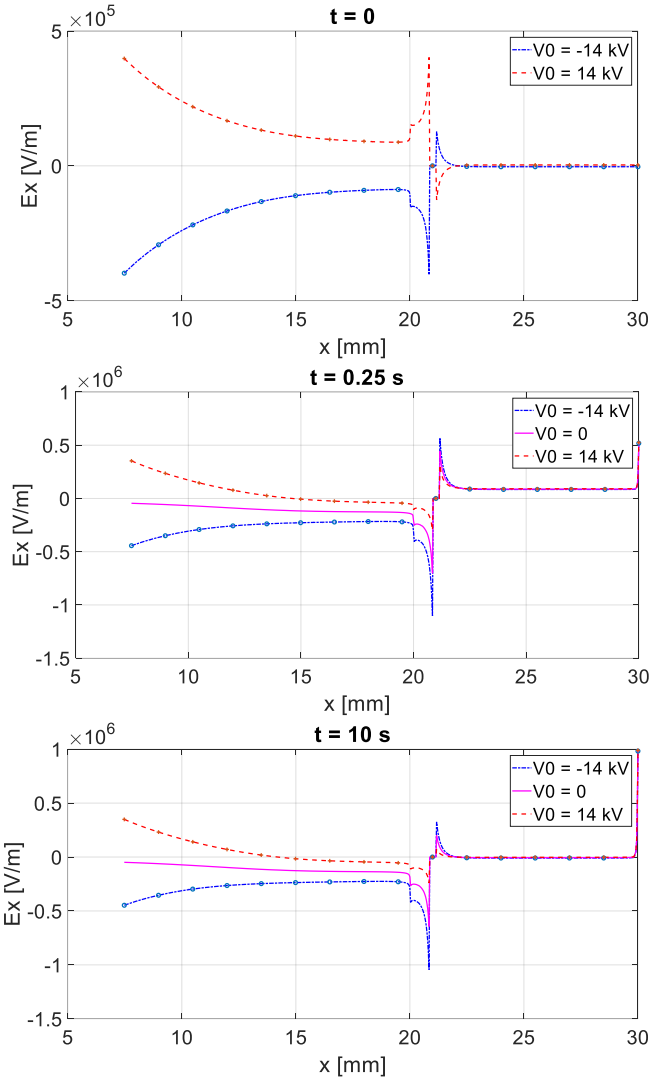

Figura 5.14 Electric potential contour plot and distribution of the x-component of the electric field along Γ with a floating mesh, for Actuator 2 [59].

5.3.4 Biological results

Biological tests have been done on *Candida Albicans*, in the same way illustrated in Chapter 3. In this case, *Candida* was treated only in Agar substrate. Petri dishes were made by the Department of Veterinary Medical Sciences, University of Bologna [28]. To quantify the living yeast present after the treatments, the number of Colony Forming Units (CFU) of untreated suspension initial is 10^6.

The firstly tests have been performed, in open air, only by Teflon linear actuator, with the mesh between the actuator and the sample, and without it. In fact, charged particles disinfection efficiency, produced by Teflon linear actuator was investigated. Set-up is equal to the set-up describe in Figure 1.14 in Chapter 1. The sample, at the distance of 2 cm from the actuator, were treated with a plasma-on time of 10 and 20 minutes. The duty cycle is the same used in the previous tests: 1 second on and 1 second off. The electrical parameters are equal to the parameters chosen for the charge particles measurements: a sinusoidal voltage of 14 kV peak with a frequency of 36 kHz and an average power of 18 W. In the following graph, the results obtained by the Teflon linear are compared with the PVC annular, analysed in Chapter 2.

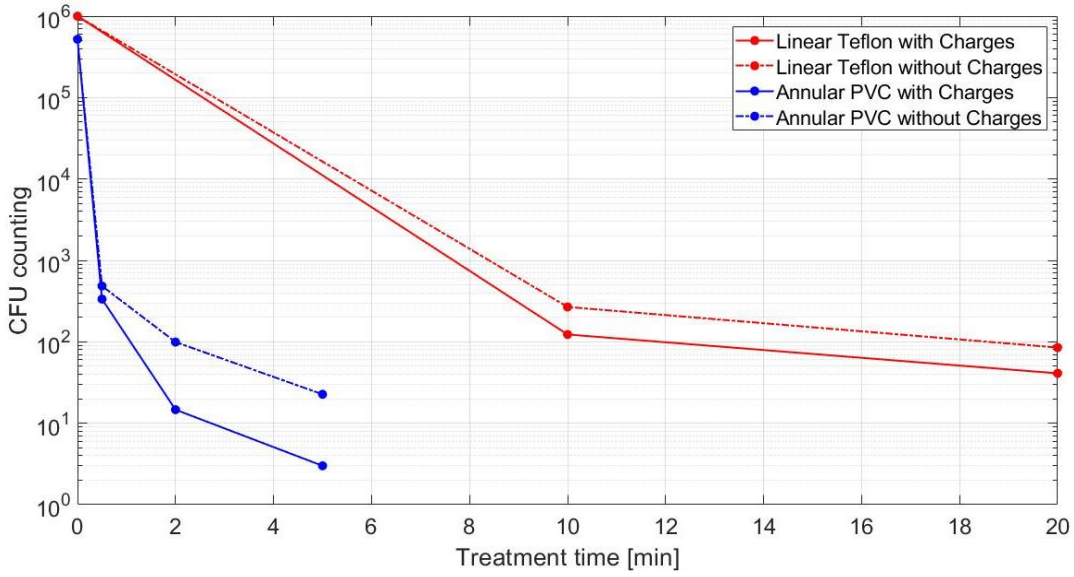

Figure 5.14 *Candida Albicans* CFU reduction. Teflon linear (red line) and PVC annular (blue line) comparison, with and without mesh (continuos and dot line respectivily).

Dot lines represents the treatment without charges, they are blocked by the mesh, while for the continue lines the charges are free to reach the sample. In red, it is shown the results obtained by using Teflon linear actuator and in blue the treatments are performed by PVC annular one.

When the geometry is linear charged particles effect is not so important. In fact, the difference between the dot and continuous red lines (Teflon actuator) is a half with respect the gap between the blue lines (PVC annular actuator). Despite the charged particles production by the linear actuator is higher than the annular, as shown in Figure 5.7, their biological effect is less. This behaviour can be correlated to the velocity profiles highlights in Figure 5.4, in which the annular actuator has a velocity profile broader and faster with respect linear one. As a matter of fact, the morphology of the induced jets is different for the two geometries and influence the biological results.

In figure 5.15 it is shown a picture of the Petri dishes treated by Teflon linear actuator. A control sample (Figure 5.15.a) is compared with a sample after 10 minutes of plasma treatment (Figure 5.15.b) and 20 minutes (Figure 5.15.c), the treatment has been performed with mesh grounded (GND). In Figure 5.15.b, a preferential direction of the disinfection effect is possible to identify. It is in the middle of the Petri Dishes, corresponding to the rectangular shape of the actuator. After a long treatment time (Figure 5.15.c), the inactivation process on *Candida* becomes more homogeneous because in addition to EHD effect, the diffusion of the charge particles occurs. In fact, after 20 minutes of treatment there is a less quantity of *Candida* CFU, represented by the white dots in the Petri Dishes (Figure 5.15.c).

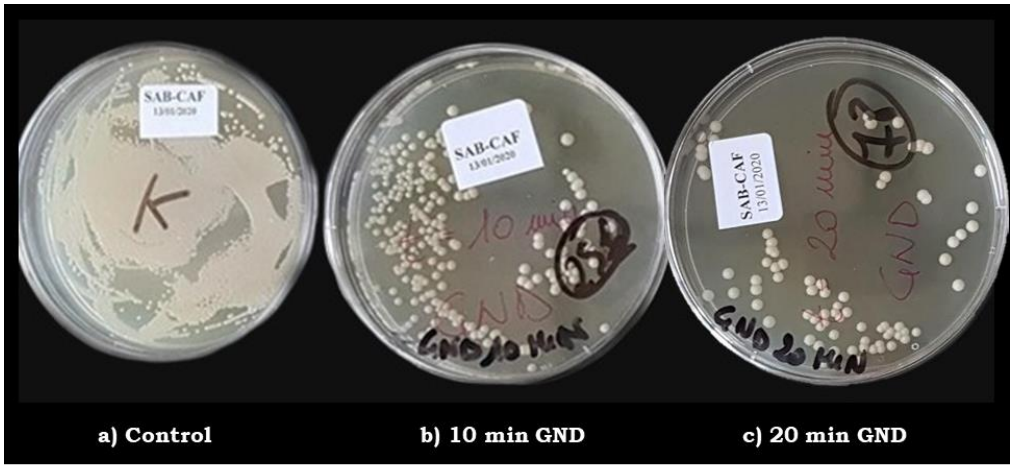

Figure 5.15 *Candida* CFU reduction in Agar substrate in a control sample (a), after 10 min (b) and 20 min (c) of treatment, with grounded mesh.

In order to carry out a quantitative comparison between velocity and charge profiles, mechanical power released to the flow by actuators has been compared with the total amount of charges deposited onto target surface. These calculations have been performed for all actuators. The mechanical power [28] [59] was calculated from the velocity profiles, $u(y)$, depicted in Figure 5.4. It is derived from the kinetic energy of the jets, by means of the following expression for the linear case ($P_{m,L}$) and for the annular ($P_{m,A}$):

$$P_{m,L} = \frac{1}{2}\,\rho\, L \int_{Y_{min}}^{Y_{max}} u^3(y)\, dy \qquad (5.2)$$

$$P_{m,A} = \frac{1}{2}\,\rho\,\pi \int_{Y_{min}}^{Y_{max}} |y|\, u^3(y)\, dy \qquad (5.3)$$

In both expressions, ρ is the atmospheric air pressure density, L is the electrode length in the z-direction (50 mm, see Figure 5.1), Y_{max} and Y_{min} correspond positive and negative limits of the y coordinate respectively (Pitot position in Figure 5.4) and *u(y)* is the velocity profile.

Total amount of deposited charges onto target surface, has been evaluated for both linear (Q_L) and annular (Q_A) actuators, by utilizing following expressions:

$$Q_L = L \int_{Y_{min}}^{Y_{max}} \mathrm{q}(y)\, dy \qquad (5.4)$$

$$Q_A = \pi \int_{Y_{min}}^{Y_{max}} |y|\, q(y)\, dy \qquad (5.5)$$

where *q(y)* represents the charge distribution displayed in Figure 5.7, and Y_{max} and Y_{min} are positive and negative limits of the y coordinate respectively (Probe position in Figure 5.7).

The actuator efficiency is defined as the ratio between the mechanical and electrical power. In the table below, the value of deposited charge, electrical and mechanical power, and efficiency of the three actuators are summarised.

	PVC annular	**PVC linear**	**Teflon linear**
Deposited charge [nC]	33	53	96
Electrical Power [W]	10	6.8	18
Mechanical Power [W]	$8.5e^{-04}$	$2.9e^{-04}$	$11e^{-04}$
Efficiency [%]	$8.5e^{-03}$	$4e^{-03}$	$6e^{-03}$

Table 1 Deposited charge, electrical and mechanical power and efficiency for the three actuator anayzed.

The comparison between PVC annular and linear shows that the former is characterized by the lowest mechanical power, about one third with respect that of Teflon linear actuator. Despite this, Teflon linear actuator is able to deposit over the target surface a quantity of charge 60% higher with respect PVC annular. As already pointed out, this behaviour underlines a higher amount of free charges existing within the jet produced by linear actuator. Teflon linear actuator presents the highest value of mechanical power and it is capable of depositing a higher amount of electric charges on the target. The electrical characterization and surface potential distribution measurements suggest that it is possible to strongly increase the number

of charged particles transported by a plasma actuator by modifying actuator geometry and supply conditions. Despite this, the biological experimental results show that the fluid-dynamic of jet is a fundamental parameter in the indirect treatments.

Conclusion

Non-thermal atmospheric pressure plasma treatments have been intensively investigated in the last decades. In this work, Plasma Synthetic Jet Actuators (PSJAs) have demonstrated their ability to inactivate different species of pathogens in indirect way. In particular, the advantage of combining together fluid-dynamics and physical-chemical properties of Dielectric Barrier Discharge (DBD) was studied. The Electro Hydro Dynamic (EHD) interaction creates a flow of air containing charged particles and active species. It is able to propagate for several centimeters at a velocity of several meters per seconds.

In addition, EHD effect was investigated for a Stremear Corona discharge used in cancer cells treatments. Also in this case, the ionic wind velocity is in the order of some meters per second despite the discharge dimension is much smaller if compared to PSJA. Induced flow can be utilized to facilitate the reactive species carriege into the medium and consequently to treat the cancer cells. This treatment, in fact, is called Plasma Activated Medium (PAM).

The precence of charged particles produced by PSJA, when the discharge is ignited, has been measured and their inactivation effect has been eximaneted. Inactivation efficacy of plasma annular reactor against *C. Guilliermondii* was demonstrated as first. Subsequently charged particles ability in disinfection enhacement was studied. The results suggest that an increase of them could be related to higher treatment efficacy. Besides, the influence of air humidity and electric parameters on the discharge regime and the charged particles has been analysed. The results show that humidity variation does not significantly influence the discarge regime. Therefore, the ambient condition is already an optimized working environment, in which the PSJA can be utilized withouth decreasing its biocidal effect. PSJA can deliver, toward a target, a higher amount of free charges, when supplied with higher voltage and lower frequency, despite the same average power and EHD effects. This could lead to an increase of

biocidal effects of this device without increasing its power consumption, and thus, increasing both efficacy and efficiency.

In order to enhance the charge delivery process, a comparison was carried out between two types of linear DBD actuators, made of different dielectric material, and an annular one. It was revealed that linear actuators produce a wider profile of the deposited charge and higher maximum values. On the contrary, its biological efficacy is reduced respect to the annular one. These results show that it is possible to strongly increase the number of charged particles transported by a plasma actuator by modifying actuator geometry and supply conditions. Moreover, the morphology of the induced jets strongly influences the biological results.

In conclusion, this work shows the efficacy of indirect plasma treatment for disinfection purposes. Most important application's advantage is the direct contact absence between sample and plasma discharge. Basically, reactive species and charged particles solely reach the sample. In particular, the annular actuator exhibits the best performances for biological applications. Directional effects, scalability and presence of charged particles enhancing inactivation effects are the main features of this type of reactors. The efficacy in disinfection field opens new perspectives in control of pathogen, widely diffuse in nature and able to induce diseases in immunocompromised humans and animals, with the aggravating factor to express a natural resistance to some drugs. The use of ambient air as carrier gas and the simple actuator set up, make this device suitable for real-life, large areas, indirect treatments applications. Further studies are needed to understand which chemical species reach the sample and their role in disinfection process.

Bibliography

[1] Akishev Y et al. 2019 Special issue on recent developments in plasma sources and new plasma regimes. *J. Phys. D: Appl. Phys.* **52**

[2] Vandamme M et al 2012 ROS implication in a new antitumor strategy based on non-thermal plasma. *Int. J. Cancer.* **130** 2185–94

[3] Dayun Y et al 2017 Cold atmospheric plasma, a novel promising anti-cancer treatment modality. *Oncotarget.* **8** 15977–95

[4] Fridman A 2012 *Plasma Chemistry* (Cambridge: Cambridge University Press)

[5] Laourssi M 2004 Evaluation of the roles of reactive species, heat, and UV radiation in the inactivation of bacterial cells by air plasmas at atmospheric pressure. *Int. J. Mass Spec.* **233**

[6] Fridman A et al 2004 *Plasma Physics and Engineering* (Boca Raton, FL: CRC Press)

[7] Fridman G et al 2007 Applied plasma medicine. *Plasma Process. Polym.* **5** 503–33

[8] Machala Z et al 2019 Chemical and antibacterial effects of plasma activated water: correlation with gaseous and aqueous reactive oxygen and nitrogen species, plasma sources and air flow conditions *J. Phys. D: Appl. Phys.* **52**

[9] Graves D B 2017 Mechanisms of Plasma Medicine: Coupling Plasma Physics, Biochemistry, and Biology. *IEEE Transactions on radiation and plasma medical sciences.* **1** (4)

[10] Machala Z et al 2008 DC Discharges in Atmospheric Air and Their Transitions. *IEEE Transactions on plasma science* **36** (4)

[11] Fridman A et al 2005 Non-thermal atmospheric pressure discharges. *J. Phys. D: Appl. Phys.* **38** R1

[12] Kogelschatz U et al 2003 Dielectric-barrier Discharges: Their History, Discharge Physics, and Industrial Applications. *Plasma Chemistry and Plasma Processing*. **23** 1

[13] Kogelschatz U et al 1997 Dielectric-Barrier Discharges. Principle and Applications. *J. Phy IV France.* **7** C4-47

[14] Lunov O et al 2015 Non-thermal plasma mills bacteria: Scanning electron microscopy observations. *Appl. Phys. Lett.* **106**

[15] Robinson M 1962 A history of the Electric Wind. *American Journal of Physics*. **30** 366

[16] Moreau E 2007 Airflow control by non-thermal plasma actuators. *J. Phys. D: Appl. Phys.* **40** 605–636

[17] Roth J.R., et al 1998 Boundary layer flow control with a one atmosphere uniform glow discharge surface plasma. *36th AIAA Aerospace and Exhibit Meeting* AIAA 0328.

[18] Neretti G 2016 Active flow control by using plasma actuators. *Recent Progress in Some Aircraft Technologies ed R Agarwal* (Rijeka: InTech)

[19] Borghi C A et al 2017 Duty cycle and directional jet effects of a plasma actuator on the flow control around a NACA0015 airfoil. *Meccanica.* **52**(2) 1-14

[20] Kurz A et al 2013 Boundary layer transition control using DBD plasma actuator. *Aerospace Lab* **2** 1–8

[21] Junhui H et al 2006 Plasma actuators for separation control of low-pressure turbine blades *AIAA J*. **44** 51–7

[22] Van Ness D K II et al 2006 Tip clearance control using plasma actuators. *44th AIAA Aerospace Sciences Meeting Exhibit Paper AIAA-2006-21* (Reno, NV, 9–12 January 2006)

[23] Amano I et al 2007 Sterilization using a wide-gap discharge formed by dielectric barrier discharge coupled with surface discharge under atmospheric pressure. *Industry Applications Conf. 42nd IAS Annual Meeting Conf. Record of the 2007 IEEE.*

[24] Riherd M et al 2013 Serpentine geometry plasma actuators for flow control *J. Appl. Phys.* **114**

[25] Kotsonis M et al 2012 Performance improvement of plasma actuators using asymmetric high voltage waveforms. *J. Phys. D: Appl. Phys*. **45**

[26] Santhanakrishnan A et al 2007 Flow control with plasma synthetic jet actuators *J. Phys. D: Appl. Phys.* **40**

[27] Neretti G et al 2016 Geometry optimization of linear and annular plasma synthetic jet actuators. *J. Phys. D: Appl. Phys.* **50**

[28] Neretti et al 2018 Indirect Inactivation of Candida guilliermondii by using a Plasma Synthetic Jet Actutator. Effect of Advected Charged Particles. *Plasma Medicine* **8** (3) 255 – 268

[29] Neretti G et al 2018 Measurement of the charge distribution deposited by an annular plasma synthetic jet actuator over a target surface. *J. Phys. D: Appl. Phys*. **51**

[30] Fridman G et al 2007 Comparison of direct and indirect effects of non-thermal atmospheric-pressure plasma on bacteria. *Plasma Process. Polym.* **4** 370 – 5

[31] Bussiahn R et al 2010 The hairline plasma: An intermittent negative dc-corona discharge at atmospheric pressure for plasma medical applications. *Appl. Phys. Lett.* **96**

[32] Machala Z et al 2010 Plasma agents in bio-decontamination by dc discharges in atmospheric air. *J. Phys. D: Appl. Phys.* **43**

[33] Janda M et al 2012 The streamer-to-spark transition in a transient spark: a dc-driven nanosecondpulsed discharge in atmospheric air. *Plasma Sources Sci. Technol.* **21**

[34] Bauer G et al 2019 Cold Atmospheric Plasma and Plasma-Activated Medium Trigger RONS-Based Tumor Cell Apoptosis. *Scientific reports.* **9**

[35] Bauer G, 2019 Cold atmospheric plasma and plasma-activated medium: antitumor cell effects with inherent synergistic potential. *Plasma Medicine* **9** 57–88

[36] Laroussi M 2014 From killing bacteria to destroying cancer cells: 20 years of plasma medicine. *Plasma Process. Polym.* **11** 1138–1141

[37] Graves D. B. 2014 Reactive species from cold atmospheric plasma: implications for cancer therapy. *Plasma Process. Polym.* **11** 1120–1127

[38] Cristofolini A et al 2012 Schlieren imaging in a dielectric barrier discharge actuator for airflow control. *Journal of Applied Physics.* **111**

[39] Settles G S 1949 *Schlieren and shadowgraph techniques*. Springer.

[40] Ricchiuto A C et al 2020 Measurement of the charge distribution deposited on a target surface by an annular plasma synthetic jet actuator: Influence of humidity and electric field. *Journal of Electrostatics.* **107**

[41] Jayasena D et al 2015 Flexible thin-layer dielectric barrier discharge plasma treatment of pork butt and beef loin: Effects on pathogen inactivation and meat-quality attributes. *Food Microbiology*, **46** 51 – 57

[42] Misra N et al 2017 Applications of cold plasma technology for microbiological safety in meat industry. *Trends in Food Science & Technology*. **64** 74 – 86

[43] Yong H I et al 2015 Evaluation of pathogen inactivation on sliced cheese induced by encapsulated atmospheric pressure dielectric barrier discharge plasma. *Food Microbiology*. **46** 46 – 50

[44] Bosi F J et al 2018 Characterization and comparative evaluation of two atmospheric plasma sources for water treatment. *Plasma Process. Polym*. **15** (3)

[45] Khan H A et al 2017 Nosocomial infections: Epidemiology, prevention, control and surveillance. *Asian Pacific Journal of Tropical Biomedicine.* **7**(5) 478-482

[46] Savini V et al 2011 What do we know about Candida guilliermondii? A voyage throughout past and current literature about this emerging yeast. *Mycoses.* **54 (**5) 434–41

[47] Neretti G et al 2018 Inactivation of Eimeria oocysts in aqueous solution by a dielectric barrier discharge plasma in contact with liquid. *J Plasma Med*. **8**(2) 155–162.

[48] Koban I et al 2010 Treatment of Candida Albicans biofilm with low-temperature plasma induced by dielectric barrier discharge and atmospheric pressure plasma jet. *New J Phys*. **7**

[49] lora-Glad Chizoba E et al 2017 A review on recent advances in cold plasma technology for the food industry: Current applications and future trends. *Trends in Food Science & Technology.* **69** 46 – 58

[50] Pon J et al 2005 Assymmetric surface dielectric barrier discharge in air at atmospheric pressure: electrical properties and induced airflow characteristics. J. *Phys. D: Appl. Phys.* **38** 3635–42

[51] Sado Kamden S et al 2011 Effects of carvacrol, (E)-2-hexenal, and citral on the thermal death kinetics of Listeria monocytogenes. *Journal of Food Protection.* **74** 2070–2078

[52] Vannini L et al 2004 Interactions between high pressure homogenization and antimicrobial activity of lysozyme and lactoperoxidase. *International Journal of Food Microbiology*. **94** 123–135

[53] Ragni L et al 2016 Influence of the electrode material on the decontamination efficacy of dielectric barrier discharge gas plasma treatments towards *Listeria monocytogenes* and *Escherichia coli. Innovative Food Science and Emerging Technologies.* **37** 170–176

[54] Cabrellon G et al 2020 Application of Fluorescence-Based Probes for the Determination of Superoxide in Water Treated with Air Non-thermal Plasma. *ACS Sens.* **5** 2866−2875

[55] Tampieri F et al 2018 Removal of persistent organic pollutants from water using a newly developed atmospheric plasma reactor. *Plasma Process. Polym.* **15**(6)

[56] Nani L et al 2018 Versatile prototype plasma reactor for water treatment supporting different discharge regimes. *J. Phys. D: Appl. Phys*. **51**(27)

[57] Borghi C A et al 2008. Electrohydrodynamic interaction induced by a dielectric barrier discharge. *J. Appl. Phys*. **103**

[58] Meeker D C, Finite Element Method Magnetics, Version 4.2, http://femm.info

[59] Ricchiuto A C, Borghi C A, Cristofolini A, Neretti G 2021 Atmospheric pressure plasma actuators: enhancement of the free

charges transport mechanism. *Plasma Processes and Polymers.* e2000214.

[60] Boeuf J P, LAgmich Y, Unfer Th, Callegari Th and Pitchford L C 2007 Electrohydrodynamic force in dielectric barrier discharge plasma actuators. *J. Phys. D: Appl. Phys.* **40** 652-662